Title
Photochemical restoration of visual responses in blind mice

Author
Polosukhina, Aleksandra

Publication Date
2013

Peer reviewed|Thesis/dissertation

Photochemical restoration of visual responses in blind mice

by

Aleksandra Polosukhina

A dissertation submitted in partial satisfaction of the
requirements for the degree of
Doctor of Philosophy

in

Vision Science

in the

Graduate Division

of the

University of California, Berkeley

Committee in charge:

Professor Richard Kramer, Chair
Professor Marla Feller
Professor Diana Bautista

Spring 2013

Photochemical restoration of visual responses in blind mice

Abstract

Photochemical restoration of visual responses in blind mice

by

Aleksandra Polosukhina

Doctor of Philosophy in Vision Science

University of California, Berkeley

Professor Richard Kramer, Chair

This dissertation addresses two non-genetic therapeutic approaches for treating inherited retinal diseases such as retinitis pigmentosa and age related retinal degeneration. The first approach utilizes a light sensitive molecule Azobenzene-acrylomide-quaternary amonium (AAQ) to restore light sensitivity to retinal degenerated (rd1) mice. AAQ molecules permeate through the cell membrane and photosensitize voltage-gated K^+ channels in response to different wavelengths of light. Consequently, we achieved robust photosensitization of most retinal cells *ex-vivo* upon application of AAQ on rd1 mouse retinal explants. We then characterized the effect of AAQ on mouse behavior and restored a pupillary light reflex and light elicited behavior in these blind rd1 mice.

The third chapter addresses improvements to the AAQ therapeutic approach. We utilize Di-ethyl-amine-azobenzene quaternary ammonium (DeNAQ) that also confers light sensitivity on RGCs by photosensitizing voltage-gated channels in response to 480 nm light and silencing the channels in the dark (*trans* form). The property of DeNAQ being sensitive in the visible range is one of the major advantages of this therapeutic. The quick relaxation of DeNAQ in the dark is also an advantage, since only one wavelength is required for photosensitization. In addition to the red-shifted properties we found that DeNAQ can confer light sensitivity to retinal cells for several weeks and restores light elicited behavioral responses.

The fourth chapter addresses the question of whether the physiological and anatomical changes that accompany retinal degeneration lead to functional changes in the retinal ganglion cells (RGCs). We used a membrane impermeable Quarternary-azobenzene-quaternary molecule (QAQ) molecule that can only enter the cells and render them light sensitive through large pore openings, those seen during pore dilation of P2X and TRP channels. We characterized the path of entry of QAQ using pharmacology and found that photosensitization of RGCs could be reduced by adding P2XR antagonists. In agreement with other studies suggesting that pore dilation has been associated with neurodegenerative processes, we show that QAQ can only confer light sensitivity to RGCs from rd1 and not from wild-type (WT) mice. We also demonstrate that QAQ does not photosensitize RGCs in glaucoma

mouse models, suggesting that this physiological change in permeability is specific to retinal degenerating disease.

The therapeutic approaches addressed in this thesis apply to a variety of retinal disease genotypes. The high promiscuity of AAQ delivery allows us to optically stimulate any cell type in the retina. Additionally, the red-shifted molecule DeNAQ, combined with its ability to target only diseased tissue, offers a promising clinical alternative for vision restoration. Finally, using another photosensitive molecule, QAQ, we study the physiological impact of retinal degeneration on pore-dilating ion channel activity. Understanding the sources of physiological changes could help prevent further damage caused by degenerative retinal diseases.

Contents

List of Figures

Acknowledgments

First and foremost, I would like to thank my advisor Richard Kramer for providing me with scientific guidance, encouragement, and patiently providing advice and inspiration; I learned immeasurably from his creative way of pursuing questions. I would also like to thank Marla Feller, who introduced me to electrophysiology and provided priceless guidance throughout my graduate studies, Diana Bautista and John Flannery for additional guidance and support, I am grateful for Udi Isacoff's invaluable encouragement and career advice, my collaborators Dirk Trauner and Russ Van Gelder. Special thanks to my undergraduate advisor Marcelo Camperi who introduced me to neuroscience.

I would like to thank my collaborators over the years, Jeff Litt for scientific discussions, advice, encouragement, and for being a wonderful scientist and friend. Thank you to Alexis Fedorchak, Alex Mourot, Doris Fortin, Christian Herold, and the rest of the lab for their companionship, making my graduate experience fun and motivating, and for teaching me how to excel in volleyball. Semyon Dyatlov, Justin Elstrott, Anastasia Anishchenko for their guidance with analysis. Thank you to our lab manager Rachel Montpetit who has provided invaluable support, advice, and friendship. I want to thank the administrative staff in the Vision Science Graduate Group, Inez Bailey for her energy, help, and support over the years.

I dedicate this dissertation to my family, friends, and Pierre, for always being there for me and for being incredibly wonderful human beings.

Chapter 1

Introduction

Vision is one of the most vital senses, allowing us not only to effortlessly navigate through our daily life, but to also appreciate the beauty of this world. This visual information consists of movement, contrast, brightness, and color, each of which is encoded in different neural circuits in the retina. Once extracted, the retinal ganglion cells send this information to higher order processes of the brain. However, many diseases of the retina disrupt this intricate circuitry rendering the person completely blind. It is crucial to enhance our understanding of these diseases in order to find cures and develop more precise tools that could restore visual sensitivity.

1.1 Retina

The retina is the first image processing unit in our body that extracts information from the light reflecting off the objects. Vision begins when light is absorbed by the visual pigment molecules in rod and cone photoreceptors. The visual pigment is found primarily in the outer segments of photoreceptor cells and consists of an opsin protein that is covalently attached to 11-cis-retinal. In the dark, photoreceptors rest at -40 mV and maximally release glutamate. When a photon is absorbed, the 11-cis retinal is isomerized to *all-trans* and activates the visual pigment. The visual pigment activates the G protein, where the Gt alpha subunit in turn activates the phosphodiesterase (PDE) enzyme to break down cyclic GMP (cGMP). The decrease in cGMP leads to the closure of cGMP-gated cation channels causing hyperpolarization of the outer segment plasma membrane. Due to the hyperpolarization, the photoreceptors decrease the amount of neurotransmitter (glutamate) released. These changes in glutamate release drive information processing by bipolar cells, horizontal cells, and amacrine cells in the inner nuclear layer (INL). Finally, all the signals converge onto retinal ganglion cells (RGCs), which send information via action potentials to the visual cortex and the lateral geniculate nucleus.

Photoreceptors synapse onto bipolar cells in the outer plexiform layer which then transmit the signals to retinal ganglion cells in the inner plexiform layer. Horizontal cells play

an important role inregulating the signals from photoreceptors to bipolar cells and in formation of bipolar cell receptive fields. Photoreceptors release glutamate in the dark thereby depolarizing the OFF bipolar cells, located in the OFF lamina and hyperpolarizing the ON bipolar cells. When photoreceptors are exposed to light, they hyperpolarize and cease releasing glutamate, thereby depolarizing the ON bipolar cells and hyperpolarizing the OFF bipolar cells (Nelson et al., 1978; Raviola and Dacheux, 1983). Signals from bipolar cells to retinal ganglion cells are modulated by amacrine cells. The rod bipolar cells connect to ON and OFF cone bipolar cells via the AII amacrine cell. The AII amacrine cell excites ON cone bipolar cells through gap junctions and inhibits the OFF cone bipolar cell through glycine release. Amacrine cells play a role in extracting contrast, color, movement, as well as brightness. Ganglion cells then process the signals in terms of action potentials and send them via the optic nerve to the higher order processes of the brain. However, diseases like retinitis pigmentosa could slowly degenerate the sensitive photoreceptor layer, rendering the rest of the circuitry mostly anatomically in tact but unable to respond to light.

1.2 Inherited Retinal Degenerating Diseases

1.2.1 Retinitis Pigmentosa

Millions of people suffer from retinal degenerating diseases, including retinitis pigmentosa, age related macular degeneration, glaucoma, Lebers congenital amaurosis and many others. Retinitis pigmentosa is the most commonly inherited retinal degeneration worldwide, occurring in approximately 1 in 5000 individuals, affecting around 1.5 million people in the world (Shintani et al., 2009). RP can develop due to a mutation in up to as many as 100 different genes, 13% inphosphodiesterase-b. This disease can be inherited as an autosomal dominant (30-40% of cases), autosomal recessive (50-60%), x-linked trait (5-15%), but though there are genetic variations of this disease, they all share a common phenotype (Hartong et al., 2006). RP is clinically characterized by lack of night vision and often progresses over time to tunnel vision and then to complete blindness. These effects occur due to the progressive degeneration of rod and then cone photoreceptors, followed by degeneration of the retinal pigment epithelium layer.

1.2.2 Stages of Degeneration

The rd1 mouse model has a mutation in phosphodiesterase-b, and photoreceptor degeneration begins around postnatal day (P)14 and by P17 only 2% of rod photoreceptors remain (Carter-Dawson et al., 1978). This model goes through three main stages of degeneration. The first phase of degeneration begins before eye opening, around P8. By P30-P40, only the light insensitive photoreceptor bodies remain connected to bipolar cells. The dendritic glutamate receptor expression of iGluRs and mGluRs in bipolar cells is down-regulated, but the expression of iGLuRs on bipolar cells is double than in WT mouse retinas (Marc et al.,

2007). At this time the retinas have normal spontaneous retinal waves, which consist of correlated spontaneous action potentials.

The second stage begins after eye opening (P14), bipolar cells have retracted their dendrites and have begun to form sprouts to make connections with the cone pedicles. The full-field flashes of light induce ON and OFF responses; from P17 to P28, OFF responses begin dominating (Stasheff, 2008). It is not clear though whether ON cells become OFF cells, or whether they simply stop receiving the appropriate synaptic inputs. By the time light-evoked responses have dissipated, rd1 RGCs fire at much higher spontaneous frequency than normal and remain so after P28. Throughout the second and third stages of degeneration, neuronal sprouting occurs from bipolar and amacrine cells. Simultaneously, bipolar and amacrine cells migrate into the RGC layer and sometimes RGCs have been observed to migrate up to the IPL (Jones et al., 2012). It would be interesting to determine whether the organizational change in the ONL and INL may have an effect on the physiological responses of RGCs.

The degeneration of photoreceptors is accompanied and preceded by hyperactivity, which appears to originate in the inner retina This hyperactivity has been found to be attributed to inner retinal circuitry reorganization, similar to what has been observed in other systems (Cuenca et al., 2005). Margolis et al. (2008) have found the RGCs in rd1 mice fire rhythmically at around 10 Hz, even in the later stages of degeneration, due to oscillatory synaptic inputs (Margolis et al., 2008; Margolis and Detwiler, 2011). This oscillating network is most likely to drive synaptic activity to downstream circuits. RGCs are affected by these oscillations independently of their class. Oscillations have been identified to originate from the electrically coupled network of ON cone bipolar and AII amacrine cells (Borowska et al., 2011). The hyperactivity of the retina is a very significant characteristic to be aware of especially when developing vision restoration tools.

These oscillations could greatly interfere with the effectiveness of many vision restoration tools; since the majority of these tools target the inner circuitry, they have to evoke a response that is significantly greater or that silence this abnormally heightened activity. Anatomically, RGCs retain normal dendritic morphology, structure and projections to higher visual centers (Mazzoni et al., 2008). Margolis et al. (2008)also concluded that RGCs do not undergo any significant physiological changes, by showing that throughout retinal degeneration ON and OFF RGCs retain their firing properties, rebound spiking, and dendritic Ca^{2+} signaling (Margolis et al., 2008). However, the studies did not investigate changes in channel or receptor expression in RGCs during degeneration. It would be interesting to examine whether these are affected since it could provide insight on the mechanisms accompanying RP diseases and open new therapeutic targets to delay their progression.

Though the death of rod photoreceptors has been extensively studied, the consequent death of cones is still poorly understood. Some studies posit that death of cones is caused by toxins released by dying rods, or from the loss of rod-cone gap junctions, oxidative stress, microglia mobilization, or cone starvation due to disruption of the epithelium cell function (Ripps, 2002; Punzo et al., 2008; Cronin et al., 2007). Despite various causes that evoke photoreceptor death, ultimately the cells die due to caspase-dependent and caspase-

independent apoptotic mechanisms (Doonan et al., 2005; Lohr et al., 2006; Sanges et al., 2006). These are characterized by cell soma shrinkage, blebbing of the plasma membrane, and breakdown of the cell into apoptotic bodies. Significant elevations of intracellular calcium and an increase in channel permeability were found in rd1 photoreceptor cells compared to wild-type (WT) (Acosta et al., 2005; Doonan et al., 2005). There have been two families of receptors associated with an increased intracellular calcium upon activation, the first is the purinergic family and the second is the transient potential super family, TRP.

P2X Receptors P2X7 receptor from the purinergic family has gained attention in due to its involvement in neurotransmitter release and mediation of neuronal injury (Khakh and North, 2012). ATP acts as a neurotransmitter and the expression of P2X7 receptors on immune cells suggests their involvement in immune function and inflammatory responses. A brief activation of P2X7Rs with low concentration of adenosene-tri-phosphate (ATP), a P2XR agonist, causes an increase in intracellular calcium, whereas sustained activation at high concentrations of ATP or benzyl-ATP (a very potent P2XR agonist) leads to pore formation (Erb et al., 1990; Gonzalez et al., 1989), letting molecules up to 900 Da through, such as the fluorescent YO-PRO dye (Surprenant et al., 1996) and Rassendren:1997wg. The ability of this receptor to pore dilate may have a large impact on physiological function and neuronal health (Sorge et al., 2012). Additional evidence of this receptors role in neurodegeneration was provided in an in-vivo study of spinal cord injury. In this study, extensive oligodendrocyte death was found in areas located primarily around the injury site, as identified by high ATP release. Application of P2X antagonist oATP, significantly improved cell survival and functional recovery, whereas bzATP enhanced cell death (Wang et al., 2004).

TRP channels A member of the TRP family, capsaicin-sensitive vanilloid subunit 1 (TRPV1) receptor is expressed throughout the CNS, including the retina. TRPV1 receptors are expressed throughout the retina and have similar pore dilating properties as P2XRs (Leonelli et al., 2009; Sappington et al., 2008). They're expressed in retinal glia (microglia and Muller cells) as well as localized to RGC dendrites and cell bodies. TRPV1 channels are known to act as Ca^{2+} entry pathways in the plasma membrane or modulating the driving force for Ca^{2+} by changing the membrane polarization, and thereby contributing to alterations in the cytosolic free Ca^{2+} concentrations. For example, activation of TRPV1 channel has also been associated with a drastic Ca^{2+} conductance linking them with neuronal cell death, especially in glaucoma (Sappington et al., 2008). TRPV1 demonstrate pore dilating properties after prolonged exposure to capsaicin, a TRPV agonist, showing a five fold increase in calcium conductance.

In the retina, these receptors may contribute to neuronal cell death during retinal degeneration. P2X7 receptors are expressed throughout various retinal cell layers: IPL, OPL, and RGCs (Mitchell et al., 2009). In the early stages of development of the slow retinal degenerating mouse model (rds), P2X7 receptor expression is upregulated in the retina and the brain compared to the WT mice (Franke et al., 2005). Injection of ATP led to photoreceptor death, whereas injection of ATP and Pyridoxalphosphate-6-azophenyl-2',4'-disulfonic (PPADs), a potent P2X receptor inhibitor, led to a decrease in the photoreceptor death (Fletcher, 2010). High concentrations of intravitreal ATP that are seen during retinal degeneration may not

only affect photoreceptors, but also may activate P2X7 receptors on other retinal neurons, thereby compromising their health.

One way of characterizing pore dilation is to use a fluorescent dye in conjunction with an agonist of a specific receptor and measure the amount of dye loaded in a cell of interest. The most common fluorescent dye used is YO-PRO. The specific agonists used to induce pore dilation in P2XRs and TRPV1 channels are bzATP or ATP and capsaicin, respectively. To make sure that the dye is loading through the desired receptors, a variety of pharmacological blockers are used; however, there are currently no specific pharmacological aqueous pore blockers. Most of the blockers for P2XRs are competitive antagonists such as brilliant blue G, PPADs, and TNP-ATP, all of which just block the ATP binding site rather than the aqueous pore. For TRPV1 channels, capsazepine is commonly used antagonist; however, just like the P2XR antagonists it does not block the aqueous pore. Ruthenium Red (RR) has been widely used blocker of TRP channel aqueous pore, but it has a wide range of other targets making results hard to interpret (Charuk et al., 1990; Cibulsky and Sather, 1999; Hirano et al., 1998).

To demonstrate that activation of P2X receptors can have detrimental effects on RGCs, in Hu et al, 2010, injections of bzATP into neonatal rats led to RGC death, which was prevented by addition of P2X7 receptor blocker brilliant blue G (Hu et al., 2010). To determine whether P2X7 receptors are susceptible to pore dilation, Innocenti et al. (2004), co-applied bzATP and YO-PRO on WT rat retina, and observed YO-PRO loading only in microglia and not in retinal neurons. Microglia were labeled in-vivo with Cy3-conjugated isolectin B4 (ILB-4) and RGCs were loaded with crystals of micro-ruby. However, even though RGCs did not load YO-PRO, loading was not tested in retinas undergoing retinal degeneration or under a TRPV1 agonist conditions.

1.3 Glaucoma

P2X and TRPV1 receptors have also been implicated in diseases such as glaucoma, a family of diseases that are clinically characterized by the visual field defects and excavation of the optic disk. There are several factors that may lead to glaucoma: elevated intraocular pressure, age, corneal thickness, vascular dysfunction, and genetic background. For example, intraocular pressure (IOP) is usually accompanied with axonal degeneration of retinal ganglion cells and followed by apoptotic death (Sommer, 1989).

Though the exact reason for the death of RGCs is still unknown, there are many possible contributing factors. The reduction of IOP is one common method of slowing down the degenerative effects of glaucoma; though it does not terminate the progression of neurofiberthinning and the visual field defects (Leske et al., 2004). The IOP elevation may lead to changes in the optic nerve head extracellular matrix composition; disruption of retrograde axonal transport of neurotrophic factors has been proposed to play a role in the RGC death (Martin et al., 2006). Oxidative stress in RGCs has also been postulated in RGC death, due to decrease of enzymes in the antioxidant defense system (Moreno et al., 2004). The

next question was whether ATP release caused by heightened IOP leads to damage of the RGCs. Mechanical stress and changes in pressure in the retina lead to ATP release in the extracellular space via neural and non-neural cells (Bodin and Burnstock, 2001).

During the traumatic brain injury, cell death has also been linked to a rise in intracranial pressure (Yang et al., 2005). In the eye, increase in IOP leads to an increase in the extracellular ATP concentrations (Zhang et al., 2007). Another hypothesis that may explain the death of RGCs in glaucoma is that increase in IOP leads to activation of TRV1 or P2X receptors, causing them to pore dilate and overload cells with Ca^{2+}. Moreover, TRPV1 channels may serve as mechanosensors in addition to indirectly responding to ATP. Sappington et al. (2008), has demonstrated that RGCs also express TRPV1 channels which cause Ca^{2+} overload in cells under the increase of the hydrostatic pressure. To test whether reducing Ca^{2+} would lead to a decrease of RGC death through the TRV1 channels, Sappington et al. (2008), reduced the extracellular Ca^{2+} concentration in these dissociated neurons and showed a reduction in apoptotic cells. Moreover, elevated pressure increased intracellular Ca^{2+} concentrations, whereas TRPV1 antagonist reduced it fourfold. Thus, glaucoma is another disease where it would be interesting to determine how P2X7 or TRV1 receptors affect RGCs and whether these conditions cause pore dilation.

1.4 Treatments for Retinal Degeneration

1.4.1 Implantable Electrode Arrays

Neural prostheses have been widely accepted as possible treatment tools in a variety of fields such as hearing as well as vision. For the implants to be successful in the eye, they need to be made out of non-reactive material, must sense light, be able to directly stimulate the corresponding ganglion cells, as well as have good spatial resolution as determined by electrode spacing. The chip is usually implanted on the epiretinal surface (the inner limiting membrane) or in the subretinal space, in place of the degenerated photoreceptors.

Currently, epiretinal prosthetics are implanted in the inner limiting membrane. Image data is processed by an external image processor which then sends the information wirelessly to the implant. The implant converts the data into a pattern of electrical stimulation and excites the remaining retinal neurons. Wireless stimulation allows for minimal implantable amount of microelectronics and thus easy technological upgrades without a need for surgery. Another advantage is the heat from the electronics would mostly be absorbed by the vitreous instead of the neuronal tissue. The disadvantages include inconsistent attachment of the device to the inner retina as well as stimulation of the outer retina requires more sophisticated algorithms, which have currently not been developed.

The subretinal approach requires a microchip to be surgically implanted between the bipolar cell layer and the RPE. This implantation requires a surgical implantation of this device via scleral incision or through the vitreous cavity. Such close proximity to retinal cells allows for direct stimulation of surviving neurons, potentially shaping a clearer neu-

ral/processing response. The advantage of this technique is that it makes use of the inner circuitry by directly stimulating the inner nuclear layer, either bipolar cells, amacrine cells, or both. Also, this method does not require an external processing unit and the subjects eye movements could still be used to locate objects, unlike in the epiretinal prosthetics. However, because the electronics are so close to the neurons there is a high probability of thermal injury, thus limiting the number of possible implantable electrodes. Moreover, since the electrode array requires a cable to connect to the external electronics, the cable will be crossing a highly vascularized choriocapillaris and in the long term may induce formation of subretinal hemorrhages or retinal detachment (Weiland et al., 2005). Finally, the greatest disadvantage is that the microphotodiodes do not provide enough current to stimulate the retinal neurons (Javaheri et al., 2006).

1.4.2 Gene Therapy

Another approach to treating retinal degeneration is to introduce light sensitive proteins such as channelrhodopsin and halorhodopsin, that render the surviving neurons that express these proteins light sensitive. Upon exposure to light these opsins can bring the membrane potential of the neurons to or away from the action potential firing threshold, overriding the hyperactive natural activity of the rd1 retina.

Channelrhodopsin-2 (ChR2): Currently a widely used tool (Boyden et al., 2005), ChR2 is a non-selective seven transmembrane rhodopsin that has been cloned from the green algae Chlamydomonas reinhardtii (Oesterhelt, 1998). It uses an attached chromophore to absorb photons and allows for reversible photoisomerization of the all-trans isoform of retinaldehyde. This conformation change directly allows ion movement through the membrane. Moreover, ChR2 has been shown to drive neurons in a temporally and spatially precise manner. One of the advantages to using ChR2 is that one can use viral delivery to target a specific subset of cells. For example, in later stages of retinal degeneration, photoreceptors degenerate leaving the rest of the circuitry intact. Photosensitization of cells presynaptic to the ganglion cells may partially restore processing capacity such as center-surround. In fact, Lagali et al. (2008) used ChR2 to target ON-Bipolar cells, using a 200-base pair promoter sequence of the mouse Grm6 gene encoding mGluR6. Center surround responses as well as transient responses were restored, verified by whole cell recording and multielectrode array. Moreover, ChR2 rd1 mice seemed to have visually guided behavior restored in the light-dark box protocol as well as the optomotor reflex (Lagali et al., 2008). Currently new types of channel-rhodopsins are being developed in order to address the problem of low conductance and fast inactivation, as well as the required high intensity of light (Lin et al., 2009).

Halorhodopsin (eNpHR): eNpHR is a chloride pump discovered in halobacteria. Unlike ChR2, eNpHR is used to silence excited neurons. Brief flashes of 570 nm light cause an opening of a Cl- channel thereby hyperpolarizing the neuron. eNpHR was also utilized to restore visual function to mice suffering from retinal degeneration by expressing it in photoreceptors via an adeno-associated virus (AAV) (Busskamp et al., 2010). After it was introduced into a degenerating mouse retina it restored ON and OFF pathways of the retinal

circuitry and reactivated some cone function, enabling mice to successfully perform visually guided behavioral tasks.

1.4.3 Light Sensitive Molecules

Recently, another vision restoration technique was developed, which uses light sensitive photochromic ligand compounds. These compounds are designed around the azobenzene molecule which gives these chemicals a distinct advantage, by allowing for *cis* or *trans* conversion under specific wavelengths, picosecond photoisomerization, and finally stability therefore ability to repetitively photoisomerize. Since these light sensitive chemicals do not require the use of gene expression, they allow for very quick and reversible studies of neuronal circuits by taking advantage of the native channels and rendering them light sensitive. Another advantage of using photoswitchable compounds is that it is relatively simple to alter their function and target via modifying their chemical properties (Banghart et al., 2009). The three main compounds this thesis focuses on are acrylamide-azobenzene-quarternary-ammonium (AAQ), Quaternary ammonium-azobenzene-quaternary ammonium (QAQ), and di-ethylamine-quarternary ammonium (DeNAQ).

AAQ AAQ permeates through cell membranes and photosensitizes voltage gated Kv channels (Banghart et al., 2009). The quaternary ammonium group blocks the Kvs pore by entering the intracellular vestibule. Under 500 nm light, the molecule turns into a *trans* form and blocks the channels and thereby depolarizes cells. Illumination of 380 nm light turns the molecule into a *cis* form and thereby relieves the block. Fortin et al. (2008) used AAQ to photoregulate cultured hippocampal neurons in a non-invasive and precise manner (Fortin et al., 2008). In Chapter 2, we use the AAQ molecule to restore light sensitivity to blind rd1 mice *in vitro* and *in vivo* (Polosukhina et al., 2012).

DeNAQ Di-ethyl-amine-azobenzene quaternary ammonium is another light sensitive molecule that we use to install vision sensitivity to blind mice, discussed in Chapter 3. DeNAQ molecule is a red-shifted compound which is a cis-blocker, thus upon illumination of 480 nm light, it blocks voltage gated channels, and in the dark it quickly relaxes into the *trans* form and relieves the channels of a block (Mourot et al., 2011). One of the advantages of DeNAQ is that the molecule has no effect on cells in the dark (*trans* form) and thus prevents any possible cytotoxicity from continuously depolarizing the cells. Consequently, we found that this new generation of compounds is an even more promising option for vision restoration and lasts in the eye for a week longer than AAQ.

QAQ Another synthesized molecule is a doubly charged quarternary-azobenzene-quaternary molecule (QAQ). Unlike AAQ and DeNAQ, QAQ is membrane impermeable and works like lidocaine by entering a pore dilated channel and blocking voltage gated Na^+ channels, Ca^{2+}, and K^+ channels. Since it is membrane impermeant, Mourot et al. (2012) targeted the nociceptors by applying capsaicin (TRPV1 agonist) and allowing QAQ entry through the pore dilated channel. After entering a cell through these endogenous channels which are activated by noxious stimuli, it accumulates and blocks voltage-gated ion channels in the *trans* but not the *cis* form and thereby in *trans* form prevents cells from firing action potentials.

Thus, QAQ provided selective photosensitivity to only those neurons that were involved in pain signaling. In Chapter 4, we utilize QAQ to determine whether there are physiological differences between rd1 and WT RGCs. Consequently, in conjunction with dye loading we demonstrate that P2X receptors and/or TRPV receptors on RGCs undergo pore dilation and allow us to target them with QAQ.

Chapter 2

Photochemical restoration of visual responses in blind mice

Preface: This chapter has been published in the journal, *Neuron:* Aleksandra Polosukhina, Jeffrey Litt, Ivan Tochitsky, Joseph Nemargut, Yivgeny Sychev, Ivan De Kouchkovsky, Tracy Huang, Katharine Borges, Dirk Trauner, Russell N. Van Gelder, and Richard H. Kramer (2012).

2.1 Summary

Retinitis pigmentosa (RP) and age-related macular degeneration (AMD) are degenerative blinding diseases caused by the death of rods and cones, leaving the remainder of the visual system intact but largely unable to respond to light. Here we show that, AAQ, a synthetic small molecule photoswitch, can restore light sensitivity to the retina and behavioral responses *in vivo* in mouse models of RP without exogenous gene delivery. Brief application of AAQ bestows prolonged light sensitivity on multiple types of retinal neurons, resulting in synaptically amplified responses and center-surround antagonism in arrays of retinal ganglion cells (RGCs). Intraocular injection of AAQ restores the pupillary light reflex and locomotory light avoidance responses in mice lacking retinal photoreceptors, indicating reconstitution of light signaling to brain circuits. AAQ and related photoswitch molecules present a new drug strategy for restoring retinal function in degenerative blinding diseases.

2.2 Introduction

Inherited degenerative diseases of the retina including retinitis pigmentosa (RP) affect 1 in 3,000 people worldwide. As differentiation of rods and cones ceases soon after birth in mammals, disorders resulting in photoreceptor degeneration lead to a permanent visual deficit. At present, there is no effective treatment for preventing this degenerative process. Without some means of restoring photoreception, patients with advanced RP face the prospect of irreversible blindness.

Retinal ganglion cells (RGCs) are the sole output neurons of the retina. Hence all of the information about a visual stimulus that reaches the brain is encoded by the spatial and temporal pattern of RGC action potentials elicited by that stimulus. Several strategies have been advanced to enable light to alter RGC firing in the absence of native rods and cones, with the goal of restoring visual function after the photoreceptors are lost (Jiménez et al., 1996; Marc et al., 2003; Punzo and Cepko, 2007; Strettoi and Pignatelli, 2000). Biomedical engineers have developed surgically implanted retinal "chip" prosthetics (Chader et al., 2009; Gerding et al., 2007; Shire et al., 2009), which can be electronically controlled by an external camera to enable optical stimuli to trigger RGC firing. Retinal implants have restored simple shape discrimination to blind patients (Humayun et al., 2003; Yanai et al., 2007) indicating that artificial stimulation of RGCs *in vivo* can create a useful visual experience. Second, genes encoding optogenetic tools, including light-activated ion channels (Bi et al., 2006; Lagali et al., 2008; Tomita et al., 2010), transporters (Busskamp et al., 2010) or receptors (Caporale et al., 2011; Lin et al., 2008) can be introduced with viruses to bestow light-sensitivity on the various types of retinal neurons that survive after the natural photoreceptive cells have degenerated. Expression of optogenetic proteins in RGCs (Caporale et al., 2011; Tomita et al., 2010), bipolar cells (Lagali et al., 2008), and remnant cones (Busskamp et al., 2010) can reinstate light-elicited behavioral responses in mouse models of RP. Third, embryonic stem cells can be differentiated into photoreceptors *in vitro* (Lamba et al., 2006). Injecting stem cell-derived retinal progenitors into blind animals results in integration of photoreceptors and restoration of some electrical activity in response to light (Lamba et al., 2009).

Each of these strategies has shown promise for functional restoration of visual responses, but all require highly invasive and/or irreversible interventions that introduce hurdles to further development as a therapeutic approach. Implantation of retinal chips or stem cell-derived photoreceptors requires invasive surgery, while exogenous expression of optogenetic tools leads to permanent genetic alterations in retinal neurons. Retinal chip prosthetics rely on extracellular electrical stimulation of RGCs, which when excessive can be cytotoxic (Winter et al., 2007). Stem cell therapies carry potential for teratoma formation (Chaudhry et al., 2009). Optogenetic tools require viral vectors selective for particular retinal neurons, but these can have off-target effects and the virus may elicit inflammatory responses (Beltran et al., 2010)). While the potential permanence of optoelectronic, stem cell, or optogenetic interventions would be a favorable feature in the absence of complications, any deleterious effects of these treatments could be very difficult or impossible to reverse.

Here we report an alternative strategy for restoring visual function, based on a small molecule "photoswitch" that bestows light sensitivity onto neurons without requiring exogenous gene expression. The photoswitch is injected into the vitreous cavity of the eye, but unlike the other strategies, it does not require highly invasive surgical interventions and its actions are reversible. We used AAQ (acrylamide-azobenzene-quaternary ammonium), a K^+ channel photoswitch that enables optical control of neuronal excitability (Banghart et al., 2009; Fortin et al., 2008). AAQ was originally thought to conjugate to K^+ channels (Fortin et al., 2008), but more recent work shows that the molecule interacts non-covalently with the cytoplasmic side of the channels, similar to the mechanism of action of local anesthetics (Banghart et al., 2009). The *trans* form of AAQ blocks K^+ channels and increases excitability, whereas photoisomerization to the *cis* form with short wavelength light (e.g. 380 nm) unblocks K^+ channels and decreases excitability. Relaxation from *cis* to *trans* occurs slowly in darkness, but much more rapidly upon exposure to longer-wavelength light (e.g. 500 nm), enabling rapid bidirectional photocontrol of neuronal firing with different wavelengths.

We show that AAQ confers robust light responses in RGCs in retinas from mutant mice that lack rods and cones. Moreover, after a single intraocular injection, AAQ restores light-driven behavior in blind mice *in vivo*. Because it is a rapid and reversible drug-like small molecule, AAQ represents a class of compounds that has potential for the restoration of visual function in humans with end-stage photoreceptor degenerative disease.

2.3 Materials and Methods

2.3.1 Animals

Wild-type mice (C57BL/6J strain, Jackson Laboratories) and homozygous rd1 mice (C3H /HeJ strain, Charles River Laboratories) >3 months old were used for the experiments. Opn4-/- and Opn4-/- rd/rd mice were a gift of Satchidananda Panda and John Hogenesch. Mutant genotypes were confirmed by PCR of genomic DNA. Opn4-/- rd/rd animals were >3 months old and had no pupillary light reflex before treamtne . All animal use procedures were approved by the UC Berkeley or University of Washington Institutional Animal Care and Use Committee, and were in accord with guidelines from the Association of Vision Research in Ophthalmology and the NIH.

2.3.2 Electrophysiology and pharmacology

Mouse retinas were dissected and kept in physiological saline at 36°C containing (in mM): 119 NaCl, 2.5 KCl, 1 KH_2PO_4, 1.3 $MgCl_2$, 2.5 $CaCl_2$, 26.2 $NaHCO_3$, 20 D-glucose, aerated with 95% O_2/5% CO_2. For extracellular recording, the retina was placed ganglion cell layer down onto a multielectrode array system (model number MEA 1060-2-BC, Multi-Channel Systems).

The MEA array electrodes were 30 μm in diameter and arranged on an 8 × 8 rectangular grid. Extracellular spikes were high-pass filtered at 200 Hz and digitized at 20 kHz. A spike threshold of 4SD was set for each channel. Typically, each electrode recorded spikes from 1-3 RGCs. Principal component analysis of spike waveforms was used for sorting spikes generated by individual cells (Offline Sorter; Plexon). Only cells with interspike intervals of $<$ 1 msec were included in the analysis.

Borosilicate glass electrodes of 6-11 MΩ were used for whole-cell voltage-clamp recordings. Current records were low-pass filtered at 2 kHz. For measuring voltage-gated K^+ currents, electrodes contained (in mM): 98.3 K^+ gluconate, 1.7 KCl, 0.6 EGTA, 5 $MgCl_2$, 40 HEPES, 2 ATP-Na, 0.3 GTP-Na (pH =7.25). For recording glutamatergic EPSCs electrodes contained (in mM): 125 Cs^+ sulfate, 10 TEA-Cl, 5 EGTA, 0.85 $MgCl_2$, 10 HEPES, 2 QX-314, 4 ATP-Na_2 (pH=7.25).

To block synaptic contributions of different retinal neurons to RGCs, the following neurotransmitter receptor antagonists were used: 4 μM SR-95531 (gabazine) for $GABA_A$ receptors, 10 μM 1,2,5,6 tetrahydropyridin-4-yl)methylphosphinic acid (TPMPA) for $GABA_C$ receptors, 10 μM initroquinoxaline-2,3-dione disodium salt (DNQX) for non-NMDA type glutamate receptors, 50 μM d-(-)-2-Amino-5-phosphonopentanoic acid (AP5) for NMDA-type glutamate receptors, 10 μM strychnine for glycine receptors, 50 μM d-tubocurarine chloride (curare) for nicotinic acetylcholine receptors. To block voltage-gated Na^+ channels we used 1 μM tetrodotoxin (TTX). All of these drugs were purchased from Sigma or Tocris.

2.3.3 Light Stimulation

In most MEA recordings, we used a 100 W mercury arc lamp filtered through 380 or 500 nm filters (Chroma, Inc), and switched wavelengths with an electronically-controlled shutter and filter wheel (SmartShutter, Sutter Instruments). Unless otherwise indicated, the standard incident light intensity at the retina was 13.4 mW/cm^2 ($2.56 * 10^{16}$ photons/cm^2/s) for 380 nm and 11.0 mW/cm^2 ($2.77 * 10^{16}$ photons/cm^2/s) for 500 nm.

2.3.4 PLR Measurement

Mice were sedated with an intraperitoneal injection of ketamine (6.7mg/ml) and xylazine (0.45 mg/ml) in normal saline. Animals were immobilized on a stereotaxic table (Stoelting Co.). Under microscopic visualization, an intravitreal injection of 1 μl of 80 mM AAQ in a vehicle solution (40% DMSO in saline). Injections were performed with a tapered, graduated glass micropipette (Drummond Scientific Co.) advanced through the sclerotomy with a micromanipulator.

Videos of pupillary light responses of unanaesthetized mice were recorded before and 3 hours after intraocular AAQ injection. White light was derived from halogen dissecting lamp, and intensity was controlled with neutral density filters. Animals were dark-adapted for at least 20 minutes prior to testing. An infrared CCD camera (focused 15 cm from

the objective) was used to measure pupil dilation, as described (Van Gelder, 2005). Light intensity was measured by a calibrated radiometer (Macam Photometrics Ltd.).

2.3.5 Locomotory Light Avoidance

Wildtype and *opn4*$^{-/-}$ *rd/rd* mice were sedated and intravitreal injection of 1 μl of 80mM AAQ was performed as described previously (See PLR Measurement). Following 30 minutes of dark adaptation, individual mice were placed into a narrow cylindrical transparent tube sealed with glass plates on both ends and behavior was recorded with an infrared video camera in the dark. For each light trial, a 385nm LED (log IR 15.7) was shown towards the face of mouse followed by a superimposed 480nm LED (log IR 15.2) switched on and off at 5 second intervals. Videos were recorded at three time points for each mouse: pre-injection, and 2 and 24 hours post-injection. Two light trials (one at each end of the tube) and one dark trial were performed for each time point. Two graders were asked to score rapid movements away from the light while masked to mouse genotype, injection status, and trial conditions. Light avoidance behaviors were determined as rapid aversive movements within 30 seconds of the light stimulus or the beginning of the dark trial.

2.3.6 Open-Field Test

Rd1 mice were placed in a 190 mm × 100 mm cylindrical UV-transparent chamber. The chamber was surrounded by 6 panels of 380 nm LEDs (Roithner Laserteknik), providing a light intensity of ≈7 mW/cm^2 uniformly across the test apparatus. Heating of LEDs was negligible during the time span encompassing each trial. The mice were dark adapted in their cages for 1 hr, prior to each experiment. The mice were placed in the experimental chamber and allowed to acclimate for 5 minutes. The behavior was then recorded using an IR sensitive video camera (Logitech C310) for 5 minutes in darkness under IR illumination. After 5 minutes, the 380 nm LED-panels were then illuminated, and behavior was monitored for an additional 5 minutes. The apparatus was cleaned and thoroughly dried prior to each experiment. After the open-field test, each mouse was given an intravitreal injection of AAQ (20 mM AAQ, 9:1 saline: DMSO) under general anesthesia, as previously described. The mice were allowed to recover for ≈6 hours on a heating pad with open access to food and water in their cage located in the dark room. The behavioral protocol described above was repeated to determine the effect of AAQ. The videos were analyzed utilizing motion tracking video analysis software (Tracker) in order to quantify the average velocity of the mice, the trajectory of motion throughout the test, and the total distance traveled. The animals were then immediately sacrificed and MEA recordings were conducted on their retinas.

2.3.7 Data analysis and statistics

Light-elicited changes in firing rate during test flashes were normalized with respect to initial firing rate and expressed as a Photoswitch Index (PI), defined as follows:

$$\mathrm{PI} = \frac{\text{test firing rate} - \text{initial firing rate}}{\text{test firing rate} + \text{initial firing rate}}.$$

Relative pupillary light responses were calculated as

$$1 - \frac{\text{pupil area minimum during thirty seconds of the light stimulus}}{\text{pupil area minimum during five seconds preceding the stimulus}}.$$

Relative response data for wild type and *opn4*$^{-/-}$ *rd/rd* mice were fitted with a three parameter Hill equation (SigmaPlot, Systat Software, Inc.). Data is mean ± s.e.m, unless otherwise indicated.

Latencies were calculated for every cell with a PI greater than 0.011, the upper median confidence interval PI of our control experiments (n = 13 retinas; n = 409 cells). For each cell, cellular firing rate was averaged over the first two light periods (dark and 380nm light), with a 10 msec bin size. Cellular basal activity was defined as the upper median confidence interval firing rate in 500 nm light. Cellular latency was then calculated as the time difference between the onset of 380 nm light and the first bin with a firing rate greater or equal to the cells basal activity. The median cellular latency was 45 msec (n = 10 retinas; n = 368 cells). The shortest cellular latency was 5 msec. All statistics were performed using commercially available algorithms (Matlab). Distributions were first tested for normality using the Shapiro-Wilk test. For non-normal distributions, the Wilcoxon rank sum test was used for pairwise comparisons. The 95% confidence intervals for medians were generated by resampling the original distributions and applying the bias-corrected percentile method (Efron and Tibshirani, 1986). Results with $p < 0.05$ were considered significant.

2.4 Results

2.4.1 Imparting light sensitivity on rd1 mouse retina with AAQ

We tested whether AAQ can impart light sensitivity on retinas from 6-month old *rd*1 mice, a murine model of retinitis pigmentosa (RP). The homozygous rd1 mouse (rd1/rd1) has a mutation in the gene encoding the β-subunit of cGMP phosphodiesterase-6 (PDE-6), essential for rod phototransduction. Rods and cones in these mice degenerate nearly completely within 3 months after birth, leading to a loss of electrical and behavioral light responses (Sancho-Pelluz et al., 2008). We placed the rd1 mouse retina onto a multi-electrode array (MEA) that enables simultaneous extracellular recording from many RGCs (Meister et al., 1994). Before AAQ application, light generated no measurable change in RGC firing. However, after 30 min treatment with AAQ, nearly all RGCs responded to light (Figure 2.1A).

Concentration (μM)	# Cells	Median PI	95% Confidence Interval
10	128 (3 retinas)	-0.016	-0.043 to 0.015
100	37 (2 retinas)	-0.233	-0.725 to 0.258
200	38 (1 retina)	0.221	-0.197 to 0.640
300	1025 (21 retinas)	0.423	0.394 to 0.457
800	359 (5 retinas)	0.717	0.627 to 0.762

Table 2.1: Supplemental Table 1

Time after treatment (hrs)	# Cells	Median PI	95% Confidence Interval
1	51 (1 retina)	0.787	0.728 to 0.841
3	61 (1 retina)	0.597	0.457 to 0.678
5	66 (1 retina)	0.167	-0.314 to 0.649

Table 2.2: Supplemental Table 2

Photosensitization increased with AAQ concentration (Figure 2.2, Table 2.1), but we used 300 μM for our standard *ex vivo* treatment. Light responses slowly diminished, but were still robust for >5 hours after removing AAQ from the bathing medium, (Figure 2.3a). Light responses could also be detected in 3 of 4 recordings from retinas removed from rd1 mice that 12 hours previously had received *in vivo* intravitreal AAQ injections (Figure 2.3a). The degree of photosensitivity varied, reflecting inaccurate injection in the small intravitreal volume of the mouse eye (2-3 μl).

Most RGCs exhibited an increase in firing rate in response to 380 nm light and a decrease in 500 nm light, opposite to AAQ-mediated light responses in neurons in culture (Fortin et al., 2008). To quantify the effects of light, we calculated a Photoswitch Index (PI), representing the normalized change in firing rate upon switching from darkness to 380 nm light. Positive or negative PI values reflect an increase or decrease, respectively, of firing. Before AAQ treatment, RGCs had almost no light response (median PI = 0.02); but after treatment, nearly all were activated by 380 nm light (median PI = 0.42) (Figure 2.1B). The rare light responses before AAQ treatment might result from melanopsin-containing intrinsically photosensitive RGCs (ipRGCs), which account for 3% of the RGCs in the adult mouse retina (Hattar et al., 2002). Significant photosensitization was observed in each of 21 AAQ-treated retinas. On average, we observed an 8-fold increase in RGC firing rate in response to 380 nm light (Figure 2.1C).

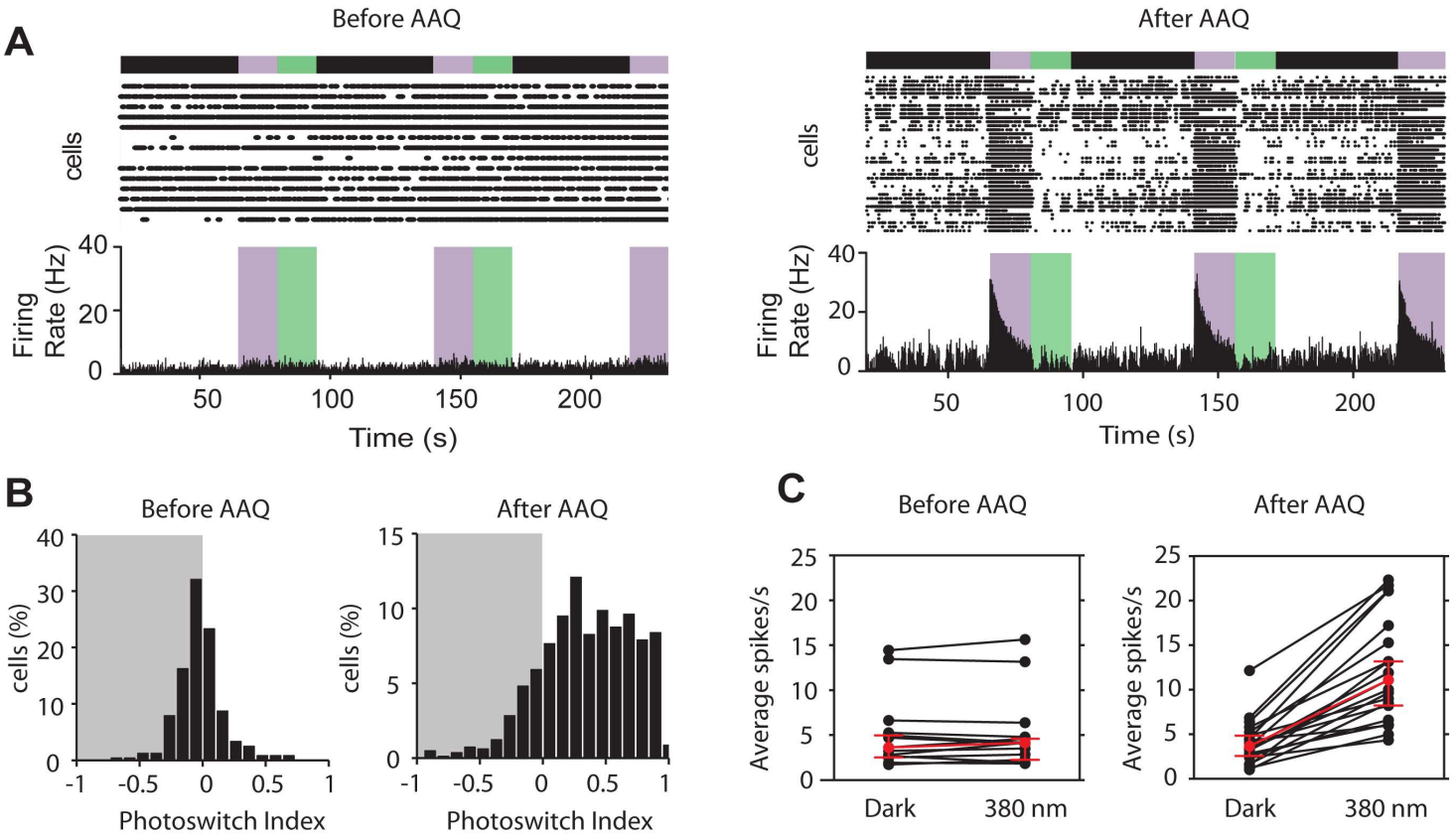

Figure 2.1: AAQ imparts light sensitivity onto blind retinas from rd1 mice. (A) Multi-electrode recordings from flat-mounted rd1 mouse retinas before and after treatment with AAQ (300 μM for 25 min, followed by washout). Top, raster plot of spiking from RGCs; bottom, average RGC firing rate calculated in 100 msec time bins. Color bars represent illumination with 380 nm (violet) or 500 nm light (green), separated by periods of darkness. (B) Analysis of photoswitching of the entire population of RGCs from all untreated retinas and all AAQ-treated retinas. Untreated retinas (n=12) had PI values near 0, indicating no photoswitching, AAQ-treated retinas (n=21) had PI values > 0, indicating an increase in firing frequency after switching from darkness to 380 nm light. (C) AAQ-mediated photosensitivity results from an increase in firing rate in 380 nm light. Average RGC firing rates in untreated retinas and AAQ-treated retinas in darkness and during the first 5 s in 380 nm light. Note that untreated retinas (n=12) fail to respond to light, but AAQ-treated retinas have RGCs that increase firing rate with 380 nm light. Red symbols show median values and error bars represent 95% confidence intervals for untreated and treated retinas ($p < 0.0001$, Mann-Whitney test).

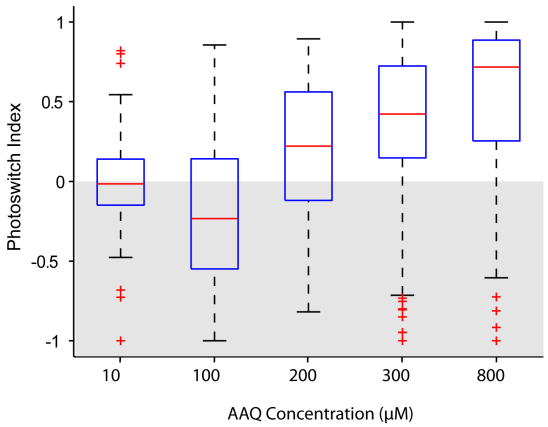

Figure 2.2: Concentration-dependence of AAQ photosensitization of rd1 retinas. See Table 2.1 for values.

2.4.2 AAQ acts on RGCs, bipolar, and amacrine cells in rd1 retinas

We were surprised that 380 nm light stimulated RGC firing because this wavelength unblocks K^+ channels which should reduce neuronal excitability. However, since RGCs receive inhibitory input from amacrine cells, RGC stimulation might be indirect, resulting from amacrine cell-dependent disinhibition. To test this hypothesis, we applied antagonists of receptors for GABA and glycine, the two inhibitory neurotransmitters released by amacrine cells. Photosensitization of RGCs by AAQ persisted after adding inhibitors of $GABA_A$, $GABA_C$, and glycine receptors (Figure 2.4A), but the polarity of photoswitching was reversed, with nearly all neurons inhibited rather than activated by 380 nm light (Figure 2.4B). These results indicate that photoregulation of amacrine cells is the dominant factor that governs the AAQ-mediated light response of RGCs.

After blocking amacrine cell synaptic transmission, the remaining light response could result from photoregulation of K^+ channels intrinsic to RGCs and/or photoregulation of excitatory inputs from bipolar cells. To explore the contribution of intrinsic K^+ channels, we obtained whole-cell patch clamp recordings from RGCs and pharmacologically blocked nearly all synaptic inputs (glutamatergic, GABAergic, and glycinergic). Depolarizing voltage steps activated outward K^+ currents that were smaller and decayed more rapidly in 500 nm light than in 380 nm light (Figure 2.4C). Comparison of current vs. voltage (I-V) curves shows that the current was reduced by ≈50% in 500 nm light (Figure 2.4D), similar to previous results (Fortin et al., 2008). However, MEA recordings indicate that photoregulation of RGC firing was nearly eliminated by blocking all excitatory and inhibitory synaptic inputs (Figure 2.5), suggesting that the light response is driven primarily by photoregulation of upstream neurons synapsing with RGCs.

To examine directly the contribution of retinal bipolar cells to the RGC light response,

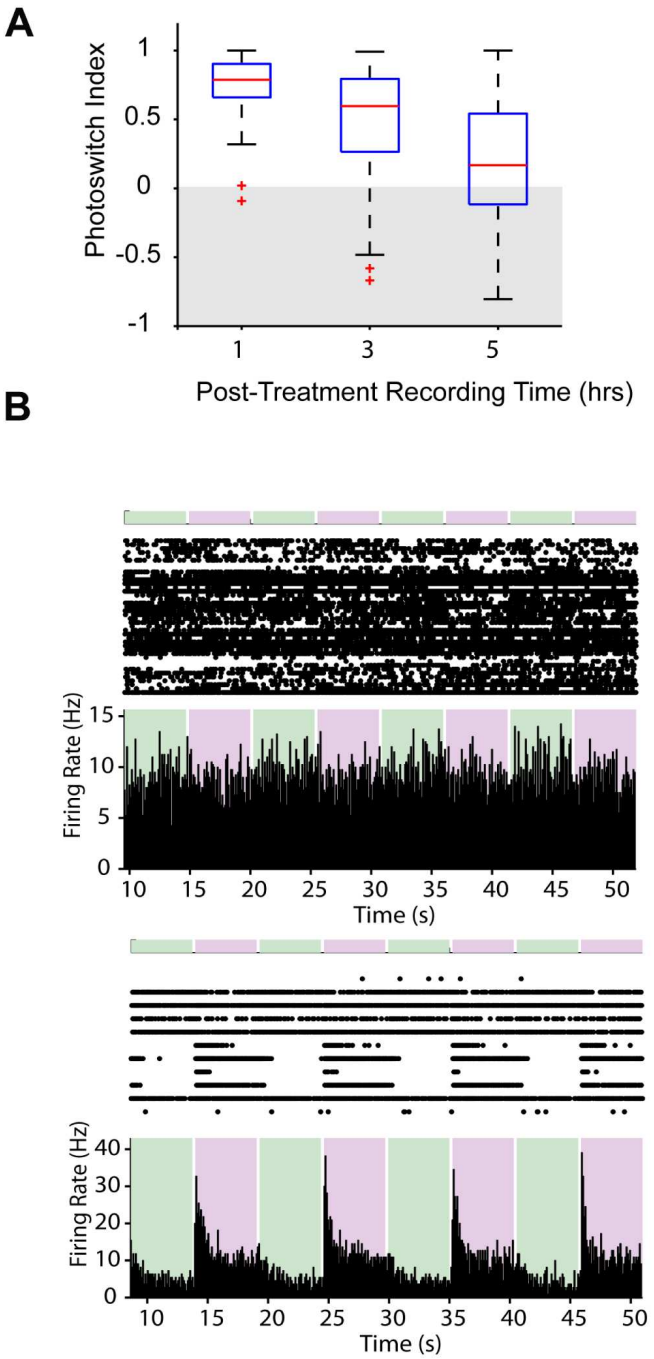

Figure 2.3: AAQ photosensitization abates slowly after treatment. (A) Decay of photosensitization following *ex vivo* treatment of rd1 retinas. See Table 2.2 for values. (B) Examples of MEA recordings obtained 12 hrs after intravitreal injection of AAQ *in vivo*.

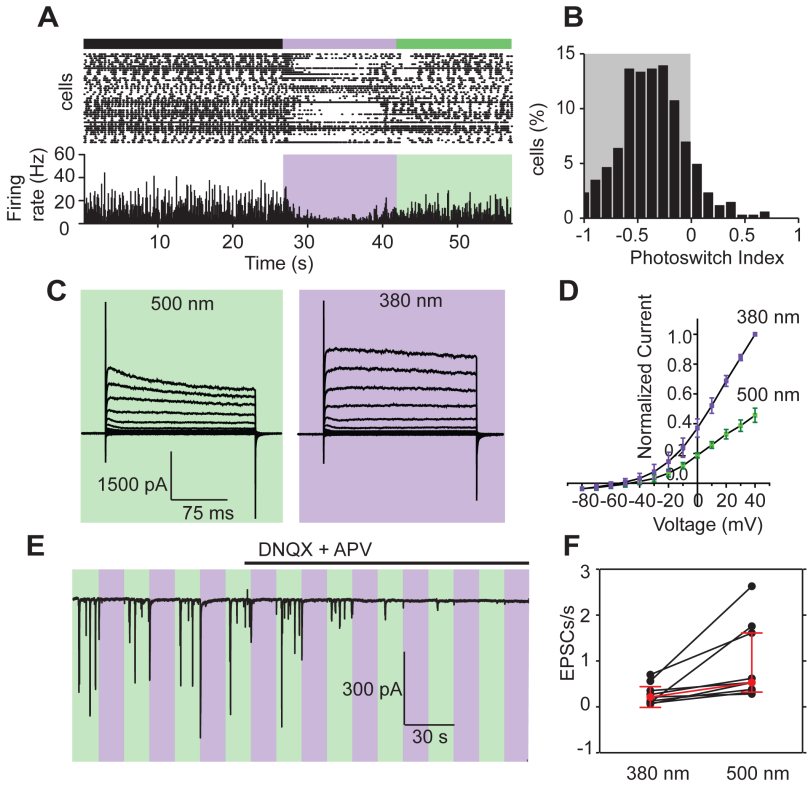

Figure 2.4: Multiple types of retinal neurons contribute to the AAQ-mediated light response of RGCs. (A) Amacrine cell-mediated synaptic inhibition dominates the RGC light response. MEA recording with antagonists of $GABA_A$ (gabazine; 4 M), $GABA_C$ (TPMPA; 10 μM), and glycine receptors (strychnine; 10 μM). Top, raster plot of RGC spiking. Bottom, average RGC firing rate. (B) After blocking inhibition, PI values show a decrease in firing frequency upon switching from darkness to 380 nm light (n=11 retinas). (C) Endogenous K^+ channels contribute to the RGC light response. Whole-cell patch clamp recording from an RGC. Currents were evoked by voltage steps from -80 to +40 mV in 20-mV increments in 380 nm and 500 nm light. Inhibitory GABAergic and glycinergic inputs were blocked as in (a), and excitatory glutamatergic inputs were blocked with DNQX (10 μM) and AP5 (50 μM). (D). Photoregulation of endogenous K^+ channels evaluated in steady-state I-V curves obtained in 380 and 500 nm light (n = 5 RGCs). Current is normalized to the maximal value at +40 mV (380 nm light). Variability among data is expressed as mean ± s.e.m.. (E) Bipolar cell-mediated synaptic excitation also contributes to the RGC light response. Whole-cell patch clamp recording from an RGC. Blockade of inhibitory synaptic inputs (as in panel A) and endogenous RGC K^+ channels (as in panel C) reveals photoregulation of EPSCs. Note the disappearance of EPSCs after superfusion with glutamate receptor antagonists DNQX (10 μM) and AP5 (50 μM). Holding potential = -60 mV. (F) Average EPSC rate in 380 nm and 500 nm light. Note the significant increase in EPSC rate in 500 nm light ($p < 0.05$, Mann-Whitney test; n=9 cells). Red symbols show median values and error bars represent 95% confidence intervals.

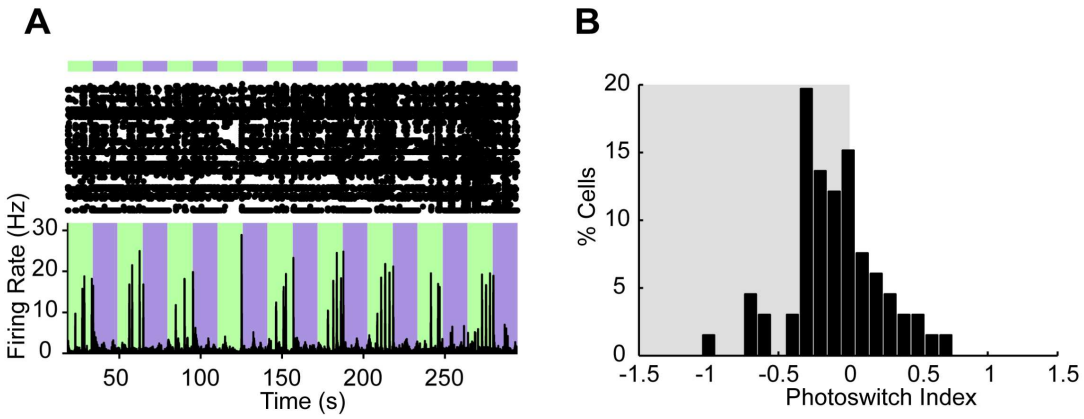

Figure 2.5: Blocking retinal synapses greatly reduces AAQ photosensitization. (A) Top, raster plot of spiking from RGCs; bottom, average RGC firing rate calculated in 100 msec time bins. Color bars represent illumination with 380 nm (violet) or 500 nm light (green). Stimulation of RGC firing in an AAQ treated retina with D-APV, Curare, DNQX, Strychnine, Gabazine, and TPMPA. (B) Analysis of photoswitching of the entire population of RGCs (n = 66) from one treated retina. PI median was -0.063 (95% CI: -0.384 to 0.258).

we blocked RGC K^+ channels with intracellular Cs^+ and added GABA and glycine receptor antagonists to block amacrine cell inputs. Flashes of 500 nm light triggered excitatory post-synaptic currents (EPSCs) in RGCs and 380 nm light suppressed these events (Figures 2.4E and 2.4F). Blocking glutamate receptors eliminated these events and bipolar cells provide the only known glutamatergic input to RGCs. Hence, we conclude that inputs from amacrine cells, bipolar cells, and to a lesser extent, the intrinsic K^+ conductances of RGCs, all combine to shape and amplify the AAQ-mediated RGC light response.

2.4.3 Spatial localization and center-surround antagonism of RGC light responses in AAQ-treated retina

Visual acuity is determined by the size of receptive fields of neurons in the visual system. In the healthy retina, the receptive field of an RGC is defined by the spatial extent of all of the photoreceptors that influence its activity. By definition, the receptive fields of RGCs in rd1 mice are eliminated after the photoreceptors have degenerated. However because AAQ makes presynaptic neurons light-sensitive, it is possible to measure the spatial extent of their light-driven influence on RGC firing. While this is not a conventional measurement of the RGC receptive field, it does indicate the spatial precision of the AAQ-mediated RGC light response.

We illuminated AAQ-treated retinas with small spots (60 μm diameter) of 380 nm light

Distance (um)	# Cells	Median PI	95% Confidence Interval
Target	11	0.517	0.455 to 0.812
200-400	95	-0.165	-0.239 to -0.090
400-600	143	-0.213	-0.284 to -0.150
600-800	97	-0.256	-0.294 to -0.206
800-1200	50	-0.296	-0.626 to 0.034

Table 2.3:

centered on one of the 60 electrodes in an MEA (Figure 2.6A). In the example shown in Figure 2.6A, upon switching from 500 to 380 nm light, the average RGC activity increased in the targeted electrode by ≈81%, but not in the surrounding electrodes. In each of a total of 8 targeted spots from 3 different retinas, only neurons near the targeted electrode exhibited a significant increase in firing (median PI = 0.517; Figure 2.6B). Since RGCs are detected by only one electrode and they are spaced 200 μm apart, this puts an upper limit on the radius of the AAQ-mediated RGC collecting area of 100 μm.

Analysis of electrodes outside the illuminated spot showed that 380 nm light significant decreased RGC firing. Decreased firing was detected in electrodes centered at 300, 500, and 700 μm from the mid-point of the targeted electrode (Figure 2.6C, Table 2.3). Hence RGCs in the center of an illuminated spot are stimulated, whereas those in a surrounding annulus (from 200 to 800 μm) are inhibited. Inhibition in the surrounding RGCs implies that a sign-inverting synapse from a laterally-projecting neuron is involved in transmitting information from the center illuminated area to the surround. Amacrine cells are known to form a mutually inhibitory network, making them the likely source of the inhibitory signal.

2.4.4 Spectral requirements of AAQ-mediated light responses

We determined the optimal wavelength for turning off RGC firing when the AAQ photoswitch is driven from the *cis* to the *trans* configuration. First, a conditioning 380 nm stimulus was used to turn on firing and then we measured suppression of firing in response to test flashes of different wavelengths. We found that 500 nm light is best at suppressing activity (Figure 2.7A), as expected from previous results (Fortin et al., 2008). To determine which wavelengths are best at triggering firing when AAQ photoisomerizes from *trans* to *cis*, we again applied test flashes of different wavelengths, but to ensure that the photoswitch started maximally in the *trans* configuration, the stimulation protocol began with a reset flash of 500 nm light followed by a period of darkness. We found that the optimal wavelength for stimulating firing was 380 nm under these conditions. However, robust firing could also be activated with 420 or 460 nm light (Figure 2.7B), and even 500 nm light could trigger an increase in firing frequency, if the preceding dark interval was sufficiently long. The history-dependence of photoswitching is a consequence of the initial ratio of the *cis* and *trans* photoisomers. Starting with all molecules in the *trans* state, even 500 nm light can

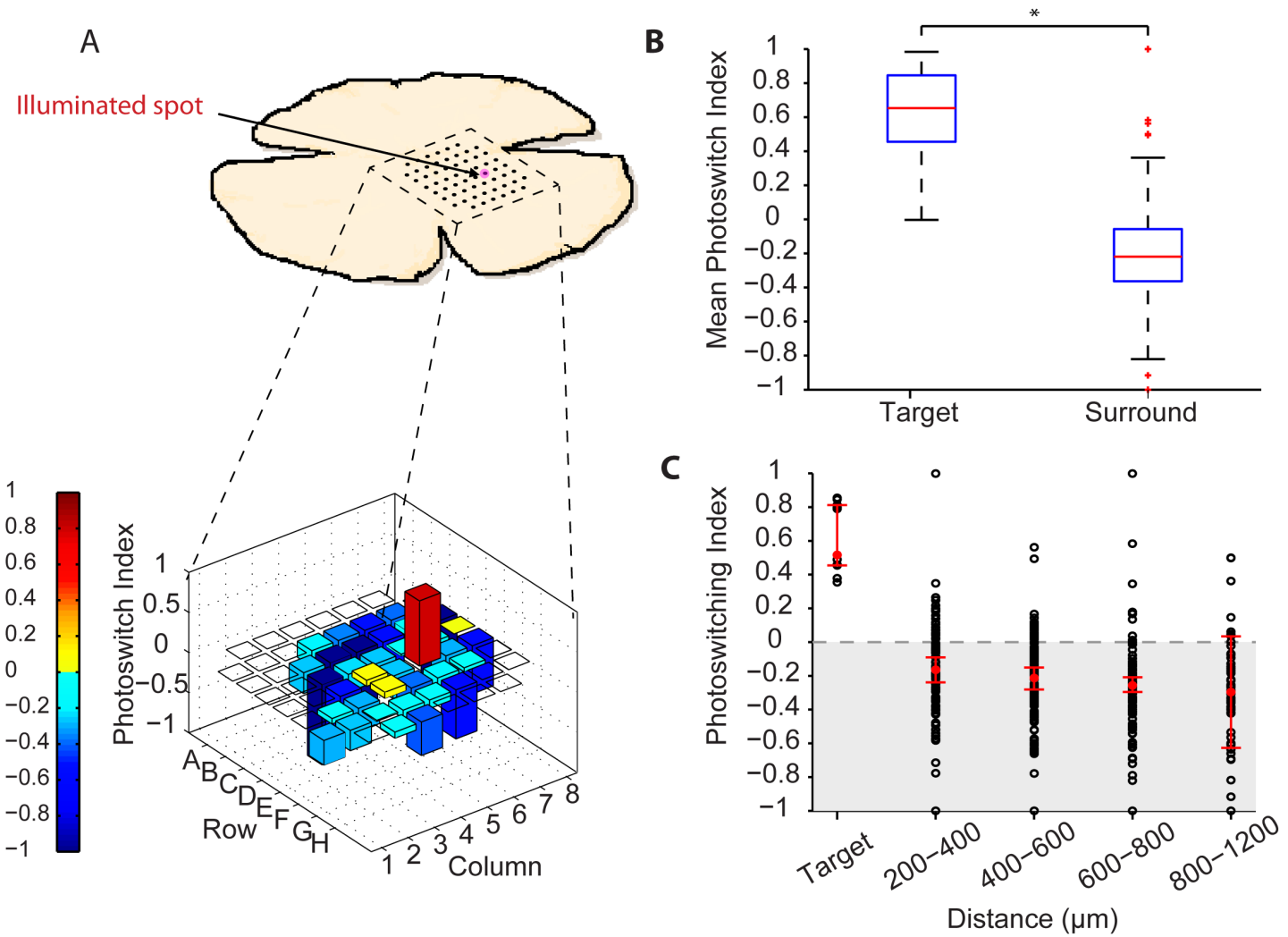

Figure 2.6: The AAQ treated retina generates spatially precise light responses. (A) Targeted illumination of a portion of the retinal centered on a single MEA electrode (top). The target (electrode E6) was exposed to 3 s flashes of alternating 380 and 500 nm light. ,Spot size = 60 μm in radius, inter-electrode spacing = 200 μm. Only the targeted electrode records an increase in RGC firing in response to 380 nm light (bottom). PI values are color-coded (scale at left) and also represented by bar height. Red bar is electrode E6 (PI 0.812; n = 1 cell) and blue electrodes are the surround (PI = -0.209; n = 56 cells). Empty squares are electrodes on which no action potentials were recorded. (B) Targeted illumination results from 3 retinas, displayed in a box plot. PI values for the target and the surround RGCs are significantly different from one another ($p < 0.005$, Mann-Whitney test). (C) Targeted illumination results in opposite responses in center and surround RGCs (n = 11 cells and n = 385 cells, respectively, from 3 retinas. PI values of RGCs (open circles) as a function of distance from the target electrode, displayed in 200 um bins. The red diamonds indicate the median plus or minus the bootstrapped 95% confidence intervals.

increase the fraction of cis molecules. Hence UV light is not essential for eliciting retinal responses. We also found that broad spectrum white light can trigger an increase in firing frequency in RGCs (Figures 2.7C and 2.7D).

We measured the absolute light intensity required to photoregulate AAQ-treated retinas from rd1 mice. The threshold intensity required to induce RGC firing was 2.6×10^{15} photons/cm^2/s of 380 nm light (Figure 2.7E). RGC firing rate increased progressively with brighter light, up to 10^{17} photons/cm^2/s, but even this intensity did not saturate the response. By comparison, retinas from rd1 mouse expressing ChR2 in bipolar cells (Lagali et al., 2008) have RGCs that exhibit a firing threshold of $6 * 10^{15}$ photons/cm^2*s.

2.4.5 Restoring behavioral light responses *in vivo* with AAQ

Given that AAQ can bestow photosensitivity onto blind retinas *ex vivo*, we asked whether it can confer light-induced behavior in blind mice *in vivo*. Although rd1 mice lose all morphologically recognizable rods and cones, a small fraction of cones with altered morphology can survive, allowing correct performance of a visual discrimination task under some illumination conditions (Thyagarajan et al., 2010). Rd1 mice also exhibit a pupillary light reflex (PLR), but this behavior is completely absent from rd1 mice lacking melanopsin, the photopigment found in the small percentage (≈3%) of RGCs that are intrinsically photosensitive (Hattar et al., 2002; Panda et al., 2003) (ipRGCs). Therefore, we tested the PLR of adult rd1 mice lacking the melanopsin gene (opn4$^{-/-}$ rd1/rd1) (Panda et al., 2003). After 3 months of age, no PLR could be elicited in any of the mice that we tested, even with brightest light available (Figure 2.8A). However, in a subset of these mice (9 out of 25), intravitreal injection of AAQ resulted in a substantial PLR, with a maximal pupillary constriction ≈65% as large as wild-type. Control experiments showed no restoration of the PLR following sham injection of vehicle alone (n = 4; Figure **??**). The AAQ-mediated response was attributable to the retina, as direct application of AAQ to the isolated iris *in vitro* did not produce light-elicited constriction. In the remaining mice, suboptimal intravitreal placement or leakage resulting from puncture damage may have limited retinal access to injected AAQ, precluding effective photosensitization.

The AAQ-mediated PLR in *opn4$^{-/-}$ rd1/rd1* mice could be triggered by photopic irradiance levels normally encountered during daytime, but the PLR threshold was 2-3 log units higher than the normal PLR in wild-type mice (Figure 2.8B). The AAQ-mediated PLR was slower than in wild-type mice and AAQ induced some basal pupillary constriction in darkness. Nonetheless, these results show that light responses in AAQ-treated retina can drive brain circuits, leading to a behavioral response that is absent from untreated blind animals.

We next tested whether locomotory light-avoidance behavior (Johnson et al., 2010; Kandel et al., 1987) could be restored in blind *opn4$^{-/-}$ rd1/rd1* mice treated with a unilateral intravitreal injection of AAQ. We placed a mouse into a narrow cylindrical transparent tube and recorded behavior with an infrared video camera (Figure 2.9A). An automated image anlaysis system was used to detect the mouse and measure how quickly it moved away from the illuminated end of the tube, toward the center. The latency to movement was signifi-

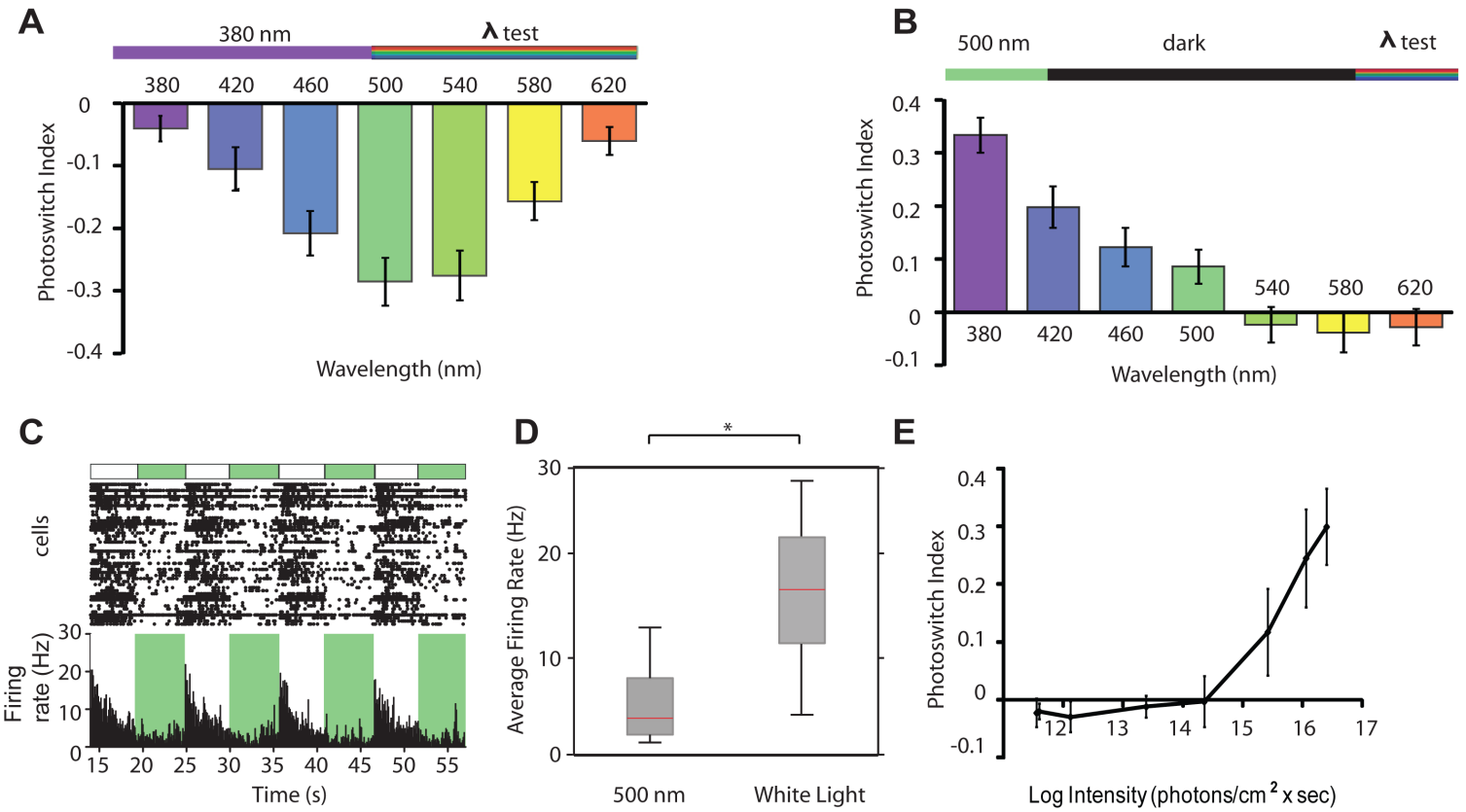

Figure 2.7: Spectral and illuminance sensitivity of AAQ-mediated photocontrol of RGC firing. (A) Spectral sensitivity of light-elicited suppression of RGC firing. Top: Light stimulation protocol. AAQ was first driven into its cis configuration with 380 nm light (5 s) and various test wavelengths triggered photoisomerization to the trans configuration. Bottom: PI values reveal the effectiveness of different wavelengths in suppressing RGC firing (n=5 retinas). (B) Spectral sensitivity of light-elicited activation of RGC firing. Top: Light stimulation protocol. AAQ was first driven into its trans configuration with 500 nm light (15 s). After an additional dark period (45 s) various test wavelengths triggered photoisomerization to the cis configuration. Bottom: PI values reveal the effectiveness of different wavelengths in stimulating RGC firing (n = 5 retinas). For (A) and (B) the PI was measured over the first 1 s after applying the test wavelength. (C) Stimulation of RGC firing in an AAQ-treated retina with white light. Top, raster plot of spiking from RGCs; bottom, average RGC firing rate. (D) Box plot representation of increased firing rate in white light vs. 500 nm. White light significantly increases peak firing rate ($p < 0.05$, Mann-Whitney test, n = 5). (E) Light intensity-response relationship for AAQ-treated rd1 mouse retinas exposed to different intensities of 380 nm light. Minimum light intensity needed for photoswitching is $2.6 * 10^{15}$ photons/cm^2/sec.

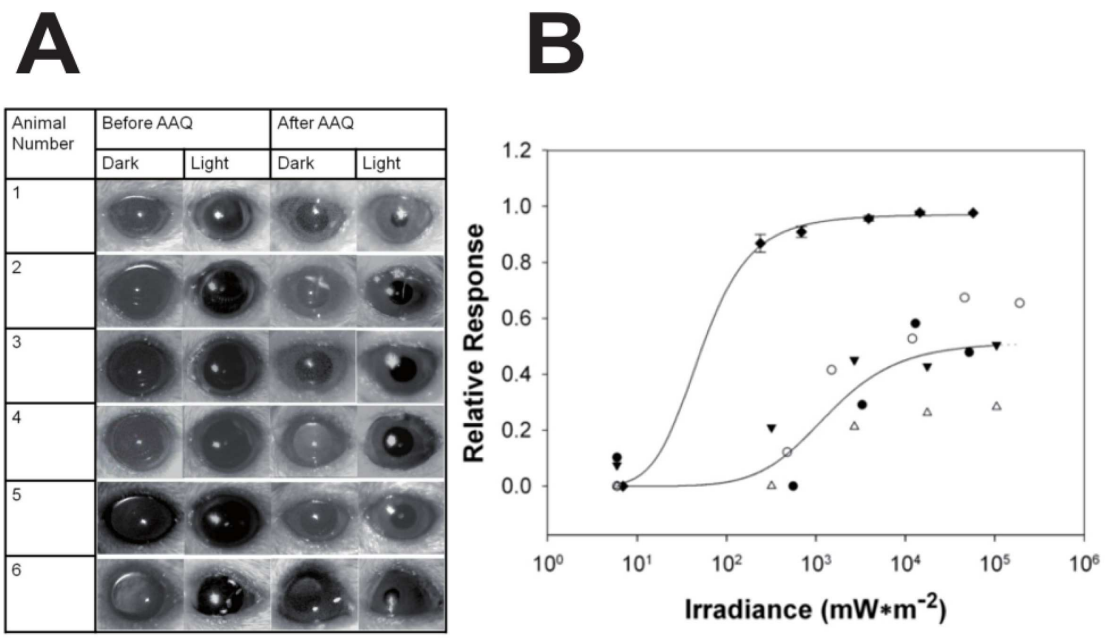

Figure 2.8: AAQ restores the pupillary light response in mice lacking all retinal photoreceptors. (A) Pupillary light responses to 5.5×10^4 mW/m^2 white light in *opn*4$^{-/-}$ *rd*/*rd* mice, before (left) and 3 hours after (right) intravitreal injection of AAQ (1 μl of 80 mM in DMSO). Dark images taken 5 s before light stimulus; light images represent maximal pupillary constriction during 30 s light exposure. Images were taken with an infrared-sensitive camera under infrared illumination. (B) Irradiance-dependence of pupillary light responses to white light. Irradiance response for wild-type mice (plotted as mean ± SD, n=5) (⬥) and four *opn*4$^{-/-}$ *rd*/*rd* mice injected with AAQ (plotted individually: • ∘ ▼ △). Data were fitted with a three parameter Hill equation.

cantly shorter in light than in darkness in wild-type mice (n=13, 26 trials, $p < 0.01$), but not in *opn4*$^{-/-}$ *rd1/rd1* mice (n = 7, 14 trials) indicating light-avoidance in the wild-type but not in the mutant mice. AAQ reinstated the light vs. dark latency difference, measured 2 hours after injection (n=7, 14 trials, $p < 0.02$), indicating restoration of light avoidance. At 24 hours after AAQ injection, there was no difference in latency in light vs. darkness, consistent with dissipation of the AAQ. These results indicate that an active light-avoidance behavior can be elicited by AAQ following a single injection into the eye.

Wild-type mice exhibit a decrease in open-field locomotion in response to light (Hascoët and Bourin, 2009). In contrast, rd1 mice exhibit no change in locomotion over at least a 10 minute period of illumination (Lin et al., 2008). We tested whether AAQ could restore this behavior by placing an rd1 mouse into a circular test chamber and monitoring movement during 5 min in darkness followed by 5 min in 380 nm light. Figure 2.10A and 2.10B show an example of the effect of AAQ on one rd1 mouse. Before AAQ, light had no effect on movement trajectory (Figure 2.10A) or total distance traveled (Figure 2.10B). After AAQ, light caused an almost immediate decrease in exploratory behavior, quantified as diminished distance traveled. Average data from 8 rd1 mice showed no light vs dark difference in movement before AAQ (Figure 2.10C). However, after AAQ there was a decrease in movement that occurred within 30 seconds of light onset. This decrease was sustained throughout the illumination period. Before AAQ there was no statistically significantly change in the speed of locomotion in light as compared to darkness (Figure 2.10D), but after AAQ injection, light caused a significant 40% slowing of locomotion. Sham injections with vehicle alone elicited no significant change in light modulated behavior (n = 4, $p > 0.6$). Further analysis of the 8 mice showed that 7 of them exhibited significant light-evoked slowing of locomotion after AAQ injection (Figure 2.10E).

After termination of the behavioral test, mice were sacrificed and retinas were placed on the MEA for electrophysiological analysis. In 5 cases, we successfully obtained MEA recordings and we were able to directly compare the AAQ-mediated photosensitization of the retina *ex vivo* with the behavioral responses *in vivo*. The one mouse that failed to exhibit light-modulated behavior (mouse A in Figure 2.10E) also failed to exhibit light-sensitive retinal responses. For all of the other 4 mice, light-elicited behavior was correlated with a light-elicited change in firing rate.

Rd1 mice possess ipRGCs, which should respond to the light used in this behavioral test. However, previous studies (Lin et al., 2008) show that ipRGCs do not mediate short-term light-elicited changes in exploratory behavior. Hence we propose that AAQ restores this behavior by photosensitizing types of RGCs that are not intrinsically photosensitive.

2.5 Discussion

The ultimate goal of vision restoration research is to develop a technology that recreates as closely as possible the activity of the entire population of RGCs in response to a natural visual scene. Since only a small fraction of RGCs are intrinsically light-sensitive (Ecker

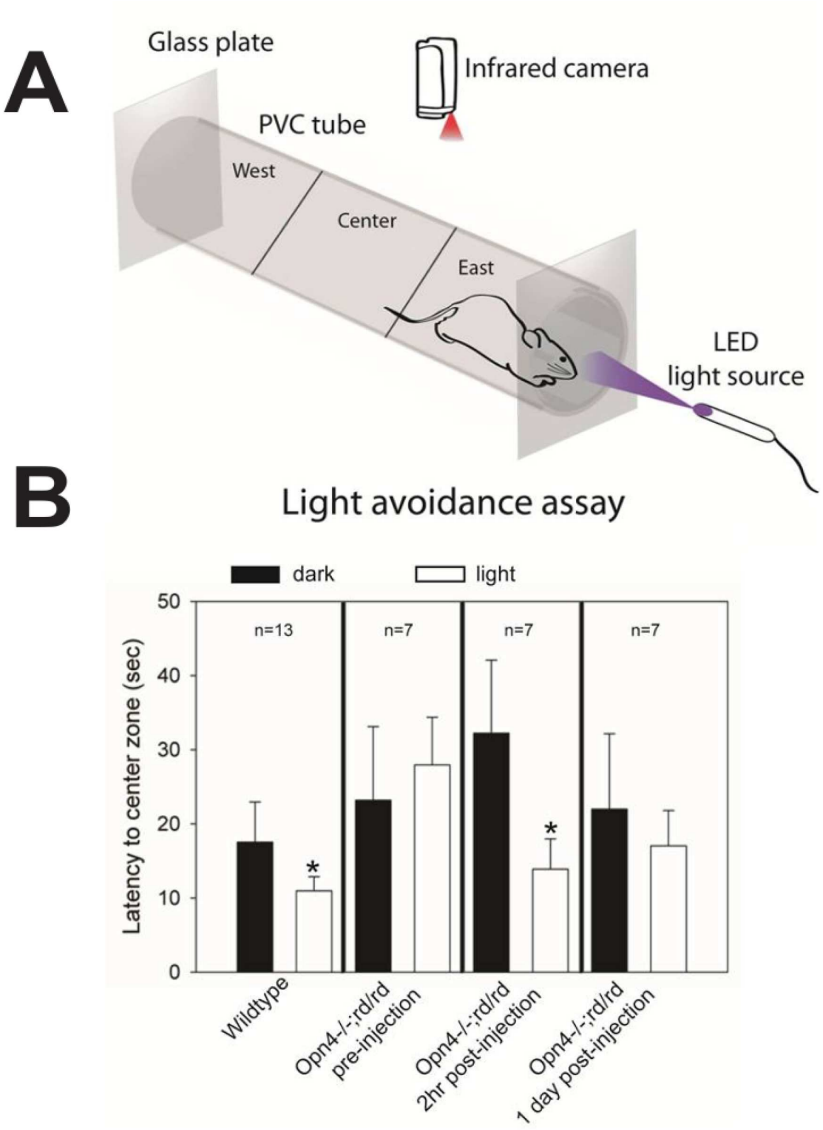

Figure 2.9: AAQ restores active light avoidance behavior in mice lacking all retinal photoreceptors. (A) Schematic diagram of the locomotory light-avoidance test chamber. (B) Restoration of light avoidance behavior in opn4-/- rd/rd mice following AAQ injection. Bars represent mean latency of movement from the East to the Center third of the tube.

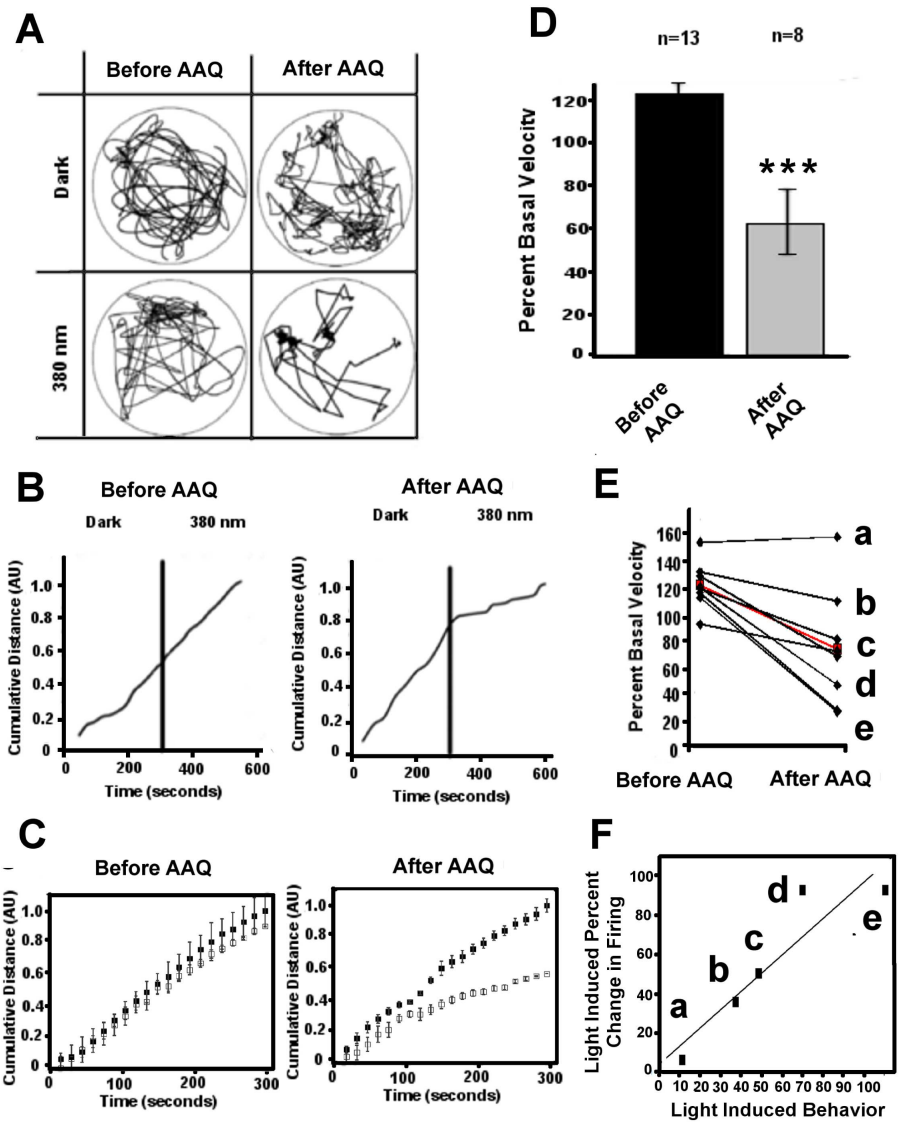

Figure 2.10: AAQ restores light-modulated locomotor behavior in an open-field test (A) Paths traveled by an rd1 mouse before and after injection with AAQ in darkness and with 380 nm illumination. (B) Cumulative distance traveled by the mouse in darkness and in 380 nm light, before and after AAQ. (C) Average cumulative distance traveled of all mice in darkness and 380 nm light, before and after AAQ. Closed squares represent time spent in darkness while open squares represent time spent in 380 nm light. (± SEM, n = 8). (D) Mean locomotory velocity in light normalized to basal velocity in darkness. Velocity decreases significantly in light (n = 8, $p < 0.0006$). (E) Light evoked change in the velocity of each of the eight mice, before and after AAQ. Red line shows the mean light evoked change, before and after AAQ. (F) Light induced behavior is correlated with the light induced change in firing rate. Data were from the five mice for which both *in vivo* behavioral measurement and *ex vivo* retinal MEA recordings were obtained (as labeled in panel (E)). The light induced percent change in firing rate was calculated from the aggregate light response for all units recorded with the MEA upon switching from darkness to 380 nm light,. The light induced behavior represents percent change in velocity upon switching from darkness to 380 nm light.

et al., 2010; Panda et al., 2003), photosensitivity must be conferred artificially by directly or indirectly making the neurons sensitive to light. Ideally, the kinetics and absolute sensitivity to light should be equivalent to natural RGC responses. The healthy retina has a remarkably broad operating range owing to light-adaptation mechanisms, so the artificial system should include gain adjustment and range extension capabilities. Ideally, the system would replicate normal encoding of contrast and color and highlight movement, with certain RGCs being directionally selective, accomplished with a minimally invasive and safe technology. To date, no restorative technology is close to meeting these criteria, but new developments are providing reason for optimism.

Broadly, three approaches have been suggested for restoring visual function to the eye in the absence of rods and cones: optoelectronic engineering with retinal chip prosthetics; genetic engineering with viral-mediated delivery of optogenetic tools; and cellular engineering, with rod or cone progenitors differentiated from stem cells *in vitro*. We now describe a fourth approach, photochemical engineering with a small molecule photoswitch. The following functional considerations suggest that the photoswitch approach would compare favorably with other methods for restoring visual function. and offers some practical advantages.

2.5.1 Kinetics

AAQ-mediated retinal light responses are rapid. MEA recordings show that the median response latency of RGC spiking is 45 msec in the AAQ-treated rd1 mouse retina, compared to ≈50 msec (Farrow and Masland, 2011) to several hundred msec (Carcieri et al., 2003) for photopic light responses from RGCs in wild-type retina. Retinal chips electrically stimulate RGCs directly, and therefore can elicit spikes with latencies of several msec. For optogenetic tools, depending on which retinal cell type expresses the tool the response latency of RGCs ranges from several msec to 150 msec (Bi et al., 2006; Busskamp et al., 2010; Lagali et al., 2008). Stem-cell based therapies would presumably restore wild-type kinetics assuming the differentiated rods and cones have full function.

2.5.2 Sensitivity

MEA recordings *in vitro* and PLR measurements *in vivo* indicate that the AAQ-treated rd1 mouse retina responds under bright photopic conditions, comparable to levels achieved in natural outdoor illumination. This is similar to light sensitivity conferred onto RGCs by optogenetic tools (Bi et al., 2006; Thyagarajan et al., 2010). Exogenous expression of NpHR in cone remnants can result in higher light sensitivity (Busskamp et al., 2010). However, it is unclear whether many patients with advanced RP have sufficient cone remnants to allow this to be a broadly applicable approach (Milam et al., 1998). High sensitivity can also be conferred by exogenously expressing melanopsin in RGCs that are not normally light-sensitive (Lin et al., 2008), but the responses are variable and slow (on the order of seconds). Stem cell-based therapies in theory might recapitulate the wild-type sensitivity of rods and

cones. However, the human retina normally contains > 100,000,000 rods and cones, and whether a significant fraction can be restored with stem cells remains unclear.

2.5.3 Spatial resolution and extent of retinal functional restoration

AAQ-mediated retinal responses have a high spatial resolution. Our spot illumination experiments places a 100 μm radius upper limit on the AAQ-mediated receptive field size. Amacrine cells, which predominate in driving RGC responses, can project over several hundred m, but mutual inhibition between these cells presumably spatially constrains RGCs responses to a smaller area. Because AAQ is a diffusible small molecule, in principle it should reach the entire retina and confer light sensitivity on all RGCs. In practice, we observed robust light responses in almost all RGCs when AAQ was applied *in vitro*, but intravitreal injections *in vivo* were less effective, with only 25-36% of injections resulting in behavioral responses to light. Drug delivery via intravitreal injections in mice can be unreliable because of the very small vitreal volume (≈5 ul), which is <1,000-fold the vitreal volume of the human eye (≈5.5 ml). Further experiments using animals with larger vitreal volumes are needed to better test and optimize the effectiveness of intravireal AAQ administration.

In contrast to the relatively high spatial resolution that could be conferred by AAQ, the spatial resolution of a retinal chip is limited by the relatively large size of the stimulating electrodes and the spread of current emanating from each electrode. While the healthy human retina contains ~1.2 million RGCs, current retinal chips have 16-64 electrodes spaced 100-200 micrometers apart (Winter et al., 2007). Chips with electrodes more densely packed exhibit crosstalk between electrodes, limiting their effectiveness. At present, the resolution that could be provided by retinal chip stimulation is several orders of magnitude lower than the theoretical limits imposed by RGC density in the macula, crucial for high-acuity vision. The area of RGC stimulation is limited by the physical size of the chip implant, which typically covers only the central 20 degrees of vision in the macula (Chader et al., 2009). Larger chips are possible, but there are challenges in power delivery and achieving stable adherence to the retina.

Similar to photoswitches, the spatial resolution conferred by optogenetic tools is defined by the size of the cell type targeted for expressing a given light-activated protein. In principle, the smaller the cell type and the more densely they are packed together, the higher the spatial resolution. In practice, viral transduction with current vectors has resulted in expression of optogenetic tools in a minority of targeted cells (e.g. 5% of bipolar cells in mice (Lagali et al., 2008); and 5-10% of RGCs in marmosets (Ivanova et al., 2010)), but it is possible that new viral vectors will be developed that improve transduction efficiency (Vandenberghe et al., 2011). Viral transduction of NpHR has resulted in more efficient transduction (50-75%) of remnant cones in blind mice (Busskamp et al., 2010), but this approach is only appropriate for the few patients thought to possess remnant cones. Viral transduction of cones requires subretinal injection, which involves local detachment of a portion of the retina

from the underlying retinal pigment epithelium. Effective viral gene transfer is limited to the detached area (Hauswirth et al., 2008).

Stem cell approaches offer the potential for greater spatial resolution but this is dependent on having a high density of differentiated photoreceptor cells that form functional and anatomically correct synapses with appropriate retinal neuron partners, and at present only a very low density of cells has been achieved (Lamba et al., 2009).

2.5.4 ON and OFF retinal output channels

Optogenetic tools have the advantage of being genetically-targetable to particular types of neurons to generate the appropriate stimulation or inhibition of firing, for example to ON- or OFF-RGCs (Busskamp et al., 2010; Lagali et al., 2008), Moreover, ChR2 and NpHR can be co-expressed in the same RGC and trafficked to different compartments to restore antagonistic center-surround responses (Greenberg et al., 2011). In contrast, all RGCs in AAQ-treated retina respond with the same polarity light response. While this pattern of responsiveness is different than the normal retina, it may not preclude a useful visual experience. Behavioral studies in primates demonstrate that selective pharmacological blockade of ON neurons does not severely impair recognition of shapes or detection of light decrements (Schiller et al., 1986). Moreover, in RP patients, electronic retinal prosthetics can restore shape recognition, even though the devices stimulate ON- and OFF-RGCs indiscriminately (Sekirnjak et al., 2009). Hence while two channels of visual information flow are important for normal vision, simultaneous activation of ON- and OFF-pathways is sufficient for visual perception. AAQ treatment enables RGCs surrounding an illuminated area to respond with the opposite polarity to those in the center. Since all RGCs respond with the same polarity light response to full-field illumination (Figure 2.1A), the opposite center vs. surround responses to spot illumination suggests that inhibitory neurons that project laterally invert the sign of the response. It seems likely that the opposite center vs. surround response would enhance perception of spatial contrast and facilitate edge detection in downstream visual regions of the brain. But ultimately, the evaluation of the quality of images produced by photoswitch activation of retinal cells will require study in primates or human patients.

2.5.5 Spectral sensitivity

In AAQ-treated retinas, RGCs respond most strongly to short wavelength light, consistent with the photochemical properties of the molecule (Fortin et al., 2008). Although 380 nm light is optimal for enhancing firing frequency, longer wavelengths (up to 500 nm) can still generate excitatory light responses, reflecting the spectral range of *trans* to *cis* azobenzene photoisomerization. This is important, because unlike in the mouse, the human lens minimally transmits 380 nm light (Kessel et al., 2010). Newly-developed red-shifted azobenzene derivatives allow K^+ channel regulation with even longer wavelengths of light and chemical modification of the azobenzene moiety results in compounds with improved quantum efficiency (Mourot et al., 2011). Ideally, second-generation AAQ derivatives would enable

photostimulation of the retina with intensities and wavelengths experienced during normal photopic vision. Alternatively, a head-mounted optoelectronic visual aid (Degenaar et al., 2009) designed to intensify and transform the palette of visual scenes to a blue-shifted wavelength could enhance the effectiveness of AAQ and related agents. Such a device would also allow switching of individual RGCs ON and OFF by rapid modulation of shorter- and longer-wavelength light.

Except for some of the optogenetic tools, the other vision restoration methods pose no particular spectral challenges. NpHR and ChR2 respond optimally to 580 and 470 nm light, respectively (Nagel et al., 2003; Zhang et al., 2007), but newly discovered red-shifted homologs (Govorunova et al., 2011) expand the toolkit for potential use for photosensitizing retinal neurons. Since they are driven by images captured by an external camera, retinal chip prosthetics can be engineered to operate over the entire visual spectrum. Similarly, assuming stem-cell derived photoreceptors express the full complement of cone opsins, these should be responsive to a broad range of wavelengths.

2.5.6 Invasiveness, safety, and reversibility

The phototswitch approach has the advantage of being relatively non-invasive and readily reversible. We envision photoswitch molecules being administered therapeutically by intravitreal injection, a safe and frequent procedure for treating macular degeneration with anti-vasoproliferative agents. Because AAQ photosensitization dissipates within 24 hrs, it may be possible to titrate the most effective dose with repeated intravitreal injections. The reversibility of AAQ will allow for upgrades as newer agents become available, perhaps with improved spectral or kinetic properties. Longer-term therapy would require an extended release formulation. We estimate that a several month supply of AAQ could be packaged into an intravitreal device like those currently used for long-term steroid treatment of ocular inflammation (London et al., 2011b).

In contrast, retinal chip prosthetics require invasive intraocular surgery. Optogenetic treatment of remnant cones and stem cell therapy both require subretinal injection, a risky procedure that begins with iatrogenic retinal detachment, which could further damage the retina. These three approaches are essentially irreversible. Should they produce undesired effects (such as chronic photophobia or disturbing visual sensations) there is no ready means for reversal of either stem cell implantation or gene therapy, and removal of chip prosthetics would require additional significant surgery.

Both retinal chip prosthetics and human gene replacement therapy have received investigational new device/drug status and have been tested in human patients under research protocols (Ahuja et al., 2011; Benav et al., 2010), without significant toxicity. However, microbial optogenetic tools would require trans-specific gene therapy, which is unprecedented. Viral gene expression in the eye can elicit late-onset inflammation, indicating an immune reaction (Beltran et al., 2010). Because the unitary conductance of ChR2 and NpHR is quite small (Feldbauer et al., 2009; Sjulson and Miesenböck, 2008; Zhang et al., 2007), photosensitivity requires very high levels of exogenous expression, raising concerns about an immune

response to the microbially-derived protein or cytotoxicity. While long-term safety of AAQ or similar compounds will require toxicology studies, to date we have not seen acute toxicity of AAQ on neural function *in vitro* (Fortin et al., 2008) or *in vivo* (Figure 2.3). The pathway for evaluating photoswitch compounds for toxicity is straightforward and will mirror those that have been followed for other approved, intravitreal agents.

Finally, in addition to its potential clinical use, AAQ has utility as a scientific tool for understanding normal retinal function and development. Using AAQ the firing activity of single cells or small regions of the retina can be controlled with high temporal and spatial resolution. This may be useful for better understanding information processing by the retina and for studying developmental plasticity in animals before rods and cones are functional (Huberman et al., 2008). AAQ-mediated photocontrol of retinal neurons also provides a unique way to investigate circuit remodeling after the rods and cones have degenerated in mouse models of RP (Marc et al., 2003).

Chapter 3

Restoring visual function to blind mice with red-shifted chemical photoswitches

Preface: This work was conducted in collaboration with Ivan Tochitsky, a graduate student at UC Berkeley. Aaron Friedman, a graduate student in Dr. Daniela Kauffer's lab conducted visual fear conditioning test. Nick Gallerani provided valuable technical assistance for histology experiments.

3.1 Summary

A large number of human retinal degenerative diseases are caused by the degeneration of rods and cones, leading to irreversible blindness. Visual responses can be restored in a mouse model of RP, by applying a synthetic ion channel photoswitch compound that confers light-sensitivity onto retinal neurons, downstream from the degenerated rods and cones (Polosukhina et al., 2012). However photosensitization persists for only a few hours and requires very high intensity, near-UV light, unsuitable for clinical application. Here we report red-shifted photoswitch compounds that generate robust responses to light with intensity equivalent to ordinary daylight. A single intravitreal injection can photosensitize the retina for several weeks, restoring electrophysiological and behavioral responses with no toxicity. We compared different strains of mice with rods and cones that were functional, non-functional, or degenerated. We found that the red-shifted photoswitches only affected mice lacking rods and cones, indicating a drug target that is selectively expressed in retinas with degenerative disease. The high light sensitivity, favorable spectral sensitivity, and selective targeting to diseased tissue make these red-shifted photoswitches prime drug candidates for clinical vision restoration in patients with end-stage RP and AMD.

3.2 Introduction

Degenerative retinal diseases including age related macular degeneration (AMD) and retinitis pigmentosa (RP) affect millions of people around the world. At present, there are no effective treatments to prevent the progressive degeneration of rod and cone photoreceptors that characterizes these disorders. Without a means for restoring photoreception, patients with advanced RP face the prospect of irreversible blindness. Several technologies are being developed to confer information about the visual world to the retinal neurons that survive after the rods and cones have degenerated. Surgically implanted electronic retinal prosthetics can stimulate RGC firing in response to light (Weiland et al., 2011), restoring some visual perception to blind human (Weiland et al., 2011). Transplantation of stem cell-derived photoreceptor progenitors can improve visual function in patients with RP (Lamba et al., 2009). Viral expression of microbial opsins (i.e. optogenetic tools) (Bi et al., 2006; Busskamp et al., 2010; Lagali et al., 2008; Thyagarajan et al., 2010) can restore visual responses to strains of blind mouse, that serve as animal models of RP. All of these strategies have shown promise for restoring visual function, but they are either invasive (i.e. implantation of electronic chips) or irreversible (i.e. transplantation of photoreceptor progenitors or viral expression of optogenetic tools). The potential permanence of stem cell or gene therapies could be a benefit if complications are absent, but the possibility of irreversible adverse effects makes these interventions risky to implement in humans.

We have introduced another strategy for restoring visual function: adding a synthetic small molecule "photoswitch" to confer light sensitivity onto retinal neurons without involving exogenous gene expression. We showed that a K^+ channel photoswitch named AAQ could bestow light responses onto RGCs and drive behavior in blind mice *in vivo* (Polosukhina et al., 2012). As a small molecule, AAQ has some advantages over alternative approaches for vision restoration. Unlike microbial opsin or stem cell-based therapies, the effect of AAQ is reversible and wears off quickly, allowing for titration of the compound *in vivo* to maximize its effect and minimize toxicity. Furthermore, AAQ can potentially photosensitize all remaining retinal ganglion cells and thus provide vision with a higher spatial resolution compared to an optoelectronic prosthetic with a limited number of stimulation electrodes.

However, several properties of AAQ limit its potential for therapeutic development. AAQ requires high intensity, UV wavelength light and the compound dissipates from the eye within a day after intravitreal injection. The human lens filters out most UV light (Artigas et al., 2012) and repeated exposure to high intensity light can be damaging (van Norren and Gorgels, 2011). AAQs short time course would necessitate daily injections of the compound into the eye, a delivery schedule unsuitable for long-term treatment. Furthermore, AAQ contains a reactive acrylamide moiety and its toxicity *in vivo* is unknown.

In order to be used in the clinic, our opto-pharmacological therapy needs to overcome all of AAQs shortcomings. This can be accomplished via new photoswitch molecules that would respond to visible, rather than UV light, and be at least as sensitive to light as the microbial opsins previously tested for vision restoration (Busskamp et al., 2010; Thyagarajan

et al., 2010). These molecules would persist *in vivo* for days to weeks and demonstrate no toxicity in the eye. In order to extend our therapy to the largest number of patients suffering from vision loss, including those with non-end-stage RP or AMD, we also need to ensure that our compounds do not interfere with any remaining photoreceptor-mediated vision. To address these requirements, we have synthesized several red-shifted K^+ channel photoswitches (Mourot et al., 2011) and have now tested them for their ability to photosensitize blind retinas and restore visual function to blind mice.

3.3 Materials and methods

3.3.1 Animals

WT mice (C57BL/6J strain, Jackson Laboratory), homozygous *rd*1/*rd*1 mice (C3H/HeJ strain, Charles River Laboratories), heterozygous *rd*4/+ mice (In56Rk-Rd4 strain, Jackson Laboratory) and triple knockout mice ($tra^{-/-}$ $cnga3^{-/-}$ $opn4^{-/-}$, gift of King-Wai Yau) >3 months old were used in our experiments. All animal use procedures were approved by the UC Berkeley Institutional Animal Care and Use Committee.

3.3.2 Electrophysiology

Mouse retinas were dissected and kept in physiological saline at 37C containing (in mM) 119 NaCl, 2.5 KCl, 1 KH_2PO_4, 1.3 $MgCl_2$, 2.5 $CaCl_2$, 26.2 $NaHCO_3$, and 20 D-glucose, aerated with 95%O_2/5%CO_2. For extracellular recordings, the retina was placed ganglion cell layer down onto a multielectrode array system (MEA 1060-2-BC, Multi-Channel Systems). The MEA electrodes were 30 m in diameter and arranged in an 8×8 rectangular grid. Extracellular spikes were high-pass ltered at 200 Hz and digitized at 20 kHz. A spike threshold of 4SD was set for each channel. Typically, each electrode recorded spikes from one to three RGCs. Principal component analysis of the spike waveforms was used for sorting spikes generated by individual cells (Ofine Sorter, Plexon).

3.3.3 Light Stimulation

A 100W mercury arc lamp was used for MEA light stimulation. The photon flux equivalent for DENAQ-treated retinas was calculated using 470nm (photoswitch absorbance peak) photon energy, and 450nm photon energy for BENAQ-treated retinas. The incident white light intensity for *rd*1, WT and TKO retinas was 3.3×10^{15} photons/cm^2/sec, and 3×10^{14} photons/cm^2/sec for *rd*4 retinas, unless stated otherwise. AAQ-treated retinas were stimulated with filtered 380nm and 500nm light from the same lamp using narrow-pass filters (Chroma, Inc), with the same light intensity as previously described (Polosukhina et al., 2012). A Polychrome 5000 (Till Photonics, Germany) monochromator was used to determine the action spectrum of DENAQ in the retina.

3.3.4 Data Analysis and Statistics

Light-elicited changes in ring rate in *rd*1, *rd*4 and TKO retinas during test ashes were normalized and expressed as the Light Response Index (LRI), defined as follows:

$$\text{LRI} = \frac{\text{mean firing rate in the light} - \text{mean ring rate in darkness}}{\text{mean firing rate in the light} + \text{mean ring rate in darkness}},$$

and Light sensitivity = abs(LRI). Light-elicited changes in ring rate in WT retinas during test ashes were normalized and expressed as the Peak Light Response Index (PLRI), dened as follows:

$$\text{PLRI} = \frac{\text{peak firing rate in the light} - \text{peak ring rate in darkness}}{\text{peak firing rate in the light} + \text{peak ring rate in darkness}}.$$

The first second of the light and dark intervals was used to measure the peak firing rate. Statistical significance (p value) calculations were performed using the two tailed unpaired Students t test, unless stated otherwise. LRI and PLRI distributions were rst tested for normality using the Shapiro-Wilk test. For non-normal distributions, the Wilcoxon rank sum test (Matlab) was used for pairwise comparisons. Results with $p<0.05$ were considered signicant.

3.3.5 Cryosections

Animals were euthanized by CO_2 asphyxiation and cervical dislocation. For retinal cross sections, the eyes were enucleated, the cornea and lens were removed, and the resulting eye-cups were fixed in 4% PFA for 1 hour at room temperature. The tissues were then cryoprotected in 30% sucrose overnight at 4C and frozen in OCT compound (Tissue-TEK, Sakura) with dry-ice ethanol slurry. Retinal sections were cut (15μm) with a cryostat and collected on Superfrost Plus slides (MenzelGlaser, Braunschweig, Germany).

3.3.6 Histology

Slides were incubated in nuclei stained with 1 μM DAPI in PBS (GIBCO, pH 7.4) for 30 minutes. They were then washed with PBS (GIBCO, pH 7.4) and incubated in 2.5 μM sulforhodamine in PBS (GIBCO, pH 7.4) for five minutes. Fluoromount-G (Southern Biotech) was used to mount coverslips (Fisherbrand 22×50-1.5) onto slides. Images were captured using a Pris microscope through the 40× oil objective. One section from each eye was selected and four 2-6 μm thick z-stack images were taken at the periphery and center of the section. Images were analyzed using ImageJ. Inner and outer nuclear layer thickness was measured in microns at four equidistant positions along the image. RGCs were counted over a 100 μm section. Two counts were made per image and averaged.

3.3.7 Open-Field Test

*Rd*1 mice were placed in a 190×100 mm circular chamber. The chamber was surrounded by six panels of 500nm LEDs (Roithner Laserteknik), providing uniform illumination with a light intensity of 10 mW/cm^2. The mice were dark-adapted for 1 hour prior to each experiment, then habituated to the experimental chamber for 5 min. The exploratory behavior was recorded using an IR sensitive video camera (Logitech C310) for 5 min in darkness under IR illumination, then the chamber was illuminated by the 500nm LEDs, and locomotory behavior was monitored for an additional 5 min. The apparatus was cleaned after each experiment. After the open-eld test, mice were given an intravitreal injection of DENAQ (20 mM DENAQ, in 90%PBS/10%DMSO) or sham (90%PBS/10%DMSO) and were allowed to recover for 6 hours on a heating pad with open access to food and water in their cage located in a dark room followed by a second round of behavioral testing. The videos were analyzed with motion tracking software (Tracker) in order to record the animals' velocity and position. The ratio of

$$\frac{\text{activity light}}{\text{activity darkness}} = \frac{\text{mean velocity in the light}}{\text{mean velocity in darkness}}.$$

3.3.8 Visual Fear Conditioning Test

Fear conditioning was conducted in $12 \times 10 \times 12$ inch chambers with 3 metal and one clear plastic wall and electrified metal bar floors (context A), closed within outer sound and light attenuating chambers (Coulbourn Instruments, Whitehall, PA, USA). Prior to experiments, animals were habituated by two days of handling and one five minute exposure to the chamber. On day one, groups of WT mice, uninjected and DENAQ-injected (6 hours after intravitreal injection of 10 mM DENAQ in 90%PBS/10%DMSO) *rd*1 mice, were subjected to paired conditioning (5 min of habituation with no stimuli, followed by three 10 s full field constant white light cues co-terminating with 2 s footshock, with 15 s between cues, followed by 5 min of no stimuli) or unpaired stimuli (same procedure except stimuli were 3 footshocks and 3 light cues randomly interleaved with 5-12 s between stimuli). On day two, the chamber context was altered (context B) by removing the electric grid floor and inserting laminated cork board walls. The mice were then tested for recall of the light-cued conditioning (5 min habituation with no stimuli followed by 2 min continuous light cue followed by 5 min no stimuli). Chambers were cleaned with 70% ethanol before and after each animal. Two house lights provided very dim illumination (5 μW/cm^2) sufficient to allow video recording throughout the experiment, but below the threshold for DENAQ activity. The bright light cue was provided by two white LED arrays attached to the inner chamber ceiling (500 μW/cm^2). Locomotor activity was analyzed as in the open field assay.

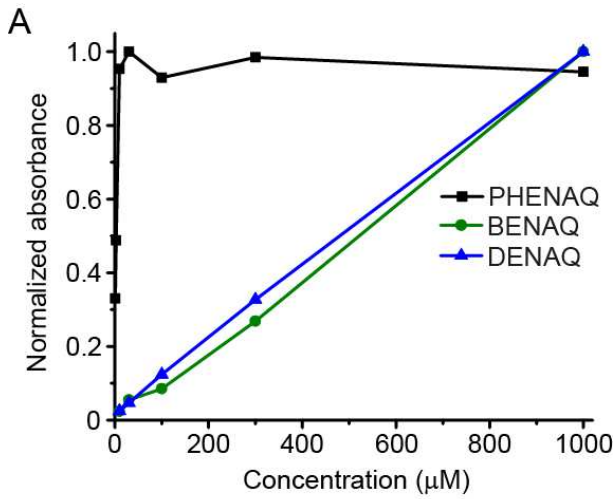

Figure 3.1: Solubility of the photoswitch compounds in PBS, pH 7.4 with 10% DMSO. Absorbance measurements were normalized to 1.

3.4 Results

Mourot et al. (2011) described 3 red-shifted photoswitch compounds that confer light sensitivity on K^+ channels: DENAQ, BENAQ, and PhENAQ. As a first step in evaluating the potential suitability of these compounds for therapeutic vision restoration, we measured their solubility in aqueous solution. Both DENAQ and BENAQ were soluble up to at least 1 mM in phosphate buffer saline (pH 7.4), but PhENAQ proved highly insoluble (Figure 3.1) and therefore was not used in further experiments.

We tested the actions of DENAQ and BENAQ on the retinas of >3 month old rd1 mice, which lose nearly all rods and cones within 1 month after birth (Sancho-Pelluz et al., 2008). We measured the effect of light on action potential firing by RGCs recorded with an extracellular multi-electrode array (MEA). Before photoswitch application, light caused no significant change in firing (Figure 3.2A). A subsequent 20 min treatment with 300 μM DENAQ rendered the same retina photosensitive, with nearly all units responding to the onset of white light with an increase in firing rate (Figure 3.2B). The firing frequency declined somewhat during the 15 sec light flash. At light offset, firing rate returned quickly to baseline (within 45 msec). BENAQ application resulted in a similar light response (Figure 3.1). The rapid dark turn-off of DENAQ and BENAQ response reflects the fast spontaneous *cis* to *trans* relaxation rate of these compounds in the dark (Mourot et al., 2011). This is in contrast to AAQ, which persists in the *cis* state for minutes (Fortin et al., 2008).

We next examined the spectral sensitivity of DENAQ-mediated photosensitization of the rd1 retina. A wide range of wavelengths, between ≈420 to ≈540 nm, can elicit the light response, with blue-green light (480-500 nm) being most effective (Figure 3.2C). The

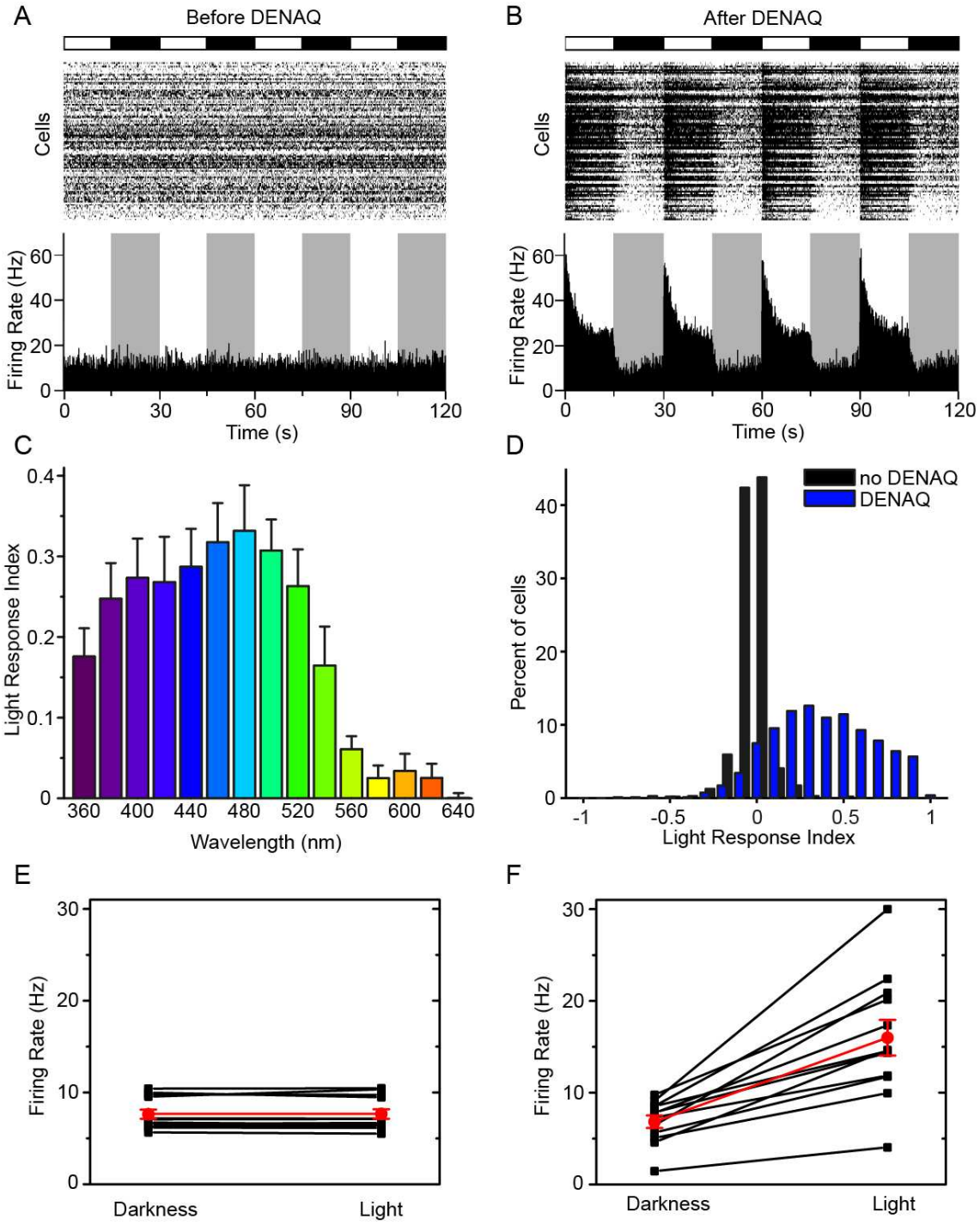

Figure 3.2: A-B) MEA recording from an rd1 retina before DENAQ treatment (A) and after treatment with 300μM DENAQ (B). C) Spectral sensitivity of the DENAQ-mediated light response. D) LRI value distributions for RGCs from untreated (black) (median LRI=0, n=12 retinas) and DENAQ-treated (blue) rd1 retinas (median LRI=0.42, n=12 retinas, p<0.001, rank sum test). E-F) Mean RGC firing rate in light and darkness before (n=12 retinas, p=0.94, rank sum test) (E) and after DENAQ treatment (n=12 retinas, p<0.001, rank sum test) (F). MeanSEM values are shown in red.

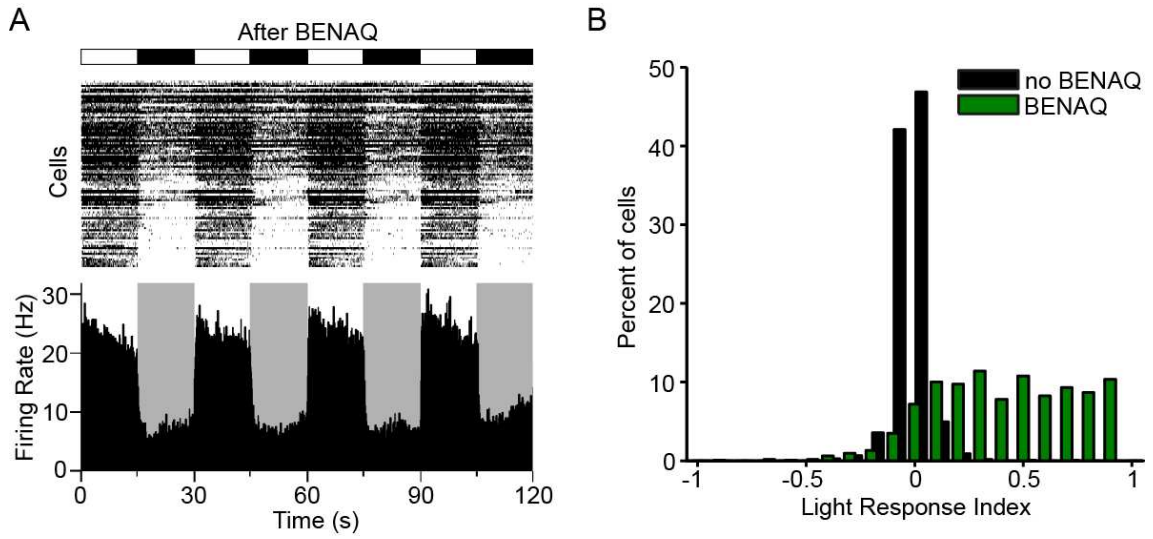

Figure 3.3: A) MEA recording from a BENAQ-treated rd1 retina. B) LRI values for RGCs from untreated (black) and BENAQ-treated (green) rd1 retinas (median LRI=0.46, n=11 retinas, p<0.001, rank sum test).

action spectrum of retinal photosensitization closes matches the absorption spectrum of *trans*-DENAQ in solution (Mourot et al., 2011). Stimulation with broad spectrum white light is also quite effective. To quantify the degree of photosensitization, we calculated a Light Response Index (LRI), which represents the normalized change in average firing rate upon switching from darkness to white light. RGCs from untreated rd1 retinas showed no detectable light response (median LRI=0, n=12 retinas); while nearly all DENAQ-treated rd1 RGCs were activated by white light (median LRI=0.42, n=12 retinas, p<0.001, rank sum test) (Figure 3.2D). We observed no significant change in firing rate upon light stimulation of untreated rd1 retinas (n=12 retinas, p=0.94, rank sum test) (Figure 3.2E), while DENAQ-treated rd1 retinas increased the RGC firing rate by an average of 2.4-fold in response to light (n=12 retinas, p<0.001, rank sum test) (Figure 3.2F). Treatment of rd1 retinas with BENAQ likewise resulted in a robust light response upon white light stimulation (median LRI=0.46, n=11 retinas, p<0.001, rank sum test) (Figures 3.3A, 3.3B).

We found that the light intensity threshold for DENAQ-mediated RGC responses in the rd1 retina was $4{\times}10^{13}$ photons/cm^2/sec (Figure 3.4A), with slightly brighter light ($3{\times}10^{14}$ photons/cm^2/sec) needed to photosensitize the majority of RGCs (Figure 3.4B). BENAQ treated retinas were slightly less sensitive to light (threshold = $8{\times}10^{13}$ photons/cm^2/sec). For comparison, the intensity threshold for responses mediated by AAQ (Polosukhina et al., 2012), ChR2 expressed in RGCs (Thyagarajan et al., 2010) and halorhodopsin (NpHR) expressed in remnant cones (Busskamp et al., 2010) was 4×10^{15}, 4×10^{14}, and 1×10^{14} photons/cm^2/sec, respectively. The sensitivity of DENAQ-treated retinas is thus at least as great as that of retinas expressing microbial optogenetic tools.

Photosensitivity can also be installed into the rd1 retina by injecting DENAQ into the

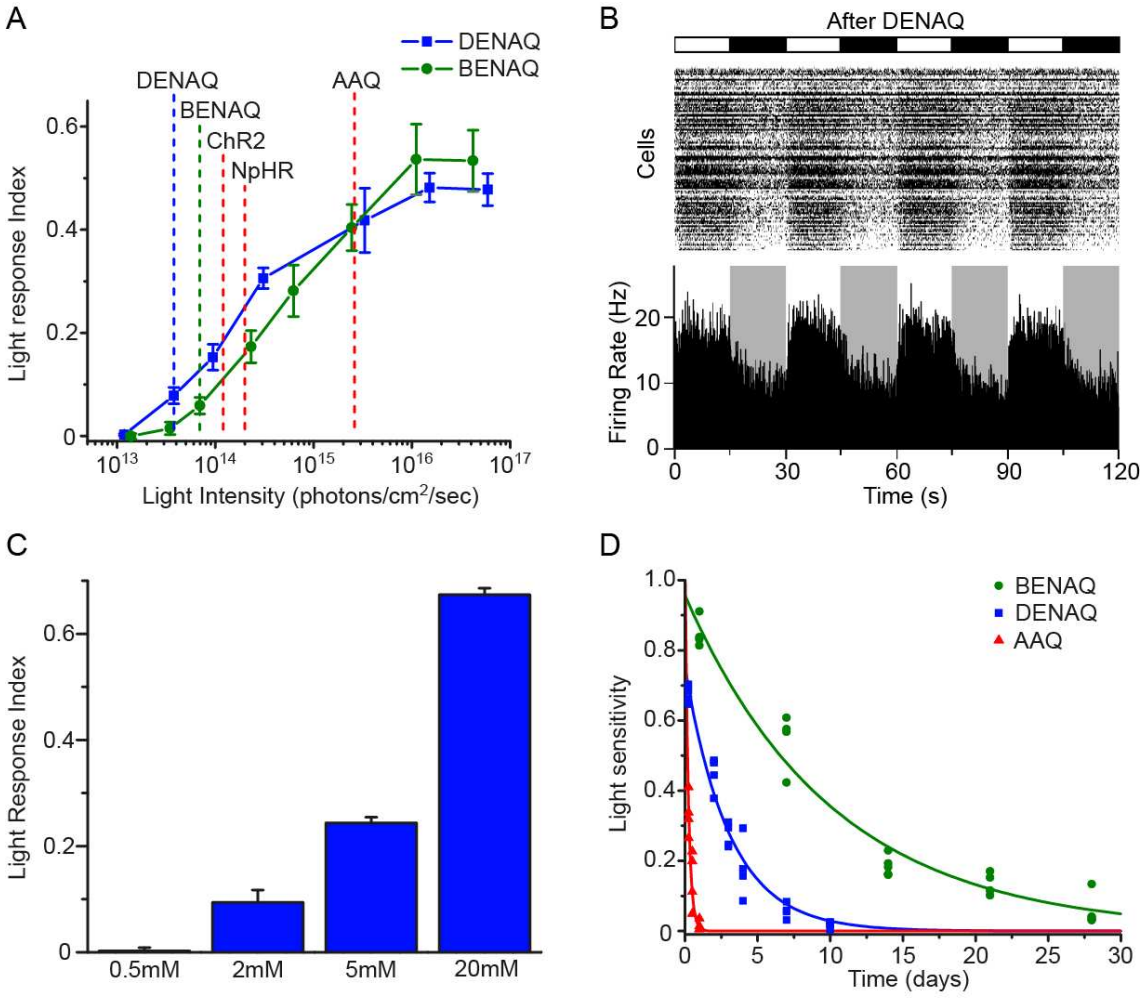

Figure 3.4: A) Light intensity dose response curves for DENAQ (blue) and BENAQ (green). The thresholds for activation of DENAQ (blue), BENAQ (green), ChR2 (red), NpHR (red) and AAQ (red) are represented by dotted lines and labeled appropriately. B) MEA recording from a DENAQ-treated rd1 retina stimulated with low intensity (3×10^{14} photons/cm^2/sec) white light. C) MEA-recorded *ex vivo* light responses of retinas after intravitreal injection of various concentrations of DENAQ (n=4 retinas each). Data are mean ± SEM. D) Persistence of AAQ (red, half-life=3.6 hours), DENAQ (blue, half-life=2.1 days) and BENAQ (green, half-life=7 days) in the retina as measured on the MEA *ex vivo* after intravitreal injection (n=4 retinas per time point). The rate of photoswitch decay was calculated by fitting the data with monoexponential decay function.

vitreous cavity of eye in vivo. The effectiveness of *in vivo* injection was assessed 6 hours later by sacrificing the mouse and obtaining *ex vivo* MEA recordings from isolated retinas. A single 2 μl bolus injection containing ≥2 mM DENAQ was necessary to produce significant photosensitization and the effect increased with DENAQ concentration (Figure 3.4C). This is likely an over-estimate of the minimum required dose because of the efflux of some of the injected compound from the eye. MEA recordings at later times after injection showed that DENAQ photosensitization persists for several days (half-life=2.1 days) and BENAQ photosensitization for several weeks (half-life=7 days), in contrast to AAQ, which dissipates within 24 hours after intravitreal injection (half-life of 3.6 hours) (Figure 3.4D).

Photoreceptor degeneration slowly progresses from peripheral to central retina in RP and regions retain intact neural circuitry for years. It would be ideal for any vision restoration treatment to selectively act on diseased retinal tissue while sparing healthy tissue. To assess the actions of photoswitch compounds on healthy and diseased retina, we compared the effects of DENAQ in wild-type (WT) and rd1 retinas. The light stimulus parameters were the same as employed above. In WT retina, almost all RGCs exhibited strong light responses before photoswitch treatment, with light-onset triggering an increase in firing frequency in some ON-RGCs exhibiting a decrease in OFF-RGCs (Figure 3.5A). Surprisingly, DENAQ treatment resulted in little change in the light response, with no apparent change in the number of RGCs generating On or Off responses (Figure 3.5B). In order to quantify photoreceptor-mediated RGC light responses, we calculated the Peak Light Response Index (PLRI) value, which represents the normalized change in peak firing rate upon switching from darkness to light. The distributions of PLRI values from RGCs measured from six WT retinas before and after DENAQ treatment were not significantly different (n=6 retinas, p=0.34, rank sum test) (Figure 3.6C). Likewise, the light responses of a wild type retina prior to and after treatment with BENAQ were quite similar (Figures 3.7A, 3.7B). The distributions of PLRI values measured from untreated and BENAQ-treated WT RGCs were not significantly different from one another (n=6 retinas, p=0.76, rank sum test) (Figures 3.7C, 3.7D).

We decided to investigate this apparent selectivity of DENAQ and BENAQ for degenerated but not healthy retinas further. For our next target, we tested DENAQ on a triple knockout (TKO) (tra$^{-/-}$ cnga3$^{-/-}$ opn4$^{-/-}$) mouse retina, which lacks functional rods and cones, as well as the photopigment melanopsin, but retains the architecture and connectivity of a healthy retina (Hattar et al., 2003). These TKO retinas did not respond to white light stimulation prior to or after DENAQ treatment (n=6 retinas, p=0.21, rank sum test) (Figure 3.5D), suggesting that intact, healthy retinas are not affected by DENAQ to any noticeable extent. In order to determine whether the action of DENAQ was specific to *rd*1 mice or was broadly applicable to other degenerated retinas, we applied the photoswitch onto an *rd*4/+ mouse retina. *Rd*4 mice suffer from a different genetic defect compared to *rd*1 mice (Kitamura et al., 2006), but share a similar phenotype where photoreceptors die soon after birth, eventually leading to complete blindness (Roderick et al., 1997). Untreated *rd*4 mouse retinas did not generate a light response as measured on the MEA, but DENAQ treatment conferred robust photosensitivity to these retinas (n=6 retinas, p<0.001, rank sum test) (Figure 3.5D). Thus, it seems that retinal degeneration itself, and not any particular

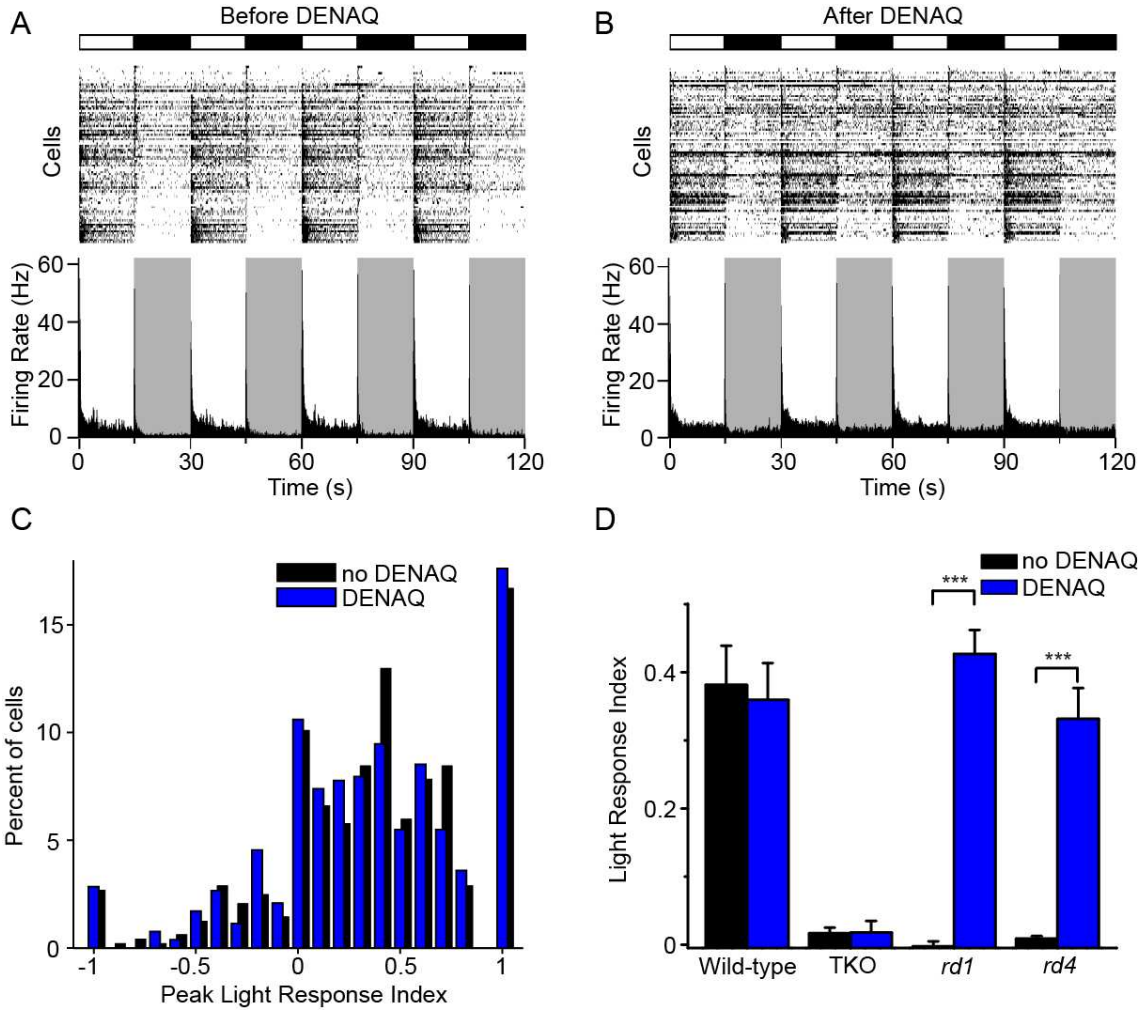

Figure 3.5: A-B) MEA recording from a WT retina before (A) and after (B) treatment with 300 μM DENAQ. C) RGC PLRI values for WT retinas before (black) and after (blue) DENAQ treatment (n=6 retinas, p=0.34, rank sum test) D) Light responses of untreated and DENAQ-treated WT (n=6 retinas, p=0.72), TKO (n=6 retinas, p=0.97), rd1 (n=12 retinas, p<0.001) and rd4 retinas (n=6 retinas, p<0.001). Mean PLRI values are shown for WT retinas and mean LRI values for TKO, rd1 and rd4 retinas. Data are mean ± SEM.

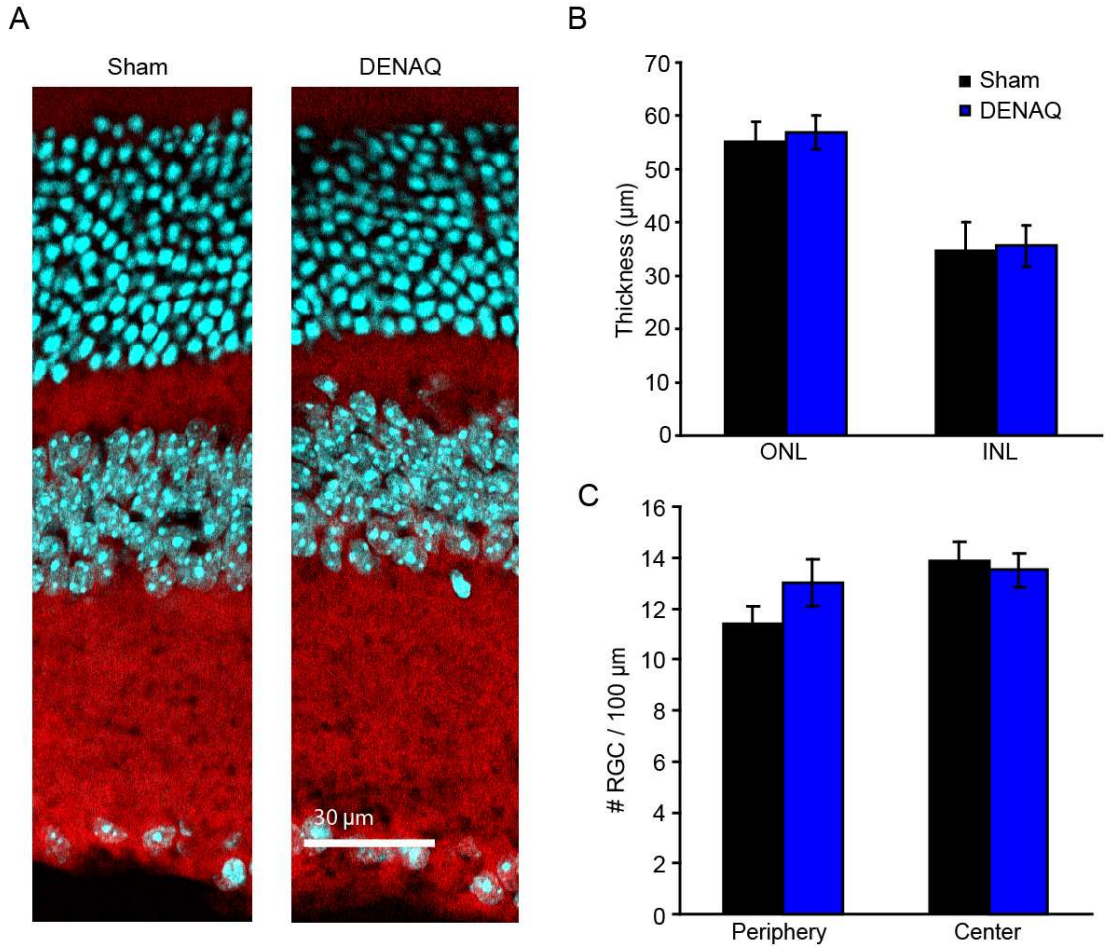

Figure 3.6: A) Retinal cross-section from a PBS-injected eye (left) and a 5mM DENAQ-injected eye (right). (scale bar=50 μM) B) Outer nuclear layer (ONL) and inner nuclear layer (INL) thickness in PBS-injected (black) and DENAQ-injected (blue) retinas. C) RGC number per 100 μm in PBS (black) and DENAQ-injected (blue) retinas.

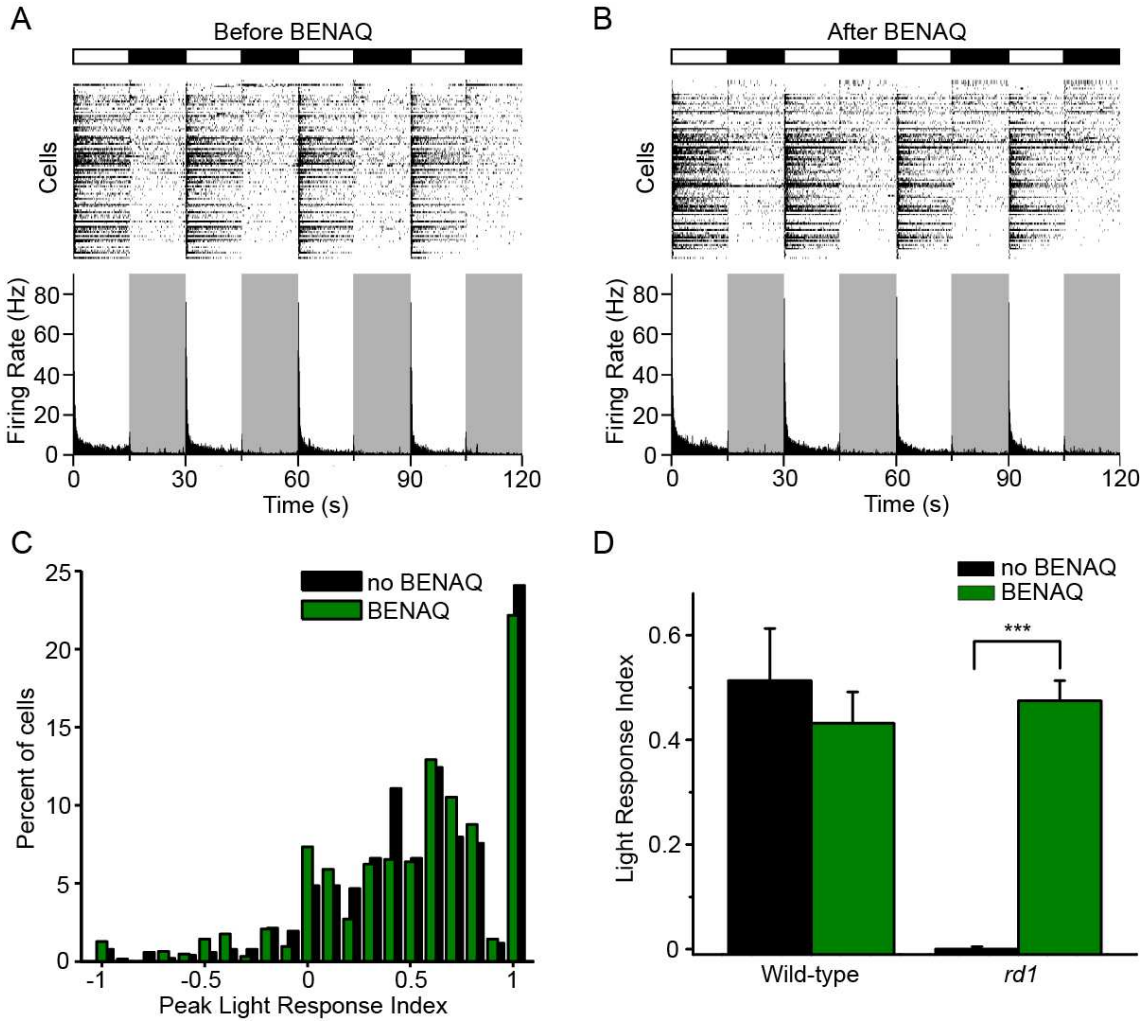

Figure 3.7: A-B) MEA recording from a WT retina before (A) and after (B) BENAQ treatment. C) RGC PLRI values for WT retinas before (black) and after (green) BENAQ treatment (n=6 retinas, p=0.76, rank sum test).

mutation, is the factor enabling the selectivity of DENAQ. This selectivity is highly advantageous for the proposed clinical use of these red-shifted photoswitches, as it would in principle allow us to target our therapy specifically to degenerated tissue.

In order to ensure the safety of the photoswitch compounds *in vivo*, we performed a histological analysis of WT retinas after intravitreal injection of 5mM DENAQ. Cross-sections of retinas from 8 WT mice injected with PBS or DENAQ were examined 10 days post injection. No gross pathological changes were observed in either the DENAQ-injected or PBS-injected retinas (Figure 3.6A). There was no significant difference in the thickness of the outer nuclear layers (n=8 retinas, p=0.5) (Figure 3.6B) or the inner nuclear layers (n=8 retinas, p=0.7) between the two groups. The retinas showed normal organization of all cell layers and there was no change in total RGC number in the central (n=8 retinas, p=0.62) or peripheral retina (n=8 retinas, p=0.1) (Figure 3.6C).

We then evaluated the ability of DENAQ to restore visually guided behavior *in vivo*. Blind *rd*1 mice showed no difference in exploratory behavior during 5 minutes spent in green light versus 5 minutes in darkness in an open field locomotory assay (Figures 3.8A, 3.8B). Six hours after intravitreal injection of 20mM DENAQ, the animals displayed an increase in locomotory activity in light compared to darkness (Figures 3.8A, 3.8B). This is consistent with previously reported results from an *rd*1 mouse expressing ChR2 in its ON-bipolar cells (Lagali et al., 2008). We quantified the activity of mice in the open field experiment by measuring the ratio of mean velocity in the light divided by mean velocity in darkness. The ratio of activity in the light to activity in darkness increased by an average of 48% after injection of DENAQ (n=20 mice, p<0.001) (Figure 3.8C). Sham injection of PBS produced no significant change in basal activity or relative activity in light versus darkness (n=6 mice, p=0.88) (Figure 3.8C).

Sensory perception, e.g. visual object recognition, may not be immediate after photoswitch treatment, but rather could improve with training. To test whether *rd*1 mice can use DEAQ-mediated light responses as a stimulus for a learned behavior, we performed a visual cued fear conditioning assay. In sighted mice, this classical conditioning paradigm associates a light cue with a fearful electric foot shock, such that subsequent exposure to the light cue alone elicits a learned fear response including freezing behavior (Li et al., 2012; Newton et al., 2004; Sacco and Sacchetti, 2010). We exposed animals to either paired conditioning (3 trials of 10 s full field constant white light cues co-terminating with 2 s foot shock) or unpaired stimuli (same light and shock cues randomly interleaved rather than overlapping), and then presented a 30 s light cue alone (recall) one day later (Figure 3.9A). We analyzed the locomotor activity in the recall trial using the same metric as in the open field task (mean velocity in the light divided by mean velocity in darkness), so that we could directly compare changes in activity in the two assays. Basal activity in darkness was not significantly different among the three groups of animals that had undergone paired-conditioning. As expected, paired conditioned wild-type mice responded to light onset in the recall trial by decreasing their locomotor activity (n=10 mice, p<0.001) (Figures 3.9B, 3.9C). Wild-type C57BL/6J mice exposed to unpaired stimuli instead showed an increase in locomotor activity in the light compared to darkness (n=10 mice) (Figure 3.9C), similarly to previously reported observa-

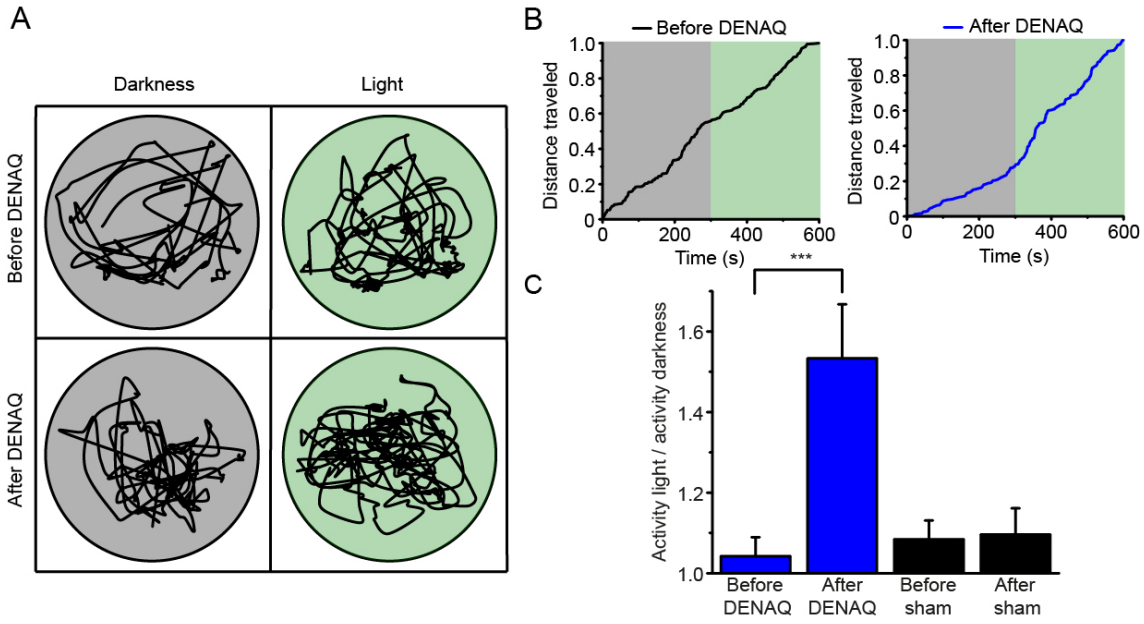

Figure 3.8: A) Movement trajectory of an rd1 mouse exploring an open cylindrical cage in the dark (top left) and under 500nm illumination (top right) before DENAQ injection. Movement trajectory for the same rd1 mouse exploring the cage in the dark (bottom left) and under 500nm illumination (bottom right) after intravitreal injection of 20mM DENAQ. B) Cumulative distance traveled by an rd1 mouse before (left) and after (right) injection of DENAQ. C) Bar graph of activity in the light divided by activity in darkness for rd1 mice before and after intravitreal injection of 20mM DENAQ (n=20 mice, p<0.001) or 20mM PBS (n=6, p=0.88) (sham). Data are mean ±SEM.

tions (Trullas and Skolnick, 1993). Uninjected blind *rd*1 mice did not show any change in locomotor activity upon light onset following either paired or unpaired conditioning (n=10 mice, p=0.98) (Figures 3.9B, 3.9C), suggesting that the melanopsin containing ipRGCs are incapable of driving learned visual freezing behavior. After intravitreal injection of 10mM DENAQ, only the *rd*1 mice that received paired conditioning, but not those exposed to unpaired stimuli, displayed a decrease in locomotor activity in the light compared to darkness during the recall trial (n=10 mice, p<0.001), exhibiting the same degree of freezing as the paired conditioned wild-type mice (n=10, p=0.51).

3.5 Discussion

Vision restoration to blind patients is the ultimate goal of all of the therapeutic interventions currently being investigated, including optoelectronic prosthetics, cell replacement therapy and gene therapy with light-sensitive microbial opsins. Our novel opto-pharmacological strategy for vision restoration has been shown to be effective in restoring light sensitivity to

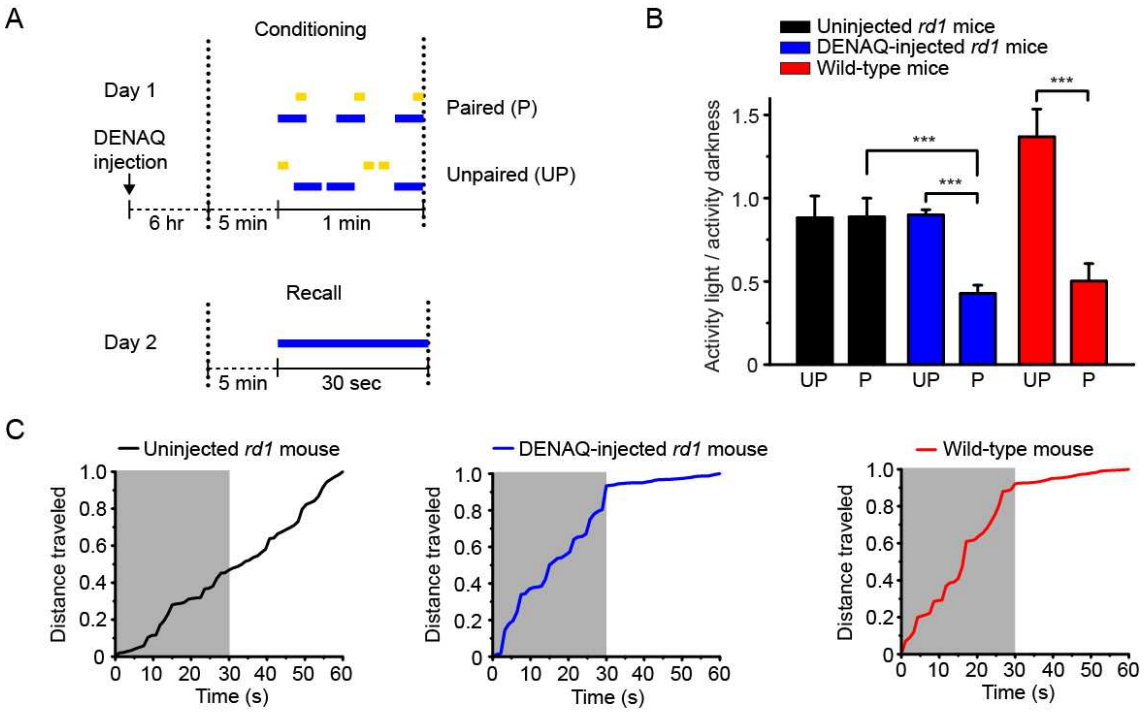

Figure 3.9: A) Diagram of the paired, unpaired conditioning and recall protocols for the visual fear conditioning assay. Electric footshock (yellow) and light flash episodes (blue) are shown. B) Bar graph of activity in light divided by activity in darkness for uninjected rd1 (n=10 mice, p=0.98), 10mM DENAQ-injected rd1 (n=10 mice, p<0.001) and WT mice (n=10 mice, p<0.001) during the recall trial of the experiment. Data are mean ± SEM. C) Cumulative distance traveled by an uninjected rd1 mouse (left, black), a 10mM DENAQ-injected rd1 mouse (middle, blue) and a WT mouse (right, red) during the 30 seconds in darkness preceding the light flash and subsequent 30 seconds in the light.

blind mice *in vitro* and *in vivo*. However, the first generation photoswitch AAQ possessed a number of properties which rendered it unsuitable for clinical testing in patients. The novel compounds presented in this study, DENAQ and BENAQ, overcome all of AAQs shortcomings. They obviate the need for retinal stimulation with UV light as well as demonstrate greatly increased light sensitivity, even proving to be more sensitive to light than the microbial opsins ChR2 and NpHR. Unlike AAQ, these compounds persist up to several weeks in the eye and are not toxic *in vivo*. Given their long-lasting effect, DENAQ and BENAQ can potentially be administrated in the clinic through a monthly schedule of intraocular injections, which is already well-established and safely utilized for other treatments of AMD (Comparison of Age-related Macular Degeneration Treatments Trials Research et al., 2012). Additionally, we hope to extend the compounds lifetime *in vivo* through the use of appropriate slow release formulations (London et al., 2011a). The pharmacological nature of our therapy means that a molecules dose can be titrated for optimal effect in individual patients,

and its reversibility should minimize potential retinal damage. Additionally, a preliminary injection of a photoswitch molecule can also be used to evaluate the function of remaining visual pathways in a blind patient, before selecting the therapeutic approach most suited to that individual.

Our red-shifted photoswitches are selective for degenerated, but not healthy retinal tissue, suggesting there may be a difference in the molecules access to degenerated retinal neurons or a molecular target upregulated during degeneration. The fact that DENAQ and BENAQ do not alter WT mouse retinal light responses suggests they will not interfere with photoreceptor-mediated light responses in human patients. Our compounds may thus not only provide a therapeutic benefit to patients with end-stage degenerative diseases by restoring light sensitivity to the entire retina, but also improve the diminishing vision of patients with mid-stage degeneration by selectively photosensitizing areas of the retina undergoing degeneration while leaving the remaining intrinsic light responses intact.

Intravitreal injection of DENAQ not only restores light sensitivity to blind mice in an open field locomotory assay, but creates a sufficiently useful visual perception for learning to take place. More sophisticated tests of visual acuity, such as restoration of the optomotor response, have not yet been conclusively demonstrated after expression of microbial optogenetic tools (Thyagarajan et al., 2010). These assays may require extended training of the animals. Training has also been shown to improve the visual task performance of patients implanted with optoelectronic prosthetics (Humayun et al., 2012), and the hearing of patients with cochlear implants (Stacey et al., 2010). The fact that the polarity of the behavioral response to light in DENAQ-injected mice can be reversed by the appropriate conditioning leads us to believe that, with the appropriate training, human patients should be able to interpret the novel visual stimulus conferred by the administration of our red-shifted photoswitches and obtain a useful visual perception of their surroundings.

While further screening of our chemical library may well generate molecules with even more favorable properties, DENAQ and BENAQ are the first candidate molecules ready to be tested in large animal models of blindness and eventually in humans suffering from retinal degeneration. We believe that these compounds and our opto-pharmacological approach in general, will prove capable of restoring vision to blind patients.

Chapter 4

Physiological Changes of Retinal Ganglion Cells during Retinal Degeneration

Preface: Laboratory technician Andy Noblet provided valuable technical assistance.

4.1 Summary

During retinal degeneration, anatomical and physiological changes have been observed in the outer nuclear layer (ONL); however, it is unclear whether RGCs also undergo physiological changes. We specifically focused on P2XRs and TRPV1 channels, due to their active role in many neurodegenerative diseases. Our lab developed a molecule, QAQ, which enters cells through active P2XRs and TRPV channels and acts as a reporter of inflammatory events in the nervous system. This method enables us to optically manipulate RGCs from retinal degenerated mice. Using QAQ we found that P2XRs and TRPV1 channels are either upregulated or chronically activated on RGCs only during retinal degeneration.

4.2 Introduction

Retinal degeneration is a blinding disease that leads to degeneration of rods and then cones, causing drastic anatomical and physiological changes of the downstream retinal circuitry (Punzo and Cepko, 2007; Strettoi and Pignatelli, 2000). One of the outcomes of this degeneration is an increased activity of the retina, characterized by heightened firing rates of RGCs (Stasheff, 2008). Margolis et al. (2008) found that rd1 RGCs experience rhythmic spike activity which was abolished by using synaptic blockers, therefore concluding that the hyperactivity arises exclusively from the synaptic inputs in the rd1 mice. Also, no difference was found between the rd1 and WT RGC ON and OFF RGCs rebound spiking. Anatomically, by filling the RGCs with fluorescent Ca^{2+} indicator imaging the dendritic stratification of the RGCs with two-photon fluorescence microscopy Margolis et al. (2008) also found no difference compared to the WT. Consequently, these findings suggest that retinal degeneration does not lead to any physiological or anatomical changes of the RGCs . However, during retinal degeneration apoptotic photoreceptors release large amounts of ATP and other neurotransmitters into the extracellular space and it is unknown how these high concentrations of neurotransmitters influence the physiological state of RGCs.

Purinergic receptors are activated by ATP and have been found to play a role in neurotransmitter release and mediation of neuronal injury (Khakh and North, 2012). P2X2, P2X4, and P2X7 receptors when exposed to a brief agonist application become permeable to Ca^{2+}, Na^{+}, and K^{+} ions. However, under a prolonged exposure to an agonist they enhance permeability to cations that are up to 900 Da, such as the fluorescent YO-PRO dye (Surprenant et al., 1996; Rassendren et al., 1997). TRPV1 channel from a TRP family is also expressed throughout the CNS and has similar pore dilating properties as P2X2, 4, and 7 receptors and is highly permeable to Ca^{2+} and larger cations. Due to their high permeability to Ca^{2+} and ability to pore dilate, P2XRs and TRPV1 channels have been implicated in many neurodegenerative diseases, brain trauma, and ischemia (Sorge et al., 2012; Sappington et al., 2008; Sharp et al., 2008).

P2XRs and TRPV1 channels are expressed in bipolar, amacrine, retinal ganglion cells and retinal microglia (Mitchell et al., 2009) and have also been suggested to play a pathological role during retinal degeneration and glaucoma. For example, *in-vivo* intraocular injections of bzATP, a potent P2XR agonist, into neonatal rats led to RGC death, which was prevented by the addition of P2X7 receptor blocker brilliant blue G (Hu et al., 2010). In DBA/2 glaucoma mouse model, TRPV1 levels increased with elevated intraocular pressure (Sappington et al., 2008). In the same study, TRPV1 antagonist reduced apoptosis and RGC intracellular Ca^{2+} in isolated RGCs under pressure.

To determine whether pore dilation plays a role in inducing RGC death, Innocenti et al. (2004) applied a P2X7R agonist bzATP and only induced YO-PRO (a fluorescent dye) loading in microglia and not in RGCs of WT freshly isolated WT rat retinas, implicating that these receptors do not pore dilate on RGCs. P2XR and TRPV channel pore dilation has not been explored in detail in RGCs of retinal degenerating mouse models. Given the possible pathological and functional role of these receptors, it is important to determine

whether they play a role in altering physiological state of RGCs during retinal degeneration and glaucoma.

We used a novel molecule QAQ that enables optical control of ion channels without genetic manipulation during inflammatory condition (Mourot et al., 2012). Application of ATP or capsaicin, a potent P2XR or TRPV1 agonist respectively, caused QAQ loading into HEK-293 cells through P2X7 and TRPV1 pores, which was quantified by measuring the amount of photosensitization of the cell. Using QAQ we demonstrate that P2XRs and TRPV1 channels are upregulated and/or activated during retinal degeneration. QAQ does not photosensitize RGCs in WT and glaucoma mice, enabling us to only optically control RGCs undergoing molecular remodeling during degeneration.

4.3 Materials and Methods

4.3.1 Animals

WT mice (C57BL/6J strain, Jackson Laboratory), for glaucoma experiments WT mice SV129, Jackson Laboratory) and (homozygous rd1/rd1 mice (C3H/HeJ strain, Charles River Laboratories) >3 months old were used in our experiments. All animal use procedures were approved by the UC Berkeley Institutional Animal Care and Use Committee.

4.3.2 Electrophysiology and pharmacology

Mouse retinas were dissected and kept in physiological saline at 36°C containing (in mM): 119 NaCl, 2.5 KCl, 1 KH_2PO_4, 1.3 $MgCl_2$, 2.5 $CaCl_2$, 26.2 $NaHCO_3$, 20 D-glucose, aerated with 95% O_2/5% CO_2. For extracellular recording, the retina was placed ganglion cell layer down onto a multielectrode array system (model number MEA 1060-2-BC, Multi-Channel Systems).

Mouse retinas were dissected and kept in physiological saline at 37°C containing (in mM) 119 NaCl, 2.5 KCl, 1 KH_2PO_4, 1.3 $MgCl_2$, 2.5 $CaCl_2$, 26.2 $NaHCO_3$, and 20 D-glucose, aerated with 95%O_2/5%CO_2. For extracellular recordings, the retina was placed ganglion cell layer down onto a multielectrode array system (MEA 1060-2-BC, Multi-Channel Systems). The MEA electrodes were 30 μm in diameter and arranged in an 8×8 rectangular grid. Extracellular spikes were high-pass filtered at 200 Hz and digitized at 20 kHz. A spike threshold of 4SD was set for each channel. Typically, each electrode recorded spikes from one to three RGCs. Principal component analysis of the spike waveforms was used for sorting spikes generated by individual cells (Offline Sorter, Plexon). Only cells with interspike intervals of <1 ms were included in the analysis.

To block synaptic contributions of different retinal neurons to RGCs, the following neurotransmitter receptor antagonists were used: 4 μM SR-95531 (gabazine) for $GABA_A$ receptors, 10 μM 1,2,5,6 tetrahydropyridin-4-yl)methylphosphinic acid (TPMPA) for $GABA_C$ receptors, 10 μM initroquinoxaline-2,3-dione disodium salt (DNQX) for non-NMDA type glu-

tamate receptors, 50 μM d-(-)-2-Amino-5-phosphonopentanoic acid (AP5) for NMDA-type glutamate receptors, 10 μM strychnine for glycine receptors, 50 μM d-tubocurarine chloride (curare) for nicotinic acetylcholine receptors, 10 μM D, L-2-amino-4-phosphonobutyric acid (L-AP4) mGluR4 agonist. 100μM 2',3'-O-(2,4,6-Trinitrophenyl)adenosine-5'-triphosphate tetra(triethylammonium) salt (TNP-ATP) for P2XR inhibition,
250μM 2'(3')-O-(4-Benzoylbenzoyl)adenosine-5'-triphosphate tri(triethylammonium) salt (bzATP) as a P2XR agonist, 50μM Ruthenium red (RR) as TRP channel andtagonist. All of these drugs were purchased from Sigma or Tocris.

4.3.3 Light Stimulation

In most MEA recordings, we used a 100 W mercury arc lamp filtered through 380 or 500 nm filters (Chroma, Inc), and switched wavelengths with an electronically-controlled shutter and filter wheel (SmartShutter, Sutter Instruments). Unless otherwise indicated, the standard incident light intensity at the retina was 13.4 mW/cm^2 ($2.56 * 10^{16}$ photons/cm^2/s) for 380 nm and 11.0 mW/cm^2 ($2.77 * 10^{16}$ photons/cm^2/s) for 500 nm.

4.3.4 IOP elevation protocol

Mice were injected with microbeads (2 μl of 10 μm in diameter) in the left eye and the IOP was maintained with repeated injections of microbeads every 2-4 weeks. Right eye was injected with 2 microliter of PBS (commercial grade from Invitrogen).

4.3.5 Data Analysis and Statistics

Protocol Each retina was exposed to 20 trials of 5 second alternating 380 and 500 nm lights.
Photoswitch Index (PI) To characterize RGC photosensitivity as normalized responses to light, we first calculated Photoswitch Index (PI) values defined as

$$\text{Photoswitch Index (PI)} = \frac{\text{Firing rate in 380} - \text{Firing rate in 500}}{\text{Firing rate in 380} + \text{ Firing rate in 500}}$$

For PI calculations we take only the first 1/2 of the 380 nm light and 500 nm light intervals. The threshold for 'photoswitching' is defined as RGC PI values >0.37 (n = 11 retinas, n = 803 cells). This value is the median PI for QAQ alone experiments that divided the two distributions in two, cells centered around zero and cells centered around higher positive PI values. **Maximum Firing Rate (MFR)** The firing rates for each cell are condensed into one 380 nm and 500 nm light set. Then, the MFR is calculated by finding the maximum firing rate of each cell across the two lights. The maximum firing rate is plotted in red. Blue bars denote the average MFR across cells binned at 200 ms.
Latencies Latencies are calculated only for cells that passed the photoswitching threshold of PI > 0.37 and defined as the time it took to reach the first 100 ms MFR density bin. Distributions were first tested for normality using the Shapiro-Wilk test. For non-normal

distributions, the Wilcoxon rank sum test was used for pairwise comparisons. The 95% confidence intervals for medians were generated by resampling the original distributions and applying the bias-corrected percentile method (Efron and Tibshirani, 1986). Results with $p < 0.05$ were considered significant.

4.4 Results

We first determined whether we can load a membrane impermeant molecule (QAQ), that enters cells through large pores in the membrane, into RGCs. After the molecule permeates into a cell we can use it to silence RGCs by optically regulating voltage gated Na^+, Ca^{2+}, and K^+ channels with 380 and 500 nm light. As described in the Thesis Introduction, 500 nm light turns the molecule into *trans*-form thus blocking voltage-gated channels and 380 nm light turns the molecule back into the *cis*-form unblocking the channels. In order to isolate RGC responses, all of the experiments were recorded from retinas on a multielectrode array in the presence of synaptic blockers (DNQX, AP5, AP4, TPMPA, Gabazine, strychnine, and curare).

In the presence of synaptic blockers and absence of QAQ treatment, light did not have any effect on the control rd1 and WT RGC firing, rd1 median PI = -0.048 [95% CI: -0.067 to -0.034] (n = 277) and WT median PI = 0 [95% CI: -0.041 to 0.01] (n = 134, $p > 0.5$), see Figure 4.1 and Figure 4.2. A PI value of +/- 0.37 was chosen to characterize the cells into photoswitching and non-photoswitching (see Methods for details). Cells that were either higher than 0.37 or lower than -0.37, were considered photoswitching. We found that out of all the RGCs recorded, only 8 % of cells photoswitched (PIs > 0.37) in both WT and rd1 retinas. Out of those RGCs, maximum firing rate densities (MFRDs) for rd1 and WT group were spread out across the two intervals, with 55% of rd1 RGCs having MFRs in the 380 nm light and for WT, 54.5% of RGCs had MFRs in 380 nm light. Intrinsically light sensitive ipRGCs could potentially account for small part of these light responses, since these cells account for about 3% of the RGCs in a mouse retina (Hattar et al., 2002).

4.4.1 QAQ only photosensitizes rd1 RGCs

We asked whether rd1 or WT RGCs have active P2XRs or TRPV channels that admit QAQ. If they are chronically active or highly expressed, QAQ would permeate into the cells and we would optically regulate the RGC firing. After treating WT retinas with 1mM QAQ for 30 minutes followed by washout, we show in Figure 4.1 that QAQ (30 minute treatment with 1mM QAQ) has no significant difference from the control untreated WT retinas, with PI = 0.05 [95% CI: 0.03 to 0.07], $p > 0.05$, only photosensitizing 7.4% of cells(Figure 4.1B,C,D).

However, when we conducted the same treatment on rd1 mice, QAQ clearly photosensitized RGCs with a significant increase of cells responding to 380 nm light and inhibiting firing to 500 nm light (median PI = 0.36 [95% CI: 0.32 to 0.41] , n = 803, $p < 0.05$) (Figure 4.2B,C,D). QAQ photosensitized 51% of rd1 RGCs with 89% of these cells having MFRs

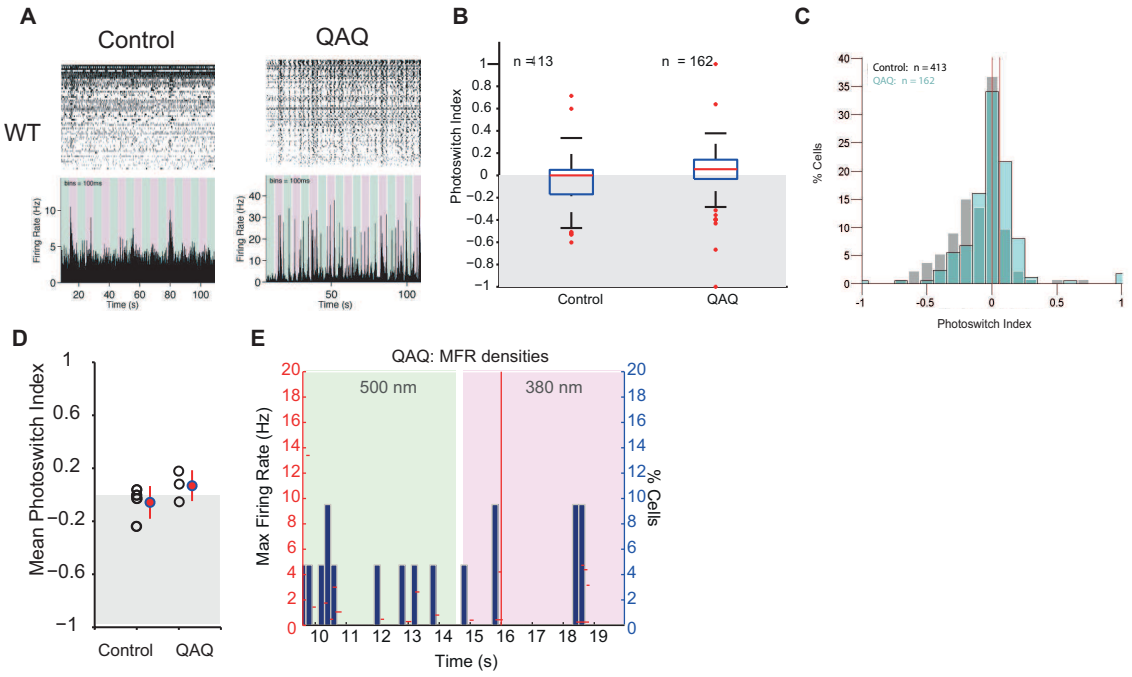

Figure 4.1: QAQ does not load into WT mouse RGCs. (A) Multi-electrode recordings from flat-mounted WT mouse retinas before (left) after treatment with QAQ (1mM for 30 min, followed by washout). Recordings were done in the presence of synaptic blockers (see Methods for details). Top, raster plot of spiking from RGCs; bottom, average RGC firing rate calculated in 100 msec time bins. Color bars represent illumination with 380 nm (violet) or 500 nm light (green). (B,C)Analysis of photoswitching of the entire population of RGCs from all untreated retinas and all QAQ-treated WT retinas. Comparison of PIs of RGCs from untreated Control retinas (n = 4) and QAQ treated retinas (n = 3), displayed in a box plot (B) and as a histogram (C). For untreated WT median PI = 0 [95% CI: -0.041to 0.01] (n = 134 cells), and for QAQ treated WT RGCs median PI = 0.05 [95% CI: 0.03 to 0.07] (n = 162 cells), indicating no photoswitching. Whiskers denote 1.5 times the interquartile range from the 25th and 75th percentile. The two groups are not significantly different ($p > 0.05$, Mann-Whitney test). (D)Average RGC PI for individual retinas in Control and QAQ treated conditions (black circles). Red symbols show mean values and error bars represent standard error of the mean (s.e.m.). (E) Maximum Firing Rate density plot of of QAQ treated RGCs that photoswitched (8%), with with 47% of RGCs, MFR density is in the light. Blue line represents the Mean Latency for the cells in the light.

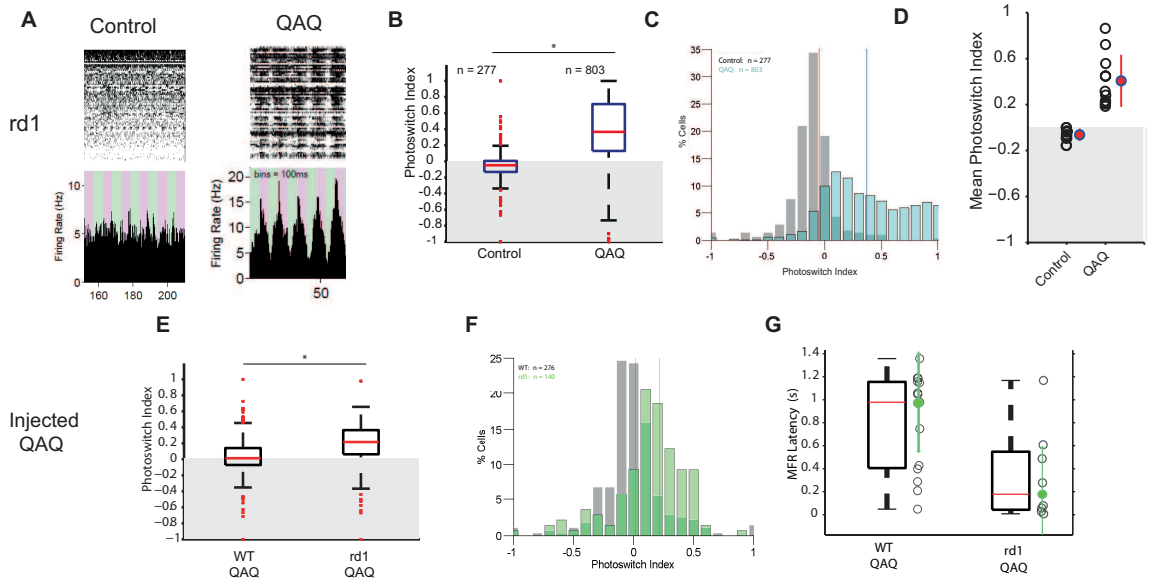

Figure 4.2: QAQ only photosensetizes rd1 RGCs. (A) Multi-electrode recordings from flat-mounted rd1 mouse retinas before (left) and after QAQ treatment (right) under the same conditions as WT. Top, raster plot of spiking from RGCs; bottom, average RGC firing rate calculated in 100 msec time bins. Color bars represent illumination with 380 nm (violet) or 500 nm light (green). (B,C)Analysis of photoswitching of the entire population of RGCs from all untreated retinas (n = 4) and QAQ-treated rd1 retinas (n = 3). Comparison of PIs of RGCs are displayed in a box plot and as a histogram (C). Median PI value for control untreated rd1 RGCs is -0.048 [95% CI: -0.041to 0.01] (n = 277) signifying no photoswitching and after QAQ treatment we see a significant increase in firing rates with median PI = 0.36 [95% CI: 0.32 to 0.41] (n = 803, $p < 0.05$, Mann-Whitney test). (D) Average RGC PI for individual retinas in Control and QAQ treated conditions (black circles). Red symbols show mean values and error bars represent standard error of the mean (s.e.m) (E) Analysis of photoswitching of the entire population of RGCs from all WT QAQ-treated retinas (n = 5 retinas) and QAQ-treated rd1 retinas (n = 3 retinas). Comparison of PIs of RGCs are displayed in a box plot and as a histogram (F). Median PI value for WT QAQ-treated RGCs is 0.01 [95% CI: 0 to 0.033] (276) signifying no photoswitching and after QAQ treatment we see a significant increase in firing rates with median PI = 0.36 [95% CI: 0.32 to 0.41] (n = 803, $p < 0.05$, Mann-Whitney test). (G) Box plots represent grouped photosensitive RGC latencies of WT and rd1 QAQ injected conditions. Open black circles represent RGC latencies, the green circles indicating the median plus or minus the bootstrapped 95% confidence intervals.

in the 380 nm light (Figure 4.4E). The majority of the cells had MFR densities concentrated at the beginning of the 380 nm light pulse, taking only 1 s for 50% of the RGCs to reach the MFR, with with median latency of 765 ms (Figure 4.4G).

4.4.2 P2XR agonist enhances QAQ induced photosensitization in rd1 RGCs

The next two questions were whether we could induce QAQ loading in WT mice by applying bzATP, a potent P2XR agonist, and if bzATP could increase photosensitization of the rd1 RGCs. We found that bzATP (250 μM) has no effect on QAQ loading in WT RGCs (median PI = 0.03, p >0.05), with no significant difference from the QAQ only (Figure 4.3), with only 7% of WT RGCs photoswitching. This is consistent with Innocenti et al. (2004) study, where bzATP did not induce YO-PRO (a large fluorescent dye) loading in WT RGCs.

However, bzATP seemed to slightly increase QAQ loading in rd1 RGCs compared to QAQ alone, with mean PI = 0.365 and p < 0.05 and 57% of RGCs responding to light(Figure 4.4). Out of the photoswitching cells, 58% had MFRs in the 380 nm light (Figure 4.4F) and even though it's a smaller percentage than was observed during QAQ-only treatment we found that the median latency light response was significantly shorter, 286 ms (p < 0.05) (Figure 4.4G) As expected, if the intracellular concentration of QAQ is higher, the time it should take for the cell to photoswitch would be much shorter. Consequently, it is possible that bzATP induced more QAQ loading by opening more pore dilated channels and thereby enhances photosensitization of RGCs, allowing for fast optical control of its firing rate.

4.4.3 TNP-ATP, P2XR antagonist, decreases QAQ induced photosensitization (loading)

In order to determine whether QAQ loading occurs only through the P2XRs, we co-applied a high concentration of a potent P2XR antagonist TNP-ATP (100 μM) with QAQ (1mM) for 30 minutes (Figure 4.5A). The TNP-ATP + QAQ treatment shows a significant decrease across all the pooled RGCs, with median PI = 0.17 (n = 525 RGCs, p < 0.05, Figure 4.5A,B,C). The average PI for individual retinas also showed a significant decrease compared to the QAQ only condition (Figure 4.5D). TNP-ATP does not completely eliminate QAQ loading, with only 34.9% of RGCs responding to light, and taking 2.3 seconds for 50% of the cells in the light to reach MFR (Figure 4.5E,F).

4.4.4 TRPV channel pores may be involved in QAQ loading

To determine whether TRP channels are involved in QAQ loading, we co-applied QAQ (1mM) and ruthenium red (RR) (50 μM), a widely used TRPV channel pore and aqueous pore blocker (Vriens et al., 2009). We found that RR reduced QAQ + bzATP loading even more compared to TNP-ATP with only with only 20.1% of cells photoswitching. There was

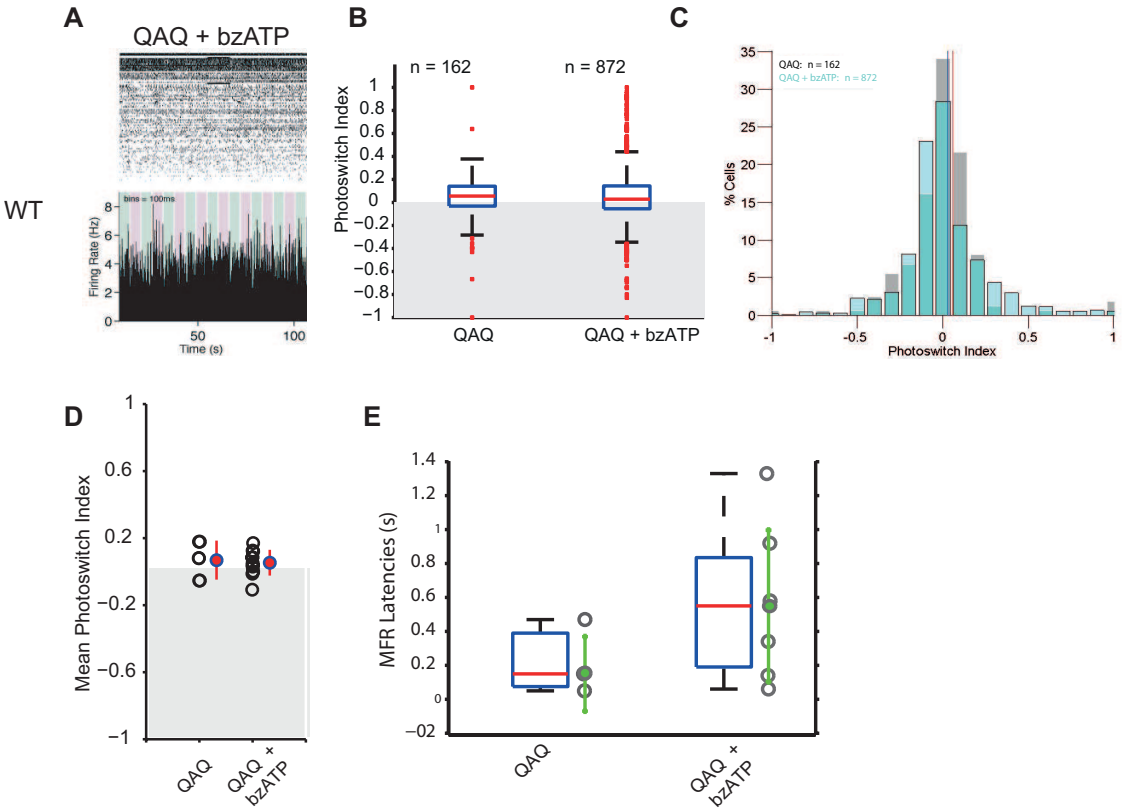

Figure 4.3: bzATP does not enhance QAQ loading in WT RGCs. (A) Multi-electrode recordings from flat-mounted rd1 mouse retinas before (left) after 30 min loading of QAQ + bzATP. Top, raster plot of spiking from RGCs; bottom, average RGC firing rate calculated in 100 msec time bins. Color bars represent illumination with 380 nm (violet) or 500 nm light (green). (B,C)Analysis of photoswitching of the entire population of RGCs from QAQ treated (n = 4) and bzATPand QAQ-treated WT retinas (n = 11). Comparison of PIs of RGCs are displayed in a box plot and as a histogram (C). Median PI value for QAQ and bzATP is -0.028 [95% CI: -0.018 to 0.037] signifying no photoswitching (n = 872 cells, p > 0.05, Mann-Whitney test). (D) Average PIs per individual retina in QAQ and QAQ+bzATP treated conditions (open black circles). Red symbols show mean values and error bars represent standard error of the mean (s.e.m.)t (E) Box plots represent grouped photosensitive RGC latencies in QAQ and QAQ+bzATP WT conditions. Open black circles represent individual RGC latencies, the green circles indicating the median plus or minus the bootstrapped 95% confidence intervals.

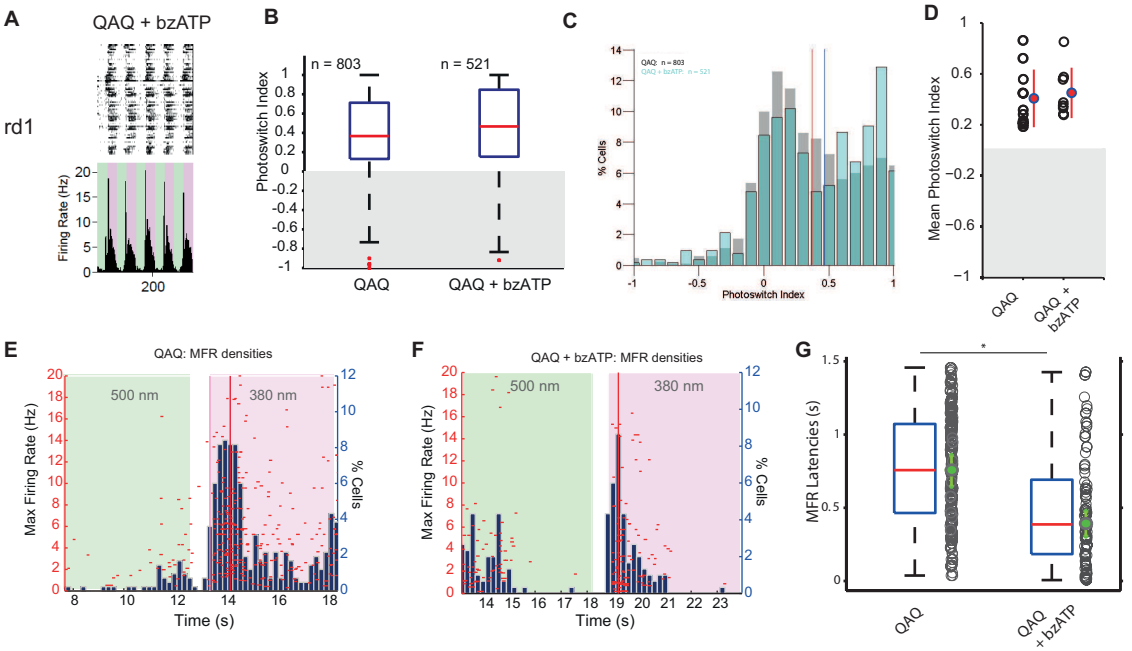

Figure 4.4: bzATP enhances QAQ loading in rd1 RGCs. (A) Multi-electrode recordings from flat-mounted rd1 mouse retinas before (left) under the same conditions as WT. Top, raster plot of spiking from RGCs; bottom, average RGC firing rate calculated in 100 msec time bins. Color bars represent illumination with 380 nm (violet) or 500 nm light (green). (B,C)Analysis of photoswitching of the entire population of RGCs from QAQ treated (n = 11) and bzATPand QAQ-treated rd1 retinas (n = 8). Comparison of PIs of RGCs are displayed in a box plot and as a histogram (C). Median PI value (shown as a blue line on the histogram) for QAQ and bzATP is 0.46 [95% CI: 0.38 to 0.57] demonstrating a significant increase in firing rate compared to QAQ only condition, (n = 525, $p < 0.05$, Mann-Whitney test). (D) Average PIs per individual retina in QAQ and QAQ+bzATP treated conditions (black circles). Red symbols show mean values and error bars represent standard error of the mean (s.e.m.) (E) Maximum Firing Rate density plot of QAQ only treated RGCs that photoswitched (51.06%), with 89.4% of these cells having MFR densities is in the light. Blue line represents the Mean Latency for the cells in the light. (F) Maximum Firing Rate density plot of QAQ + bzATP treated RGCs that photoswitched (57.39%), with with 47% of RGCs, MFR density is in the light. Blue line represents the Mean Latency for the cells in the light. (G) Box plots represent grouped photosensitive RGC latencies in QAQ and QAQ+bzATP conditions. Open black circles represent individual RGC latencies, while the green circles indicating the median plus or minus the bootstrapped 95% confidence intervals.

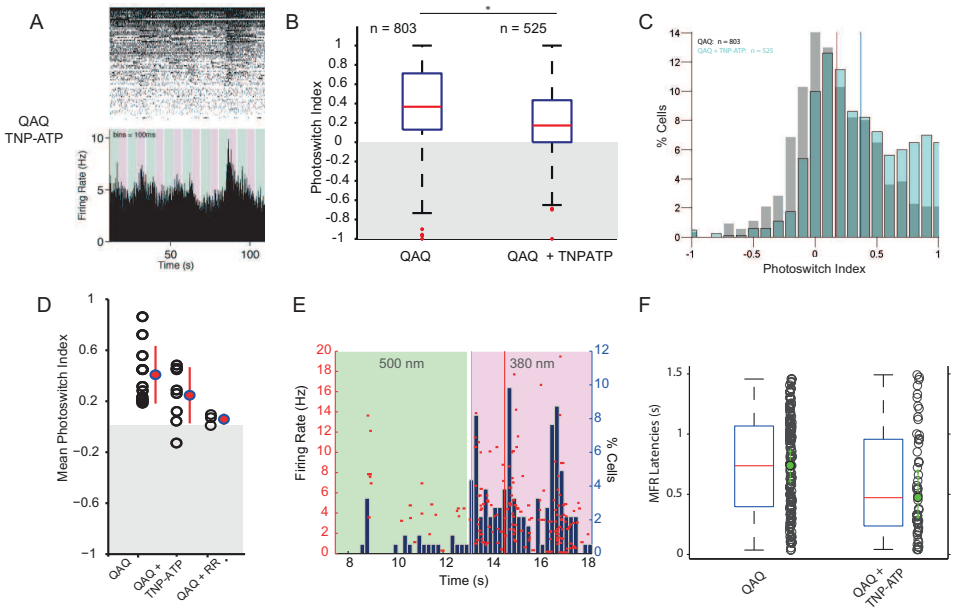

Figure 4.5: TNP-ATP decreases QAQ loading in rd1 RGCs. (A) Multi-electrode recordings from flat-mounted rd1 mouse retinas after 10 min TNP-ATP (100 μM) application, followed by a 30 min TNP-ATP + QAQ application and a washout. Top, raster plot of spiking from RGCs; bottom, average RGC firing rate calculated in 100 msec time bins. Color bars represent illumination with 380 nm (violet) or 500 nm light (green). (B,C) Analysis of photoswitching of the entire population of RGCs from QAQ treated (n = 11) and TNP-ATP + QAQ rd1 retinas (n = 8). Comparison of PIs of RGCs are displayed in a box plot and as a histogram (C). Median PI value (shown as a blue line on the histogram) for QAQ and TNP-ATP is 0.17 [95% CI: 0.14 to 0.20] signifying an significant decrease in firing rate compared to QAQ only condition, ($p < 0.05$, Mann-Whitney test). (D) Average PIs per individual retina in treated conditions (black circles). Red symbols show mean values and error bars represent standard error of the mean (s.e.m.). (E) Maximum Firing Rate density plot of QAQ +TNP-ATP treated RGCs that photoswitched (34.9%), with with only 33.3% of those RGCs have their MFR density in 380 nm light. Blue line represents the Mean Latency for the cells in the light. (F) Box plots shows a comparison of rd1 RGC latencies in QAQ and QAQ+TNP-ATP conditions. Open black circles represent individual RGC latencies, The green circles indicating the median plus or minus the bootstrapped 95% confidence intervals.

also a significant decrease in firing rates compared to the QAQ only treatment with median PI for all cells -0.056 [95% CI: -0.08 to -0.03] (n = 177, $p < 0.05$, Figure 4.6A,B). However, it is important to emphasize that RR is a non-selective blocker TRPV channel blocker and also an inhibitor of a variety of Ca^{2+} binding proteins (Charuk et al., 1990), voltage-gated L-type Ca^{2+} channels (Cibulsky and Sather, 1999), Ca^{2+} activated K^+ channels (Hirano et al., 1998), and whether it blocks P2XR pores is still to be determined.

Given the nonspecific effects of RR, we wanted to confirm that it blocks the channel pores and doesn't interfere with QAQ's ability to photosensitize voltage-gated channels. We pre-loaded the rd1 retina with QAQ and bzATP followed by a 20 min perfusion of RR with presynaptic blockers (described in Methods). In (Figure 4.6A,B) we clearly see

that QAQ was able to photosensitize 49.4% of RGCs even with RR with Median PI values of 0.40 [95% CI: 0.32 to 0.49], thus demonstrating that it does not significantly change QAQ's photosensitization ability ($p > 0.05$). (Figure 4.6D,E) shows that out of the cells that photoswitched, 83.5% of cells had their MFRs in the 380 nm light with median latency of 0.9s [95% CI: 0.5 to 1.3].

4.4.5 *In-vivo* QAQ application induces the same amount of QAQ loading into RGCs

Another concern we addressed was whether the state of pore dilation of P2XRs or TRPV channels *in-vivo* was different than *ex-vivo*. Since all the QAQ treatments were conducted after extraction of the retina, as described in the Thesis Introduction, the amount of ATP and the effects of IOP in an intact eye could lead to more activated pore dilating channels leading to different results *in-vivo* vs *ex-vivo*. Consequently, we injected 2μL of 1mM QAQ into WT and rd1 mice, extracted the retinas, and measured the amount of QAQ loading on the MEA. We found that similar to the *ex-vivo* preparation, QAQ loaded only into the rd1 mice and not into the WT (Figure 4.2E,F), WT median PI = 0.01 [95% CI: 0 to 0.033] (n = 276 cells) and rd1 median PI = 0.216 [95% CI: 0.16 to 0.251] (n = 140 cells, $p < 0.05$). The amount of photoswitching was similar to QAQ loading in an *ex-vivo* preparation ($p > 0.05$), photoswitching 34.1% of the RGCs, with 100 ms median MFR latencies for rd1 RGCs. This may imply that the difference in ATP concentrations and the IOP between the *ex-vivo* and *in-vivo* setups is not enough to trigger pore dilation in either animal model and that the *ex-vivo* experimental setup is a valid model for studying physiological changes in the RGCs.

4.4.6 QAQ does not photosensitize RGCs from induced glaucoma mice

To our surprise, QAQ did not photosensitize RGCs in the mouse model of glaucoma. Increased Intraocular Pressure (IOP) was induced in WT mice via microbead injections and maintained for either one or 10 weeks. IOP measurement curves at 1 and 10 weeks show that only the mice with microbead injections experienced heightened IOP, whereas the sham (PBS) injected mice did not (Figure 4.7A,B). We treated retinas of 1 and 10 week post bead injection WT animals for 30 minutes with QAQ and bzATP and found that QAQ does not load into any of the RGCs. Animals with high IOP after 1 week had median RGC PI = 0.065 [95% CI: 0.047 : 0.085] (n = 174) compared with sham injected animals with PI = 0.03038 [95% CI: 0.018 to 0.042] (n = 161, $p > 0.05$) (Figure 4.7CD). Retinas from the 10 week elevated IOP mice had median PI = 0.11 [95% CI: 0.088 to 0.138] (n = 486) and sham injected animals median PI = 0.143 [95% CI: 0.1 to 0.19] (n = 415, $p > 0.05$)(Figure 4.7EF). There was also no significant difference between the PI's of RGCs from both distributions ($p > 0.05$). After 10 weeks of high IOP, RGC death is usually observed, therefore the lack of

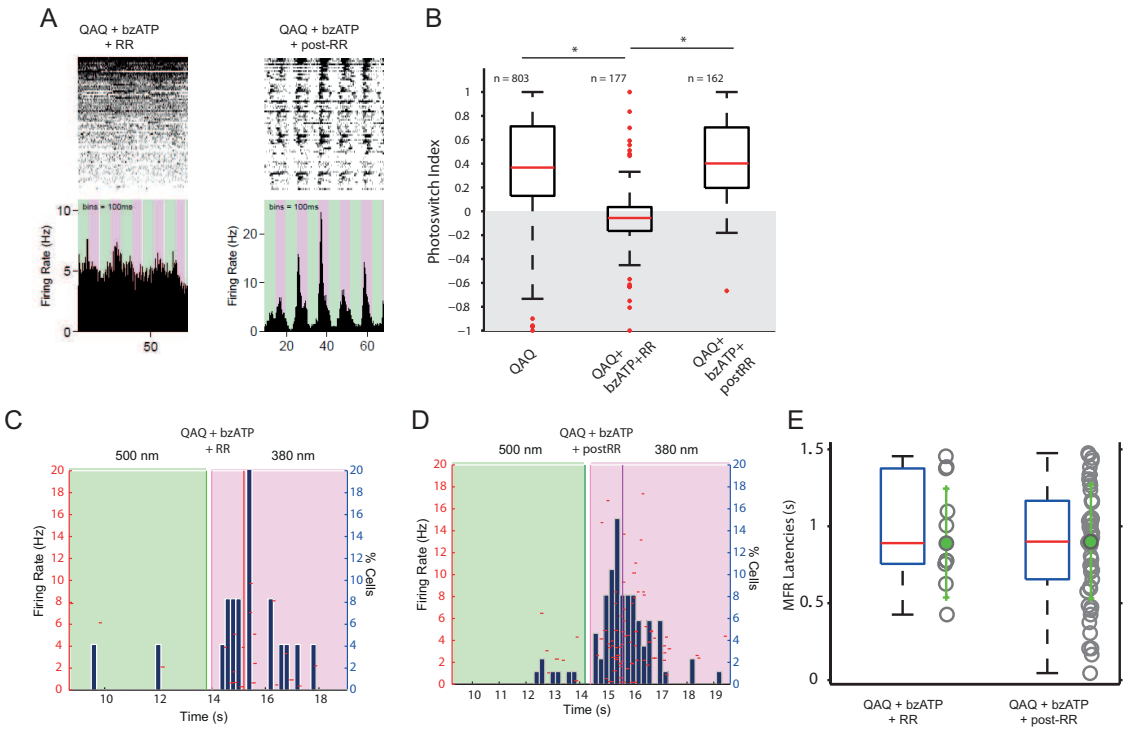

Figure 4.6: RR greatly reduces QAQ photosensitization. (A) LEFT: Multi-electrode recordings from flat-mounted rd1 mouse retinas after 10 min RR (50 μM) application, followed by a 30 min RR + QAQ + bzATP application, washout and continuous perfusion with synaptic blockers. Top, raster plot of spiking from RGCs; bottom, average RGC firing rate calculated in 100 msec time bins. Color bars represent illumination with 380 nm (violet) or 500 nm light (green). RIGHT: Multi-electrode recordings from flat-mounted rd1 mouse retinas after 30 min QAQ + bzATP treatment, a washout and perfusion with RR + synaptic blockers . Top, raster plot of spiking from RGCs; bottom, average RGC firing rate calculated in 100 msec time bins. Color bars represent illumination with 380 nm (violet) or 500 nm light (green). (B) Analysis of photoswitching of the entire population of RGCs from QAQ treated (n = 11 retinas) and RR+ bzATP + QAQ rd1 retinas (n = 3 retinas) and QAQ +bzATP with post treatment with RR (n = 2). Comparison of PIs of RGCs are displayed in a box plot and as a histogram (C). Median PI value (shown as a blue line on the histogram) for QAQ + bzATP + RR is -0.056 [95% CI: -0.08 to -0.03] signifying an significant decrease in firing rate compared to QAQ only condition, (n = 177 RGCs, $p < 0.05$, Mann-Whitney test). Median PI value for QAQ + bzATP with post-RR treatment is 0.40 [95% CI: 0.32 to 0.49], showing that RR did not alter QAQ's ability to photosensitize cells, (n = 162 RGCs, $p > 0.05$, Mann-Whitney test). (C) Maximum Firing Rate density plot of pre-RR and QAQ + bzATP treated RGCs that photoswitched (20.5 %), with 90% of those cells having FMRs in the 380 nm light. (D) Maximum Firing Rate density plot of QAQ + bzATP with post-RR treatment showing only the cells that photoswitched (49.38%), with with 83.5% cells having MFRs in the 380 nm light. (E) Box plots represent latencies in QAQ + bzATP pre and post-RR treatment conditions. Open black circles represent individual RGC latencies, The green cricles indicating the median plus or minus the bootstrapped 95% confidence intervals.

significant RGC photosensitization may suggest that the pore dilated state is more common under specific to conditions where photoreceptors degenerate, rd1.

4.5 Discussion

P2XRs and TRPV channels are the main focus of this study because of their unique ability to act as ligand-gated ion channels that become permeable to large cations and induce cell death from prolonged exposure to an agonist (bzATP or capsaicin) (Virginio et al., 1999; Virgilio et al., 2001). Their neurodegenerative function during inflammatory conditions in the CNS makes them a viable candidate for signifying pathological changes of retinal neurons during retinal degeneration. Using a QAQ molecule we showed that only during retinal degeneration, P2XRs and TRP channels on RGCs transition to an open/closed pore dilated state.

4.5.1 P2XRs are involved in pore dilation during retinal degeneration

We show that QAQ photosensitizes RGCs only in mouse models of retinal degeneration and not in WT mice. Photosensitization of 84% of rd1 RGCs with QAQ alone suggests that there are already pore dilated channels in RGCs, but it's not clear whether TRP channel or P2XRs play a bigger role. Loading QAQ with a potent P2XR agonist, bzATP, caused 64% of cells to respond to light with medium latencies of MFRs of 284 ms, compared with 780 ms of QAQ alone. This data clearly shows that bzATP alters QAQ induced responses to light, most likely by opening residual P2XR pores. This may lead to higher QAQ loading and shorter latencies due to QAQ molecules taking less time to block the voltage-gated channels.

In WT mice on the other hand, bzATP does not lead to any QAQ loading, suggesting that P2XRs are not active or not as highly expressed on RGCs under healthy conditions, which is consistent with previous studies (Innocenti et al., 2004). To confirm P2XRs role in QAQ loading, a competitive antagonist TNP-ATP led to a reduction of photosensitization of rd1 RGCs. It is thus possible that the TNP-ATP is competing for the ATP binding site and prevents channels from going into pore dilated state, but does not block the opened aqueous pores, or does not compete away all the ATP. Alternately there may be an additional pore dilating protein responsible for the remaining photoswitching.

4.5.2 TRPV Channels and Pore Dilation

TRPV channels could also be involved in QAQ loading but the lack of specific pore blocker pharmacology makes it difficult to test this hypothesis. Co-application of QAQ and RR completely prevented QAQ from loading into rd1 RGCs, suggesting that QAQ is getting into rd1 RGCs through the same pores as what RR blocks. Aware of RRs wide range of

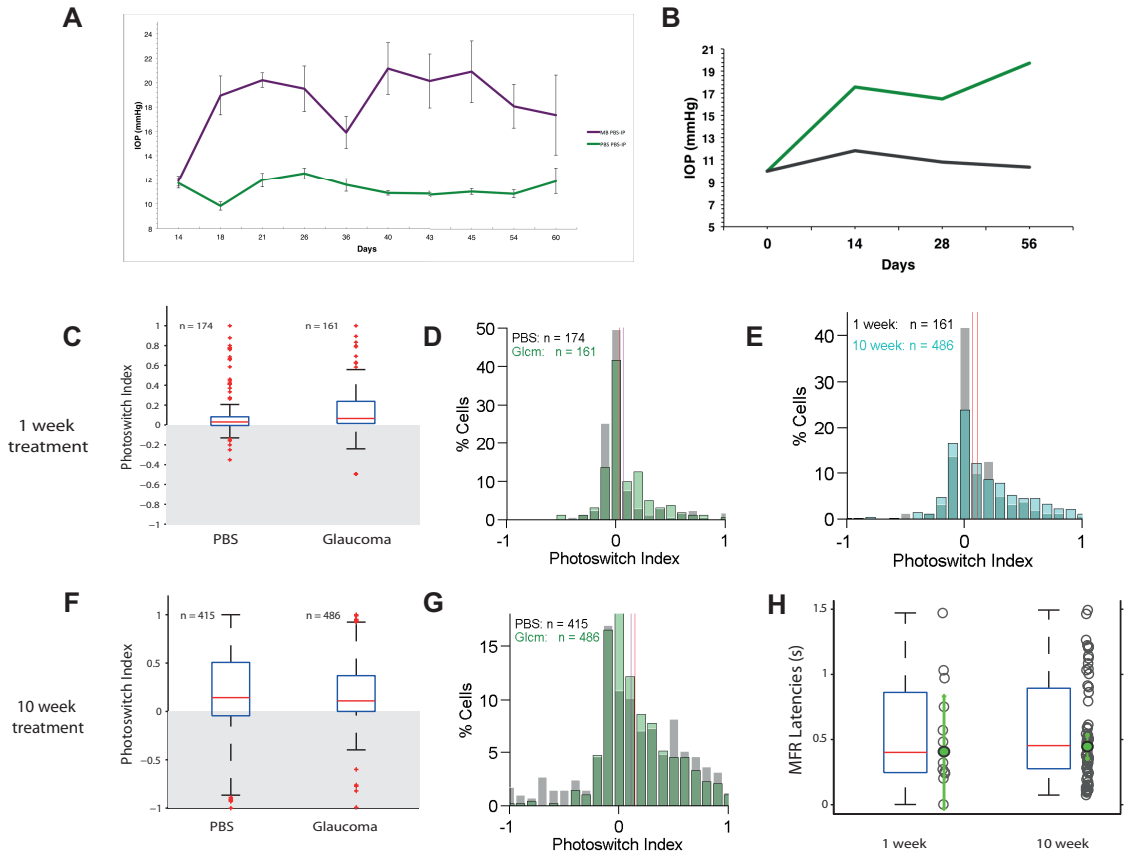

Figure 4.7: One and 10 weeks of IOP elevation is not sufficient to induce QAQ loading in WT RGCs. (A,B) IOP measurements of 10 mice over 60 days with one eye injected with microbeads in order to elevate IOP and the other (sham) injected with PBS (purple). (C) There is no photoswitching difference found between the entire population of RGCs from mice with elevated IOP for 7 days and sham (PBS-injected) mice. Comparison of all the PIs of RGCs are displayed in a box plot and as a histogram (D). Median PI value (shown as a blue line on the histogram) for microbead injected mice is PI = 0.065 [95% CI: 0.047 to 0.085] (n = 174) and the PI Median for the sham injected mice is 0.03038 [95% CI: 0.018 to 0.042] (n = 161, $p > 0.05$, Mann-Whitney test). (E) We also found no photoswitching difference found between the entire population of RGCs from mice with elevated IOP for 10 weeks and sham (PBS-injected) mice. Comparison of PIs of RGCs are displayed in a box plot and as a histogram (F). Median PI value (shown as a blue line on the histogram) for microbead injected mice is PI = 0.108 [95% CI: 0.08 to 0.136] (n = 486) and the PI Median for the sham injected mice is 0.142 [95% CI: 0.1 to 0.19] (n = 415, $p > 0.05$, Mann-Whitney test). (G) The histogram shows that there is no significant difference between the PI values of RGCs from 1 week and 10 week elevated IOP eyes ($p > 0.05$, Mann-Whitney test). (H) Box plots represent latencies one and ten week high IOP QAQ+bzATP conditions. Open black circles represent individual RGC latencies, The green circles indicating the median plus or minus the bootstrapped 95% confidence intervals.

targets, we made sure that it was not blocking the same voltage-gated channels that QAQ photoregulates.

4.5.3 Pore Dilation in Glaucoma

TRPV1 channels have also been implicated in cell death during glaucoma. We hypothesized that under a prolonged elevated IOP (1 and 8 weeks), RGCs would be more prone to QAQ loading. However, we were very surprised to find that even after 8 weeks of elevated IOP, QAQ did not load and photosensitize WT RGCs. Even an addition of bzATP with QAQ onto retinas extracted from the glaucoma induced mice did not lead to QAQ loading. We also saw no differences in photosensitization of RGCs in 1 week elevated IOP mice compared to 8 week IOP. It is not clear what conditions are needed in order to cause P2XRs or TRPV channels to pore dilate under these conditions, but perhaps high IOP leads to RGC death more quickly.

Finally, pore dilation is known to occur and let large dye molecules through the channels or via second messenger cascade (Browne et al., 2013). Though no dye or QAQ loading was seen in the healthy WT RGCs and glaucoma WT RGCs, photosensitization of RGCs in retinal degenerated mouse model may implicate pore dilation of these receptors as the first sign of a pathological state of the RGCs. This study clearly shows that RGCs undergo a physiological change during retinal degeneration.

4.6 Future Directions

This study demonstrates changes in the physiological state of the RGCs during retinal degeneration and provides a number of interesting future directions. A number of follow-up studies could help determine the pathways QAQ uses to get into the RGCs and the causes of lack of QAQ photosensitization of WT RGCs. Since clean pharmacology for blocking pore dilating channels is not available, to determine the path of entry of QAQ it would be interesting to cross TRPV1 or P2X7R knockout mice with rd1 mice, allowing us to eliminate one or both of these pore dilating channels from the system. This experiment would include MEA recordings from the knockout-rd1 mouse retinas to measure if the amount of photosensitization of RGCs has been altered compared to rd1 mice. If one of these receptors is involved in QAQ loading, then we expect to see a significant loss of QAQ induced photosensitization of RGCs. It is also possible that multiple pore dilating channels are involved and thus knocking out one of them may not have a very significant effect on QAQ loading; it may therefore be also necessary to knock out multiple channels.

It is also still unclear why QAQ does not load into WT RGCs, a few potential causes may be the inability of receptors to pore dilate or the low expression of P2XRs or TRPV channels. To address whether the protein levels of these receptors in RGCs differ in the two strains, a Western blot could be done on dissociated rd1 RGCs and wt RGCs. Fluorescence-activated cell sorting (FACS) could be used on dissociated retinas to determine which cell types and

how many cells express the desired P2XRs and TRP channels. Another possibility is that the voltage-gated channels that QAQ is photosensitizing may not be as highly expressed in the WT as in the rd1 mice, therefore in order to photosensitize the WT RGCs the same as rd1 RGCs, a higher concentration of QAQ would be required. This could be addressed by using FACS to look for surface expression of the possible candidate channels.

Bibliography

Acosta, M., E. Fletcher, S. Azizoglu, L. Foster, D. Farber, and M. Kalloniatis (2005). Early markers of retinal degeneration in rd/rd mice. *Molecular Vision 11*, 717–728.

Ahuja, A. K., J. D. Dorn, A. Caspi, M. J. McMahon, G. Dagnelie, L. Dacruz, P. Stanga, M. S. Humayun, R. J. Greenberg, and Argus II Study Group (2011, April). Blind subjects implanted with the Argus II retinal prosthesis are able to improve performance in a spatial-motor task. *The British journal of ophthalmology 95*(4), 539–543.

Artigas, J. M., A. Felipe, A. Navea, A. Fandino, and C. Artigas (2012, June). Spectral transmission of the human crystalline lens in adult and elderly persons: color and total transmission of visible light. *Investigative Ophthalmology & Visual Science 53*(7), 4076–4084.

Banghart, M. R., A. Mourot, D. L. Fortin, J. Z. Yao, R. H. Kramer, and D. Trauner (2009). Photochromic Blockers of Voltage-Gated Potassium Channels. *Angewandte Chemie International Edition 48*(48), 9097–9101.

Beltran, W. A., S. L. Boye, S. E. Boye, V. A. Chiodo, A. S. Lewin, W. W. Hauswirth, and G. D. Aguirre (2010). rAAV2/5 gene-targeting to rods:dose-dependent efficiency and complications associated with different promoters. *Gene Therapy 17*(9), 1162–1174.

Benav, H., K. U. Bartz-Schmidt, D. Besch, A. Bruckmann, F. Gekeler, U. Greppmaier, A. Harscher, S. Kibbel, A. Kusnyerik, T. Peters, H. Sachs, A. Stett, K. Stingl, B. Wilhelm, R. Wilke, W. Wrobel, and E. Zrenner (2010). Restoration of useful vision up to letter recognition capabilities using subretinal microphotodiodes. In *Annual International Conference of the IEEE Engineering in Medicine and Biology Society*, pp. 5919–5922.

Bi, A., J. Cui, Y.-P. Ma, E. Olshevskaya, M. Pu, A. M. Dizhoor, and Z.-H. Pan (2006, April). Ectopic expression of a microbial-type rhodopsin restores visual responses in mice with photoreceptor degeneration. *Neuron 50*(1), 23–33.

Bodin, P. and G. Burnstock (2001). Evidence That Release of Adenosine Triphosphate From Endothelial Cells During Increased Shear Stress Is Vesicular. *Journal of Cardiovascular Pharmacology 38*(6), 900.

Borowska, J., S. Trenholm, and G. B. Awatramani (2011). An Intrinsic Neural Oscillator in the Degenerating Mouse Retina. *Journal of Neuroscience 31*(13), 5000–5012.

Boyden, E. S., F. Zhang, E. Bamberg, G. Nagel, and K. Deisseroth (2005). Millisecond-timescale, genetically targeted optical control of neural activity. *Nat Neurosci 8*, 1263–1268.

Browne, L. E., V. Compan, L. Bragg, and R. A. North (2013). P2X7 receptor channels allow direct permeation of nanometer-sized dyes. *Journal of Neuroscience 33*(8), 3557–3566.

Busskamp, V., J. Duebel, D. Balya, M. Fradot, T. J. Viney, S. Siegert, A. C. Groner, E. Cabuy, V. Forster, M. Seeliger, M. Biel, P. Humphries, M. Paques, S. Mohand-Said, D. Trono, K. Deisseroth, J. A. Sahel, S. Picaud, and B. Roska (2010). Genetic reactivation of cone photoreceptors restores visual responses in retinitis pigmentosa. *Science 329*(5990), 413–417.

Caporale, N., K. D. Kolstad, T. Lee, I. Tochitsky, D. Dalkara, D. Trauner, R. Kramer, Y. Dan, E. Y. Isacoff, and J. G. Flannery (2011). LiGluR restores visual responses in rodent models of inherited blindness. *Molecular therapy : the journal of the American Society of Gene Therapy 19*(7), 1212–1219.

Carcieri, S. M., A. L. Jacobs, and S. Nirenberg (2003, September). Classification of retinal ganglion cells: a statistical approach. *Journal of Neurophysiology 90*(3), 1704–1713.

Carter-Dawson, L., M. LaVail, and R. Sidman (1978). Differential effect of the rd mutation on rods and cones in the mouse retina. *Investigative ophthalmology & ... 17*(6), 489–498.

Chader, G. J., J. Weiland, and M. S. Humayun (2009). Artificial vision: needs, functioning, and testing of a retinal electronic prosthesis. *Progress in brain research 175*, 317–332.

Charuk, J. H., C. A. Pirraglia, and R. A. Reithmeier (1990). Interaction of ruthenium red with Ca2(+)-binding proteins. *Analytical biochemistry 188*(1), 123–131.

Chaudhry, G. R., C. Fecek, M. M. Lai, W.-C. Wu, M. Chang, A. Vasquez, M. Pasierb, and M. T. Trese (2009). Fate of embryonic stem cell derivatives implanted into the vitreous of a slow retinal degenerative mouse model. *Stem cells and development 18*(2), 247–258.

Cibulsky, S. M. and W. A. Sather (1999). Block by ruthenium red of cloned neuronal voltage-gated calcium channels. *The Journal of pharmacology and experimental therapeutics 289*(3), 1447–1453.

Comparison of Age-related Macular Degeneration Treatments Trials Research, G., D. F. Martin, M. G. Maguire, S. L. Fine, G. S. Ying, G. J. Jaffe, J. E. Grunwald, C. Toth, M. Redford, and F. L. r. Ferris (2012, July). Ranibizumab and bevacizumab for treatment of neovascular age-related macular degeneration: two-year results. *Ophthalmology 119*(7), 1388–1398.

Cronin, T., T. Léveillard, and J.-A. Sahel (2007). Retinal degenerations: from cell signaling to cell therapy; pre-clinical and clinical issues. *Current gene therapy 7*(2), 121–129.

Cuenca, N., I. Pinilla, Y. Sauvé, and R. Lund (2005). Early changes in synaptic connectivity following progressive photoreceptor degeneration in RCS rats. *European Journal of Neuroscience 22*(5), 1057–1072.

Degenaar, P., N. Grossman, M. Memon, J. Burrone, M. Dawson, E. Drakakis, M. Neil, and K. Nikolic (2009). Optobionic vision—a new genetically enhanced light on retinal prosthesis. *Journal of neural engineering 6*, 035007.

Doonan, F., M. Donovan, and T. G. Cotter (2005). Activation of multiple pathways during photoreceptor apoptosis in the rd mouse. *Investigative Ophthalmology & Visual Science 46*(10), 3530–3538.

Ecker, J. L., O. N. Dumitrescu, K. Y. Wong, N. M. Alam, S.-K. Chen, T. LeGates, J. M. Renna, G. T. Prusky, D. M. Berson, and S. Hattar (2010). Melanopsin-expressing retinal ganglion-cell photoreceptors: cellular diversity and role in pattern vision. *Neuron 67*(1), 49–60.

Efron, B. and R. Tibshirani (1986). Bootstrap methods for standard errors, confidence intervals, and other measures of statistical accuracy. *Statistical science 1*, 54–75.

Erb, L., K. D. Lustig, A. H. Ahmed, F. A. Gonzalez, and G. A. Weisman (1990). Covalent incorporation of 3'-O-(4-benzoyl)benzoyl-ATP into a P2 purinoceptor in transformed mouse fibroblasts. *Journal of Biological Chemistry 265*(13), 7424–7431.

Farrow, K. and R. H. Masland (2011). Physiological clustering of visual channels in the mouse retina. *Journal of Neurophysiology 105*(4), 1516–1530.

Feldbauer, K., D. Zimmermann, V. Pintschovius, J. Spitz, C. Bamann, and E. Bamberg (2009). Channelrhodopsin-2 is a leaky proton pump. In *Proceedings of the National Academy of Sciences of the United States of America*, Volume 106, pp. 12317–12322.

Fletcher, E. L. (2010). Mechanisms of photoreceptor death during retinal degeneration. *Optometry and vision science : official publication of the American Academy of Optometry 87*(4), 269–275.

Fortin, D. L., M. R. Banghart, T. W. Dunn, K. Borges, D. A. Wagenaar, Q. Gaudry, M. H. Karakossian, T. S. Otis, W. B. Kristan, D. Trauner, and R. H. Kramer (2008). Photochemical control of endogenous ion channels and cellular excitability. *Nature Methods 5*(4), 331–338.

Franke, H., K. Klimke, U. Brinckmann, J. Grosche, M. Francke, B. Sperlagh, A. Reichenbach, U. G. Liebert, and P. Illes (2005). P2X7 receptor-mRNA and -protein in the mouse

retina; changes during retinal degeneration in BALBCrds mice. *Neurochemistry International 47*(4), 235–242.

Gerding, H., F. P. Benner, and S. Taneri (2007, March). Experimental implantation of epiretinal retina implants (EPI-RET) with an IOL-type receiver unit. *Journal of neural engineering 4*(1), S38–49.

Gonzalez, F. A., A. H. Ahmed, K. D. Lustig, L. Erb, and G. A. Weisman (1989). Permeabilization of transformed mouse fibroblasts by 3?-O-(4-benzoyl)benzoyl adenosine 5?-triphosphate and the desensitization of the process. *Journal of Cellular Physiology 139*(1), 109–115.

Govorunova, E. G., E. N. Spudich, C. E. Lane, O. A. Sineshchekov, and J. L. Spudich (2011). New channelrhodopsin with a red-shifted spectrum and rapid kinetics from Mesostigma viride. *mBio 2*(3), e00115–11.

Greenberg, K. P., A. Pham, and F. S. Werblin (2011, February). Differential Targeting of Optical Neuromodulators to Ganglion Cell Soma and Dendrites Allows Dynamic Control of Center-Surround Antagonism. *Neuron 69*(4), 713–720.

Hartong, D., E. Berson, and T. Dryja (2006). ScienceDirect.com - The Lancet - Retinitis pigmentosa. *The Lancet 368*, 1795–1809.

Hascoët, M. and M. Bourin (2009). *The Mouse Light-Dark Box Test*, Volume 42 of *Neuromethods0893-23361940-6045*. Totowa, NJ: Humana Press.

Hattar, S., H. W. Liao, M. Takao, D. M. Berson, and K. W. Yau (2002). Melanopsin-containing retinal ganglion cells: architecture, projections, and intrinsic photosensitivity. *Science 295*(5557), 1065–1070.

Hattar, S., R. J. Lucas, N. Mrosovsky, S. Thompson, R. H. Douglas, M. W. Hankins, J. Lem, M. Biel, F. Hofmann, R. G. Foster, and K. W. Yau (2003, July). Melanopsin and rod-cone photoreceptive systems account for all major accessory visual functions in mice. *Nature 424*(6944), 76–81.

Hauswirth, W. W., T. S. Aleman, S. Kaushal, A. V. Cideciyan, S. B. Schwartz, L. Wang, T. J. Conlon, S. L. Boye, T. R. Flotte, B. J. Byrne, and S. G. Jacobson (2008). Treatment of leber congenital amaurosis due to RPE65 mutations by ocular subretinal injection of adeno-associated virus gene vector: short-term results of a phase I trial. *Human gene therapy 19*(10), 979–990.

Hirano, M., Y. Imaizumi, K. Muraki, A. Yamada, and M. Watanabe (1998). Effects of ruthenium red on membrane ionic currents in urinary bladder smooth muscle cells of the guinea-pig. *Pflügers Archiv - European Journal of Physiology 435*(5), 645–653.

Hu, H., W. Lu, M. Zhang, X. Zhang, A. J. Argall, S. Patel, G. E. Lee, Y.-C. Kim, K. A. Jacobson, A. M. Laties, and C. H. Mitchell (2010). Stimulation of the P2X7 receptor kills rat retinal ganglion cells in vivo. *Experimental Eye Research 91*(3), 425–432.

Huberman, A. D., M. B. Feller, and B. Chapman (2008). Mechanisms underlying development of visual maps and receptive fields. *Annual review of neuroscience 31*, 479–509.

Humayun, M., J. Dorn, L. da Cruz, G. Dagnelie, J. Sahel, P. Stanga, A. Cideciyan, J. Duncan, D. Eliott, E. Filley, A. Ho, A. Santos, A. Safran, A. Arditi, L. Del Priore, and R. Greenberg (2012). Interim results from the international trial of Second Sight's visual prosthesis. *Ophthalmology 119*, 779–788.

Humayun, M. S., J. D. Weiland, G. Y. Fujii, R. Greenberg, R. Williamson, J. Little, B. Mech, V. Cimmarusti, G. Van Boemel, G. Dagnelie, and E. de Juan Jr. (2003). Visual perception in a blind subject with a chronic microelectronic retinal prosthesis. *Vision Research 43*(24), 2573–2581.

Innocenti, B., S. Pfeiffer, E. Zrenner, K. Kohler, and E. Guenther (2004). ATP-induced non-neuronal cell permeabilization in the rat inner retina. *Journal of Neuroscience 24*(39), 8577–8583.

Ivanova, E., G.-S. Hwang, Z.-H. Pan, and D. Troilo (2010, October). Evaluation of AAV-mediated expression of Chop2-GFP in the marmoset retina. *Investigative Ophthalmology & Visual Science 51*(10), 5288–5296.

Javaheri, M., D. Hahn, and R. Lakhanpal (2006). Retinal prostheses for the blind. *ANNALS-ACADEMY OF ... 35*(3), 137–144.

Jiménez, A. J., J. M. García-Fernández, B. González, and R. G. Foster (1996). The spatio-temporal pattern of photoreceptor degeneration in the aged rd/rd mouse retina. *Cell and tissue research 284*(2), 193–202.

Johnson, J., V. Wu, M. Donovan, S. Majumdar, R. C. Rentería, T. Porco, R. N. Van Gelder, and D. R. Copenhagen (2010). Melanopsin-dependent light avoidance in neonatal mice. *Proceedings of the National Academy of Sciences of the United States of America 107*(40), 17374–17378.

Jones, B. W., M. Kondo, H. Terasaki, Y. Lin, M. McCall, and R. E. Marc (2012). Retinal remodeling. *Japanese journal of ophthalmology 56*(4), 289–306.

Kandel, G., H. Bedell, R. Walker, and B. Wolf (1987). Negative phototaxis in pigmented, albinotic and RCS rat pups measured with a new technique. *Clinical vision science 1*, 357–655.

Kessel, L., J. Lundeman, K. Herbst, T. Andersen, and M. Larsen (2010). Age-related changes in the transmission properties of the human lens and their relevance to circadian entrainment. *Journal of cataract and refractive surgery 36*, 308–312.

Khakh, B. S. and R. A. North (2012). Neuromodulation by extracellular ATP and P2X receptors in the CNS. *Neuron 76*(1), 51–69.

Kitamura, E., M. Danciger, C. Yamashita, N. P. Rao, S. Nusinowitz, B. Chang, and D. B. Farber (2006, April). Disruption of the gene encoding the beta1-subunit of transducin in the Rd4/+ mouse. *Investigative Ophthalmology & Visual Science 47*(4), 1293–1301.

Lagali, P. S., D. Balya, G. B. Awatramani, T. A. Munch, D.-S. Kim, V. Busskamp, C. L. Cepko, and B. Roska (2008). Light-activated channels targeted to ON bipolar cells restore visual function in retinal degeneration. *Nature Neuroscience 11*(6), 667–675.

Lamba, D. A., J. Gust, and T. A. Reh (2009). Transplantation of human embryonic stem cell-derived photoreceptors restores some visual function in Crx-deficient mice. *Cell stem cell 4*(1), 73–79.

Lamba, D. A., M. O. Karl, and T. A. Reh (2009). Strategies for retinal repair: cell replacement and regeneration. *Progress in brain research 175*, 23–31.

Lamba, D. A., M. O. Karl, C. B. Ware, and T. A. Reh (2006, August). Efficient generation of retinal progenitor cells from human embryonic stem cells. *Proceedings of the National Academy of Sciences of the United States of America 103*(34), 12769–12774.

Leonelli, M., D. O. Martins, A. H. Kihara, and L. R. G. Britto (2009). Ontogenetic expression of the vanilloid receptors TRPV1 and TRPV2 in the rat retina. *International journal of developmental neuroscience : the official journal of the International Society for Developmental Neuroscience 27*(7), 709–718.

Leske, M. C., A. Heijl, L. Hyman, B. Bengtsson, and E. Komaroff (2004). Factors for progression and glaucoma treatment: the Early Manifest Glaucoma Trial. *Current opinion in ophthalmology 15*(2), 102–106.

Li, Y. K., F. Wang, W. Wang, Y. Luo, P. F. Wu, J. L. Xiao, Z. L. Hu, Y. Jin, G. Hu, and J. G. Chen (2012, July). Aquaporin-4 deficiency impairs synaptic plasticity and associative fear memory in the lateral amygdala: involvement of downregulation of glutamate transporter-1 expression. *Neuropsychopharmacology 37*(8), 1867–1878.

Lin, B., A. Koizumi, N. Tanaka, S. Panda, and R. H. Masland (2008). Restoration of visual function in retinal degeneration mice by ectopic expression of melanopsin. *Proceedings of the National Academy of Sciences of the United States of America 105*(41), 16009–16014.

Lin, J. Y., M. Z. Lin, P. Steinbach, and R. Y. Tsien (2009). Characterization of engineered channelrhodopsin variants with improved properties and kinetics. *Biophysical journal 96*(5), 1803–1814.

Lohr, H. R., K. Kuntchithapautham, A. K. Sharma, and B. Rohrer (2006). Multiple, parallel cellular suicide mechanisms participate in photoreceptor cell death. *Experimental Eye Research 83*(2), 380–389.

London, N. J., A. Chiang, and J. A. Haller (2011a, May). The dexamethasone drug delivery system: indications and evidence. *Advances in therapy 28*(5), 351–366.

London, N. J. S., A. Chiang, and J. A. Haller (2011b). The dexamethasone drug delivery system: indications and evidence. *Advances in therapy 28*(5), 351–366.

Marc, R., B. Jones, C. Watt, and E. Strettoi (2003). Neural remodeling in retinal degeneration. *Prog Retin Eye Res 22*, 607–655.

Marc, R. E., B. W. Jones, J. R. Anderson, K. Kinard, D. W. Marshak, J. H. Wilson, T. Wensel, and R. J. Lucas (2007). Neural Reprogramming in Retinal Degeneration. *Investigative Ophthalmology & Visual Science 48*(7), 3364–3371.

Margolis, D., G. Newkirk, T. Euler, and P. Detwiler (2008). Functional Stability of Retinal Ganglion Cells after Degeneration-Induced Changes in Synaptic Input. *The Journal of Neuroscience 28*(25), 6526–6536.

Margolis, D. J. and P. B. Detwiler (2011). Cellular origin of spontaneous ganglion cell spike activity in animal models of retinitis pigmentosa. *Journal of ophthalmology 2011*, 507037.

Martin, K. R. G., H. A. Quigley, D. Valenta, J. Kielczewski, and M. E. Pease (2006). Optic nerve dynein motor protein distribution changes with intraocular pressure elevation in a rat model of glaucoma. *Experimental Eye Research 83*, 255–262.

Mazzoni, F., E. Novelli, and E. Strettoi (2008). Retinal Ganglion Cells Survive and Maintain Normal Dendritic Morphology in a Mouse Model of Inherited Photoreceptor Degeneration. *Journal of Neuroscience 28*(52), 14282–14292.

Meister, M., J. Pine, and D. A. Baylor (1994). Multi-neuronal signals from the retina: acquisition and analysis. *Journal of neuroscience methods 51*(1), 95–106.

Milam, A., Z. Li, and R. Fariss (1998). Histopathology of the human retina in retinitis pigmentosa. *Progress in Retinal and Eye Research 17*, 175–205.

Mitchell, C. H., W. Lu, H. Hu, X. Zhang, D. Reigada, and M. Zhang (2009). The P2X(7) receptor in retinal ganglion cells: A neuronal model of pressure-induced damage and protection by a shifting purinergic balance. *Purinergic Signalling 5*(2), 241–249.

Moreno, M. C., J. Campanelli, P. Sande, D. A. Sánez, M. I. Keller Sarmiento, and R. E. Rosenstein (2004). Retinal oxidative stress induced by high intraocular pressure. *Free radical biology & medicine 37*(6), 803–812.

Mourot, A., T. Fehrentz, Y. Le Feuvre, C. M. Smith, C. Herold, D. Dalkara, F. Nagy, D. Trauner, and R. H. Kramer (2012). Rapid optical control of nociception with an ion-channel photoswitch. *Nature Methods 9*(4), 396–402.

Mourot, A., M. A. Kienzler, M. R. Banghart, T. Fehrentz, F. M. Huber, M. Stein, R. H. Kramer, and D. Trauner (2011). Tuning photochromic ion channel blockers. *ACS Chemical Neuroscience 2*(9), 536–543.

Nagel, G., T. Szellas, W. Huhn, S. Kateriya, N. Adeishvili, P. Berthold, D. Ollig, P. Hegemann, and E. Bamberg (2003, November). Channelrhodopsin-2, a directly light-gated cation-selective membrane channel. *Proceedings of the National Academy of Sciences of the United States of America 100*(24), 13940–13945.

Nelson, R., E. V. Famiglietti, and H. Kolb (1978). Intracellular staining reveals different levels of stratification for on- and off-center ganglion cells in cat retina. *Journal of Neurophysiology 41*(2), 472–483.

Newton, J. R., C. Ellsworth, T. Miyakawa, S. Tonegawa, and M. Sur (2004, September). Acceleration of visually cued conditioned fear through the auditory pathway. *Nature Neuroscience 7*(9), 968–973.

Oesterhelt, D. (1998). The structure and mechanism of the family of retinal proteins from halophilic archaea. *Current opinion in structural biology 8*(4), 489–500.

Panda, S., I. Provencio, D. Tu, S. Pires, M. Rollag, A. Castrucci, M. Pletcher, T. Sato, T. Wiltshire, M. Andahazy, S. Kay, R. Van Gelder, and J. Hogenesch (2003). Melanopsin Is Required for Non-Image-Forming Photic Responses in Blind Mice. *Science 301*(5632), 525–527.

Polosukhina, A., J. Litt, I. Tochitsky, J. Nemargut, Y. Sychev, I. De Kouchkovsky, T. Huang, K. Borges, D. Trauner, R. N. Van Gelder, and R. H. Kramer (2012, July). Photochemical restoration of visual responses in blind mice. *Neuron 75*(2), 271–282.

Punzo, C. and C. Cepko (2007). Cellular Responses to Photoreceptor Death in the rd1 Mouse Model of Retinal Degeneration. *Investigative Ophthalmology & Visual Science 48*(2), 849–857.

Punzo, C., K. Kornacker, and C. L. Cepko (2008). Stimulation of the insulin/mTOR pathway delays cone death in a mouse model of retinitis pigmentosa. *Nature Neuroscience 12*(1), 44–52.

Rassendren, F., G. N. Buell, C. Virginio, G. Collo, R. A. North, and A. Surprenant (1997). The permeabilizing ATP receptor, P2X7. Cloning and expression of a human cDNA. *The Journal of biological chemistry 272*(9), 5482–5486.

Raviola, E. and R. F. Dacheux (1983). Variations in structure and response properties of horizontal cells in the retina of the rabbit. *Vision Research 23*(11), 1221–1227.

Ripps, H. (2002). Cell death in retinitis pigmentosa: gap junctions and the 'bystander' effect. *Experimental Eye Research 74*(3), 327–336.

Roderick, T. H., B. Chang, N. L. Hawes, and J. R. Heckenlively (1997, June). A new dominant retinal degeneration (Rd4) associated with a chromosomal inversion in the mouse. *Genomics 42*(3), 393–396.

Sacco, T. and B. Sacchetti (2010, August). Role of secondary sensory cortices in emotional memory storage and retrieval in rats. *Science 329*(5992), 649–656.

Sancho-Pelluz, J., B. Arango-Gonzalez, S. Kustermann, F. J. Romero, T. Veen, E. Zrenner, P. Ekström, and F. Paquet-Durand (2008). Photoreceptor Cell Death Mechanisms in Inherited Retinal Degeneration. *Molecular Neurobiology 38*(3), 253–269.

Sanges, D., A. Comitato, R. Tammaro, and V. Marigo (2006). Apoptosis in retinal degeneration involves cross-talk between apoptosis-inducing factor (AIF) and caspase-12 and is blocked by calpain inhibitors. *Proceedings of the National Academy of Sciences of the United States of America 103*(46), 17366–17371.

Sappington, R. M., T. Sidorova, D. J. Long, and D. J. Calkins (2008). TRPV1: Contribution to Retinal Ganglion Cell Apoptosis and Increased Intracellular Ca2+ with Exposure to Hydrostatic Pressure. *Investigative Ophthalmology & Visual Science 50*(2), 717–728.

Schiller, P. H., J. H. Sandell, and J. H. Maunsell (1986). Functions of the ON and OFF channels of the visual system. *Nature 322*(6082), 824–825.

Sekirnjak, C., C. Hulse, L. Jepson, P. Hottowy, A. Sher, W. Dabrowski, A. Litke, and E. Chichilnisky (2009). Loss of responses to visual but not electrical stimulation in ganglion cells of rats with severe photoreceptor degeneration. *Journal of Neurophysiology 102*, 3260–3269.

Sharp, A. J., P. E. Polak, V. Simonini, S. X. Lin, J. C. Richardson, E. R. Bongarzone, and D. L. Feinstein (2008). $P2X_7$ deficiency suppresses development of experimental autoimmune encephalomyelitis. *Journal of neuroinflammation 5*, 33.

Shintani, K., D. L. Shechtman, and A. S. Gurwood (2009). Review and update: Current treatment trends for patients with retinitis pigmentosa. *Optometry - Journal of the American Optometric Association 80*(7), 384–401.

Shire, D. B., S. K. Kelly, J. Chen, P. Doyle, M. D. Gingerich, S. F. Cogan, W. A. Drohan, O. Mendoza, L. Theogarajan, J. L. Wyatt, and J. F. Rizzo (2009). Development and Implantation of a Minimally Invasive Wireless Subretinal Neurostimulator. *IEEE Transactions on Biomedical Engineering 56*(10), 2502–2511.

Sjulson, L. and G. Miesenböck (2008). Photocontrol of neural activity: biophysical mechanisms and performance in vivo. *Chemical reviews 108*(5), 1588–1602.

Sommer, A. (1989). Intraocular pressure and glaucoma. *American Journal of Ophthalmology 107*(2), 186–188.

Sorge, R. E., T. Trang, R. Dorfman, S. B. Smith, S. Beggs, J. Ritchie, J.-S. Austin, D. V. Zaykin, H. Vander Meulen, M. Costigan, T. A. Herbert, M. Yarkoni-Abitbul, D. Tichauer, J. Livneh, E. Gershon, M. Zheng, K. Tan, S. L. John, G. D. Slade, J. Jordan, C. J. Woolf, G. Peltz, W. Maixner, L. Diatchenko, Z. Seltzer, M. W. Salter, and J. S. Mogil (2012). Genetically determined P2X7 receptor pore formation regulates variability in chronic pain sensitivity. *Nature medicine 18*(4), 595–599.

Stacey, P., C. Raine, G. O'Donoghue, L. Tapper, T. Twomey, and A. Summerfield (2010). Effectiveness of computer-based auditory training for adult users of cochlear implants. *International journal of audiology 49*, 347–356.

Stasheff, S. F. (2008). Emergence of Sustained Spontaneous Hyperactivity and Temporary Preservation of OFF Responses in Ganglion Cells of the Retinal Degeneration (rd1) Mouse. *Journal of Neurophysiology 99*(3), 1408–1421.

Strettoi, E. and V. Pignatelli (2000). Modifications of retinal neurons in a mouse model of retinitis pigmentosa. *Proceedings of the National Academy of Sciences of the United States of America 97*(20), 11020–11025.

Surprenant, A., F. Rassendren, E. Kawashima, R. A. North, and G. Buell (1996). The cytolytic P2Z receptor for extracellular ATP identified as a P2X receptor (P2X7). *Science 272*(5262), 735–738.

Thyagarajan, S., M. van Wyk, K. Lehmann, S. Lowel, G. Feng, and H. Wassle (2010). Visual Function in Mice with Photoreceptor Degeneration and Transgenic Expression of Channelrhodopsin 2 in Ganglion Cells. *Journal of Neuroscience 30*(26), 8745–8758.

Tomita, H., E. Sugano, H. Isago, T. Hiroi, Z. Wang, E. Ohta, and M. Tamai (2010). Channelrhodopsin-2 gene transduced into retinal ganglion cells restores functional vision in genetically blind rats. *Experimental Eye Research 90*(3), 429–436.

Trullas, R. and P. Skolnick (1993). Differences in fear motivated behaviors among inbred mouse strains. *Psychopharmacology (Berl) 111*(3), 323–331.

Van Gelder, R. N. (2005). Nonvisual ocular photoreception in the mammal. *Methods in enzymology 393*, 746–755.

van Norren, D. and T. G. Gorgels (2011, July). The action spectrum of photochemical damage to the retina: a review of monochromatic threshold data. *Photochem Photobiol 87*(4), 747–753.

Vandenberghe, L. H., P. Bell, A. M. Maguire, C. N. Cearley, R. Xiao, R. Calcedo, L. Wang, M. J. Castle, A. C. Maguire, R. Grant, J. H. Wolfe, J. M. Wilson, and J. Bennett (2011, June). Dosage thresholds for AAV2 and AAV8 photoreceptor gene therapy in monkey. *Science translational medicine 3*(88), 88ra54.

Virgilio, F. D., V. Vishwanath, and D. Ferrari (2001). *On the Role of the P2X$_7$ Receptor in the Immune System*, Volume 151 / 2 of *Handbook of Experimental Pharmacology*. Springer Berlin Heidelberg.

Virginio, C., A. MacKenzie, F. A. Rassendren, R. A. North, and A. Surprenant (1999). Pore dilation of neuronal P2X receptor channels. *Nature Neuroscience 2*(4), 315–321.

Vriens, J., G. Appendino, and B. Nilius (2009). Pharmacology of Vanilloid Transient Receptor Potential Cation Channels. *Molecular Pharmacology 75*(6), 1262–1279.

Wang, X., G. Arcuino, T. Takano, J. Lin, W. G. Peng, P. Wan, P. Li, Q. Xu, Q. S. Liu, S. A. Goldman, and M. Nedergaard (2004). P2X7 receptor inhibition improves recovery after spinal cord injury. *Nature medicine 10*(8), 821–827.

Weiland, J. D., A. K. Cho, and M. S. Humayun (2011, November). Retinal prostheses: current clinical results and future needs. *Ophthalmology 118*(11), 2227–2237.

Weiland, J. D., W. Liu, and M. S. Humayun (2005). Retinal Prosthesis. *Annual Review of Biomedical Engineering 7*(1), 361–401.

Winter, J. O., S. F. Cogan, and J. F. Rizzo (2007). Retinal prostheses: current challenges and future outlook. *Journal of biomaterials science. Polymer edition 18*(8), 1031–1055.

Yanai, D., J. D. Weiland, M. Mahadevappa, R. J. Greenberg, I. Fine, and M. S. Humayun (2007). Visual Performance Using a Retinal Prosthesis in Three Subjects With Retinitis Pigmentosa. *American Journal of Ophthalmology 143*(5), 820–827.e2.

Yang, X.-f., W.-g. Liu, H. Shen, J.-b. Gong, J. Yu, W.-w. Hu, S.-t. Lü, X.-j. Zheng, and W.-m. Fu (2005). Correlation of cell apoptosis with brain edema and elevated intracranial pressure in traumatic brain injury. *Chinese journal of traumatology = Zhonghua chuang shang za zhi / Chinese Medical Association 8*(2), 96–100.

Zhang, F., L.-P. Wang, M. Brauner, J. F. Liewald, K. Kay, N. Watzke, P. G. Wood, E. Bamberg, G. Nagel, A. Gottschalk, and K. Deisseroth (2007). Multimodal fast optical interrogation of neural circuitry. *Nature 446*(7136), 633–639.

Zhang, X., A. Li, J. Ge, D. Reigada, A. M. Laties, and C. H. Mitchell (2007). Acute increase of intraocular pressure releases ATP into the anterior chamber. *Experimental Eye Research 85*(5), 637–643.